POTENCY AND PHARMACOKINETIC ENHANCEMENT OF D-PEPTIDE HIV-1 ENTRY INHIBITORS

by

Joseph Stapley Redman

A dissertation submitted to the faculty of
The University of Utah
in partial fulfillment of the requirements for the degree of

Doctor of Philosophy

Department of Biochemistry

The University of Utah

December 2012

The University of Utah Graduate School

STATEMENT OF DISSERTATION APPROVAL

The dissertation of **Joseph Stapley Redman**

has been approved by the following supervisory committee members:

Michael S. Kay	, Chair	**07/12/2012** Date Approved
Christopher P. Hill	, Member	**07/12/2012** Date Approved
Wesley I. Sundquist	, Member	**07/12/2012** Date Approved
E. Dale Abel	, Member	**07/12/2012** Date Approved
David Bearss	, Member	**07/12/2012** Date Approved

and by **Christopher P. Hill**, Chair of the Department of **Biochemistry**

and by Charles A. Wight, Dean of The Graduate School.

ABSTRACT

Peptides are a powerful class of therapeutics with high potency, high specificity, low immunogenicity, and effective methods of discovery. However, peptides often possess limitations including degradation by proteases, rapid clearance by renal filtration, and difficulty passing through membranes.

The Kay lab at the University of Utah has applied the benefits of peptide design to tackling the problem of HIV-1 transmission. In this dissertation I describe the discovery of our lead peptide candidate, PIE12, including its optimization by mirror-image phage display, its potency enhancement by defined geometric linkages and lipid conjugation, its engineered ability to prevent HIV-1 resistance, and finally the optimization of its pharmacokinetic properties. These efforts have overcome the common limitations of peptide therapeutics and produced an ideal preclinical candidate for the treatment and prevention of HIV/AIDS.

The first chapter examines the scope of the HIV pandemic, describes HIV-1's susceptible target for which we developed PIE12, and includes a brief examination of the current state of the peptide therapeutic field. The second chapter reviews methods of peptide discovery that enable protease resistance, including a discussion of well-validated techniques like mirror-image phage display followed by a review of several emerging technologies. The third chapter reveals how the aforementioned techniques were utilized in the discovery of PIE12, including early efforts to link PIE12 peptides together in order

to improve potency. The fourth chapter completes this story, illuminating our efforts to optimize the linkages between PIE12 peptides in order to increase potency, and includes information on potency-enhancing membrane-tethering moieties. The fifth chapter describes our efforts to make potent PIE12-conjugates suitable for subcutaneous delivery, including new conjugate designs and detailed evaluation of their half-life-improving properties. The final chapter discusses future directions and new opportunities revealed to us by the body of this work.

For my wife Kellie, and my little Yvette

TABLE OF CONTENTS

LIST OF TABLES

LIST OF FIGURES

ACKNOWLEDGMENTS

I am truly indebted to many people for their love, support, willingness and patience to teach me, and the opportunities provided for me to play, explore, fail, and ultimately succeed.

I give foremost appreciation to God, my wife Kellie, my daughter Yvette, and all my other family members for their support during my pursuit of this unique opportunity. I cannot thank them all enough for their love, especially during the dark times. I know they all missed me as I spent long hours in the lab, and for that I am especially grateful for their sacrifices.

I next thank my boss and PI, Michael Kay, not only for the opportunity to become involved in important research and drug design, but also because he didn't give up on me when I was ready to quit. He is truly the smartest person I know, and I admire his dedication to the sick and afflicted over the dollar. I also appreciate how high he aims, even though that often takes him (and all of us in his lab) to new and uncharted territory complete with dogma unfamiliar to all of us. To him I also credit my transition from PC to Mac; truly a godsend.

I thank my committee members, Chris Hill, Wes Sundquist, E. Dale Abel, and David Bearss who has been a friend and teacher from the beginning of my medical career. Their broad expertise was truly welcomed and helped to satisfy my own diverse interests.

I owe special thanks to friends and faculty who took the time to teach me key techniques that enabled me to complete my research. Rob Marquardt is foremost of this group, whose wisdom extended long beyond his stay in the Kay lab. Debbie Eckert also deserves special mention, often inconveniencing herself to help me complete my research. I also thank my other labmates, former labmate Brett Welch, Alan Mueller and the animal team at Navigen, Kevin Jessing, Chad Bradford, and Professor James Herron, for their expertise and contributions to my learning.

I would also like to thank a few close friends, Teran Mitchell, David Jones, and Anthony Earl, for their patience and willingness to be a sounding board as I berated them all with the esoteric details of my work. They truly don't know how much I needed a good ear over these last years. I thank them for their sharp minds, big hearts, and for being truly good people.

I also express deep gratitude to those who have helped to fund my education. From a young age my parents first put me on the path to great academic pursuits, so I thank them for that. Then the University of Utah provided me with outstanding scholarships which propelled me to even loftier goals. I thank the University of Utah's MD-PhD program and my PI who have helped to fund me over the last several years. Within the MD-PhD program I would especially like to thank Janet Bassett, who lovingly watched over me and took on every administrative challenge I managed to discover. Finally, I thank the NIH for the grants to fund our lab's work; AI076168 (R01) and AI95172 (SBIR; PK studies).

CHAPTER 1

INTRODUCTION

Scope of the HIV Pandemic

Since the AIDS pandemic was first identified in 1981 an estimated 59 million people have contracted its causal agent "human immunodeficiency virus" (HIV). To date, approximately 26 million people have died from HIV/AIDS, leaving 33 million people (including 1.2 million in the US) living with the infection (UNAIDS, 2011 UN Millennium Development Goals Report). Although five classes of antiretroviral therapies (NRTI, NNRTI, protease, integrase and entry inhibitors) are available, HIV remains a formidable pathogen. It continues to spread, affects vulnerable populations, and can develop resistance to current therapeutics. New pharmacological agents and therapeutic targets are needed in order to stay ahead of drug resistance and keep the virus under control.

Unfortunately, even new classes of inhibitors, such as the recently approved integrase inhibitor raltegravir, can succumb to the rapid emergence of HIV resistance within a few months of use[1]. As such, there is a growing need not only to develop new promising therapies against HIV, but also to anticipate and counter the problem of HIV's capacity for resistance.

HIV Entry

The general mechanism of HIV entry into susceptible host cells is well understood[2]. HIV expresses a homo-trimeric membrane protein Env (gp160), which undergoes posttranslational cleavage yielding the noncovalently associated gp120 and gp41 subunits. Posttranslational cleavage allows for trapping of these proteins in a "spring-loaded" kinetic trap. The trap is sprung when HIV virions recognize host cells through the interaction of viral gp120 with the primary receptor CD4 and one of two co-receptors (CCR5 or CXCR4). In general, CCR5-tropic virions are more transmissible, and represent the majority of early-stage HIV viral load. In ~50% of patients, HIV undergoes a switch or broadening in co-receptor tropism to begin utilizing CXCR4. This transition correlates with advanced disease and poorer clinical outcomes[3]. It is not clear what is responsible for the transition, but may simply reflect a selection for tropic virions as CCR5-expressing host cells die from CCR5-tropic virus.

After gp120 interacts with CD4 and co-receptor, it undergoes a conformational change that releases the kinetically trapped gp41. gp41 then adopts an extended conformation, plunging its N-terminal fusion peptide into the host cell membrane (Fig. 1-1). This extended conformation is semistable, lasting for several minutes (strain specific)[4]. In this state, two regions become newly defined. First, the host cell-proximal N-trimer is a trimeric coiled-coil with three inter-helical hydrophobic grooves. The highly conserved 17 C-terminal residues of the N-trimer form three deep hydrophobic pockets (Fig. 1-2). Second, the virion-proximal C-peptide region adopts an unknown configuration, possibly unstructured.

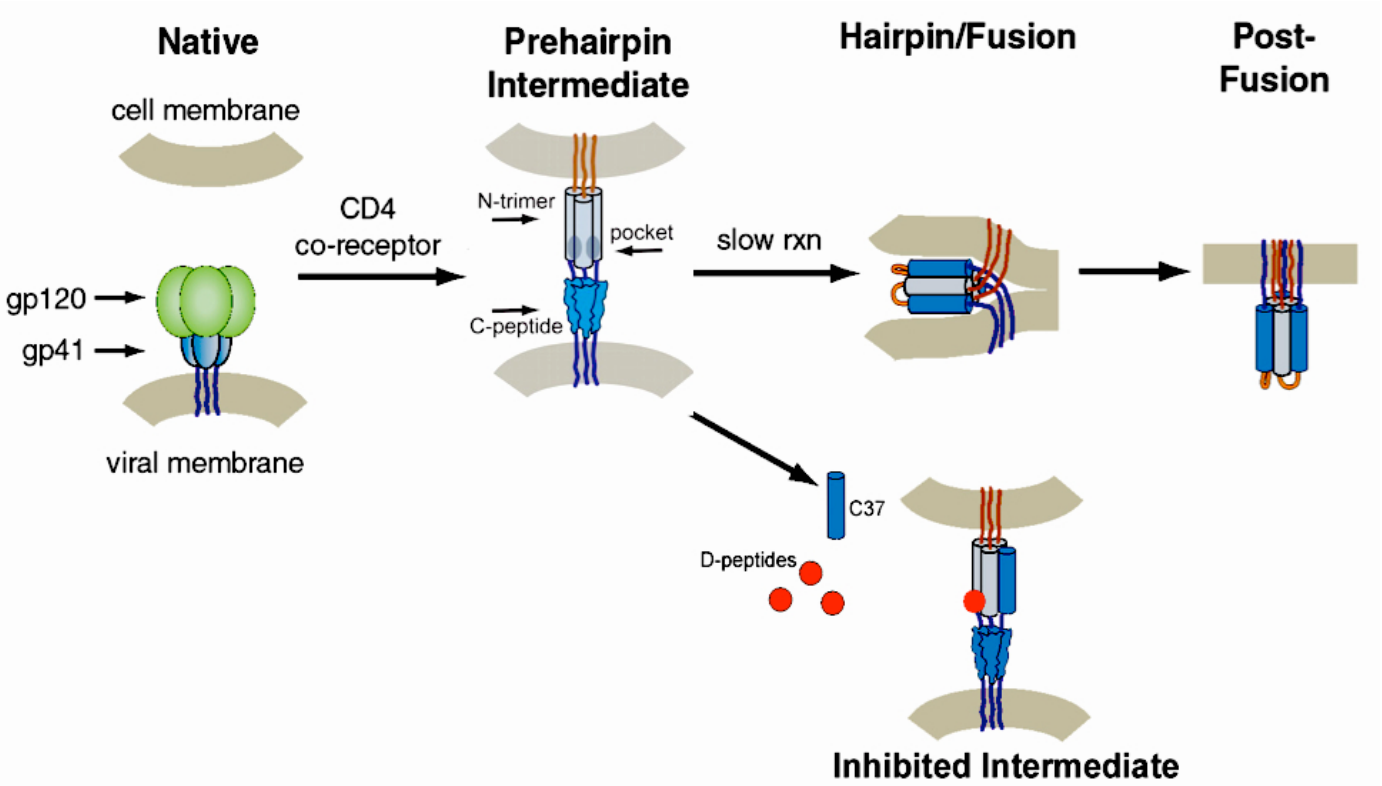

Figure 1-1. Proposed Model of HIV Fusion with Host Cells. HIV expresses several copies of the trimeric Env protein, which is post-translationally cleaved to produce gp120 and gp41. gp120 interacts with its primary receptor CD4 and a co-receptor, triggering gp41 to adopt an extended conformation that plunges its fusion peptide (red) into the host cell membrane. This prehairpin intermediate contains two regions, a host cell-proximal trimeric coiled-coil (N-trimer) and a loosely structured C-peptide region. The C-terminal residues of the N-trimer form three highly conserved deep hydrophobic pockets. The prehairpin intermediate is stable for several minutes, after which C-peptides collapse upon the N-trimer forming the trimer-of-hairpins structure that mediates fusion. Soluble C-peptide analogues (e.g., C37, Fuzeon) and/or D-peptides can bind to the prehairpin intermediate, preventing trimer-of-hairpins formation and HIV fusion. [Modified from[5]]

A)

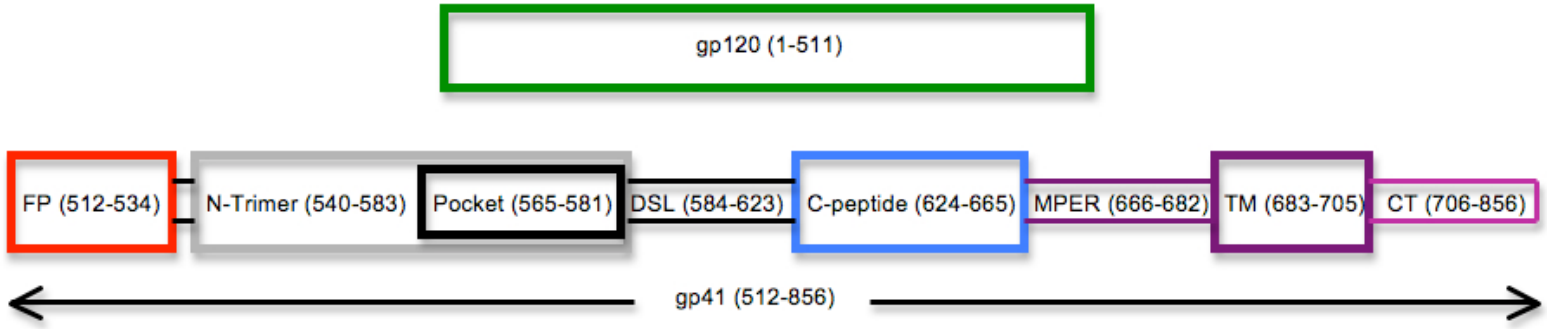

B)

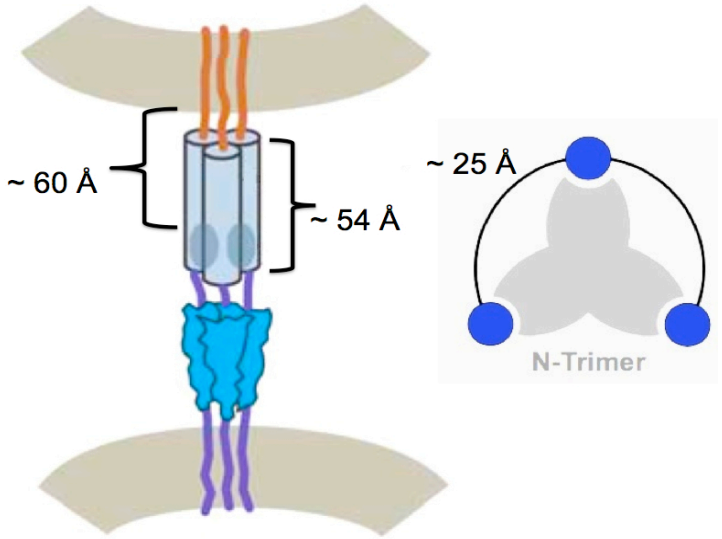

Figure 1-2. Spatial Characteristics of gp41. A) The residues assigned to each region of gp41 (HxB2 numbering). FP = fusion peptide, DSL = disulfide loop, MPER = membrane-proximal external region, TM = trans-membrane, CT = cytoplasmic tail.
B) Distances relevant to oligomerization and membrane-tethering designs. ~25 Å PEG linkers are sufficient to span two pockets.

After a brief window of time, gp41 collapses upon itself, mediating fusion of the virus and host cell. The C-peptide region becomes helical and fills in the grooves of the N-trimer region, forming the very stable "six-helix bundle" or "trimer-of-hairpins." Preventing formation of this trimer-of-hairpins is known to prevent viral infection, and is the basis of the FDA-approved entry inhibitor Fuzeon. Fuzeon is a peptide derived from the C-peptide region and can preemptively bind the N-trimer grooves and prevent fusion through a dominant negative mechanism[6]. Pocket-specific Inhibitor of Entry #12 (PIE12), an optimized nondegradable D-peptide I co-discovered in the Kay lab, binds to the deep hydrophobic pocket of the N-trimer and also prevents trimer-of-hairpins formation and fusion.

It is worth noting that CD4 and the co-receptors are located within host cell lipid rafts[7,8], which are regions of thicker membrane containing distinct lipid content. The localization of HIV's receptors here establishes viral entry at lipid rafts. Thus, entry inhibitors that are targeted to lipid rafts will have improved local concentrations and on-rates, leading to improved inhibition of fusion[9].

Despite this detailed understanding of viral entry, some aspects remain poorly understood, such as how many Env proteins are involved in fusion, and what role, if any, endocytosis plays in physiological virus entry[10].

HIV's Vulnerable Drug Target – The Pocket

The three deep hydrophobic pockets of gp41 are critical for HIV fusion[11]. Each pocket is encoded by the 17-residue sequence LLQLTVWGIKQLQARIL, and binds an essential 8-residue sequence from the C-peptide, WMEWDREI. Interestingly, this

natural ligand contains two tryptophans. A similar motif, EWXWL, was selected in our early phage display efforts and became the basis of future library designs, ultimately leading to the D-peptide entry inhibitor PIE12: HPCDYPEWQWLCELGK. PIE12 binds to the pocket with low nM affinity and potently inhibits HIV fusion[5].

The pocket is highly conserved across all major HIV-1 strains, consistent with its critical role in mediating fusion. Amino acid substitutions in this site are not well-tolerated[2]. Moreover, the nucleotide sequence that encodes this region produces the Rev-response element for Env, a critical stem-loop structure required for mRNA nuclear export[12,13], thereby discouraging mutation even at the nucleotide level.

Discovering D-Peptide Inhibitors of HIV Entry

Work in the Kay lab focuses on developing novel D-peptide therapeutics and advancing them towards promising applications such as inhibiting HIV entry. Peptides are typically defined as sequences of ≤40 amino acids[14]. D-peptides are peptides composed of D-amino acids, which are the mirror image (opposite chirality) of the L-amino acids typically utilized by living systems. D-peptides cannot be made recombinantly, so they must be made by chemical synthesis. Living systems almost exclusively utilize L-amino acids for peptide and protein synthesis, and metabolic enzymes show clear preference for their natural ligands compared to a mirror-image substrate (e.g., >1000-fold[15,16]). This makes D-peptides essentially nondegradable by proteases, endowing them with the capacity to withstand harsh physiological conditions like human plasma, the gastrointestinal system, and vaginal mucosa. This property is of obvious interest for enhancing the exposure of a peptide therapeutic.

However, the same property that makes D-peptides essentially nondegradable makes D-peptide discovery incompatible with powerful biologically-based peptide discovery techniques, because D-peptides cannot be expressed in living systems. This problem, however, can be overcome by a clever technique called "mirror-image phage display." Briefly, a library of M13 phage can be genetically designed to display billions of different L-peptides fused to their g3 proteins. There are five g3 proteins expressed on each M13 phage, so zero to five identical peptides can be displayed per phage. Phage display involves exposing a target protein or peptide to a library of L-peptides fused to these phage to select for L-peptides that bind to the target. Weak or non-binders can be washed away, while tighter binders can be eluted and the associate-phage amplified for another round of selection, thereby continually selecting for progressively better binders (Fig. 1-3)[17].

Mirror-image phage display involves the same process, but utilizes symmetry in order to discover D-peptide binders. The phage still encode L-peptides, but the target they bind to is made as a mirror image (D-chirality) of the natural L-peptide or protein. By symmetry, the L-peptide that is selected as the strongest binder to a D-target will bind to the natural L-target when synthesized as a D-peptide[18]. In our case, HIV's gp41 pocket region is the desired target, so to find a D-peptide that binds to it, an L-peptide phage library was screened against a synthetically produced D-gp41 pocket analog. The winning sequence was synthesized as a D-peptide and was found to effectively bind and inhibit the natural L-gp41 pocket region. We discovered the D-peptide HIV entry inhibitor PIE12 using a combination of mirror-image phage display and structure-aided design (described in Chapter 3)[5].

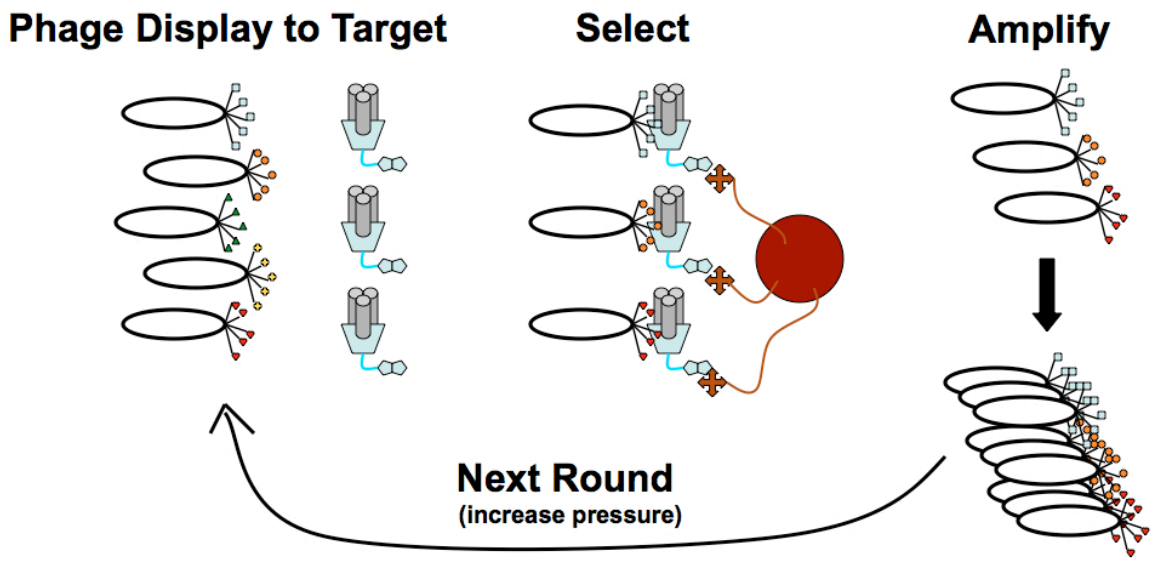

Figure 1-3. Phage Display. A library of phage displaying genetically encoded peptides is incubated with a target. The target may be tethered to a surface (solid-phase) or in solution with a handle for pull-down (solution-phase) as shown here with biotin. After incubation, the target is retrieved by adding magnetic beads coated with streptavidin. After several washes, the remaining phage contain the tightest binding peptides. These are eluted and amplified in *E. coli*. The amplified phage comprise a new library of improved binders which can be re-incubated with the target to further select for the tightest binders.

Improving Potency Through Oligomerization and Membrane Tethering

Because gp41 is a trimeric target with three symmetric pockets, we reasoned that linking three PIE12 peptides together would improve potency. Indeed, this strategy greatly improved potency ~200-fold over monomeric PIE12. We also found that discrete PEG linkers of ~22-25 Å between the C-termini of PIE12 peptides was optimal (Fig. 1-2), becoming the basis for a PEG scaffold enabling rapid synthesis of PIE12-trimer (described in Chapter 4)[9].

Through oligomerization we discovered that initial improvements in affinity (K_D) are correlated with improvements in antiviral potency (IC_{50}), but eventually a potency

plateau is reached after which further improvements in affinity no longer affect potency (Fig. 1-4). The potency plateau for HxB2 is ~100-300 pM, while it is 2-3 nM for JRFL. JRFL is a difficult-to-inhibit primary strain known to fuse more rapidly than other strains, thereby reducing its exposure to fusion inhibitors, decreasing their potency[4]. Of our D-peptide oligomers, PIE12-trimer possesses the highest affinity, but the potency plateau prevents estimation of its K_D based on IC_{50}. A direct measurement of K_D is not possible because the interaction is too tight; the extraordinarily slow off-rate prevents assessment by biosensor analysis. Nevertheless, PIE12-trimer affinity can be estimated by comparisons to the affinities and potency improvements of other D-peptide oligomers. Such estimates predict a sub-fM K_D for PIE12-trimer.

We reason that the cause of the potency plateau is the transient exposure of the prehairpin intermediate. Because potency is typically a function of both on-rate and off-rate, either increasing the on-rate or decreasing the off-rate will increase potency. However, once the off-rate exceeds the time that a target is exposed, the on-rate becomes the limiting factor for potency, and for peptides in solution (i.e., not tethered to the membrane) the on-rate is limited by three-dimensional diffusion. This on-rate limit creates the potency plateau. Although affinity can be improved by prolonging off-rates, the improvement will no longer be correlated with an increase in potency. Other groups have noticed the same potency plateau in their HIV entry inhibitors[4].

Interestingly, the potency plateau can be overcome by increasing the on-rate via prepositioning inhibitors on cell surfaces using membrane-tethering moieties. This tethering significantly improves potency (described in Chapter 4).

Resisting Resistance – the "Resistance Capacitor"

Besides contributing potent inhibitors to the armament of antiretrovirals, our work aims to build into drug design a capacity to withstand viral mutations. Drug resistance is the bane of HIV treatment, so instead of simply developing a drug that would inevitably succumb to resistance, we decided to proactively design a therapeutic that could delay it as long as possible. To this end, several design strategies have been employed. The first has already been discussed; choosing the gp41 pocket as our drug target reduces the capacity of HIV to develop drug-resistance because the pocket is highly conserved and genetically limited in its capacity to acquire mutations.

The second strategy involves a deliberate over-engineering of our inhibitor. As mentioned, a potency plateau is observed when increases in binding affinity are no longer correlated with increases in antiviral potency. At first we questioned whether to continue efforts to increase binding affinity given that no further potency improvements could be obtained. However, we found that increasing the affinity beyond the potency plateau endows the inhibitor with an excess of binding energy that can absorb the impact of affinity-disrupting resistance mutations by HIV. The greater the binding affinity is with respect to the potency plateau, the more highly charged the "capacitor" is against resistant mutations. We call this excess binding energy the "resistance capacitor." Practically, if HIV develops a mutation that damages binding affinity, the mutated virus will still be inhibited with equal potency (Fig. 1-4). The mutated virus has no growth advantage over wildtype, preventing its selection and giving little opportunity for the mutant to acquire other resistance mutations though step-wise accumulation.

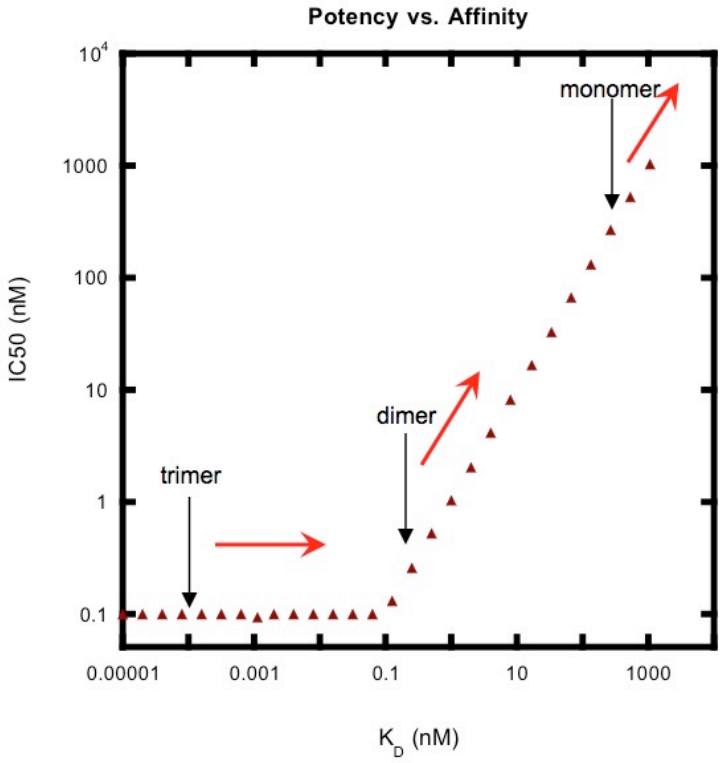

Figure 1-4. The Potency Plateau and Resistance Capacitor. An inhibitor that maintains the same potency (IC_{50}) over a range of affinities (K_D) has reached a potency plateau. Increasing affinity despite no improvements in potency creates a charged "resistance capacitor" where excess binding energy is stored that can resist HIV mutations. If HIV manages to acquire a mutation in the pocket, affinity (K_D) of the inhibitor for the pocket will be weakened. A 100-fold loss of affinity represents a particularly severe affinity-reducing mutation (red arrows). With a charged resistance capacitor, the 100-fold loss in affinity can be completely absorbed, maintaining potency.

Resistance studies conducted in collaboration with Mike Root at Thomas Jefferson University reveal how difficult it is for HIV to develop mutations to escape our pocket-binding inhibitors. PIE12-dimer and PIE12-trimer were incubated with virus at sub-therapeutic levels to encourage the development of virus resistance. Using this protocol, resistance to Fuzeon developed after only 3 weeks, while resistance to PIE12-dimer and PIE12-trimer required 40 and 65 weeks respectively[5], demonstrating the inability of HIV to readily mutate its pocket and the effectiveness of the resistance capacitor design.

Peptide Therapeutics – Powerful Yet Fragile

Peptide therapeutics have key advantages and disadvantages compared to small molecules and proteins. Compared to small molecules, peptides generally have improved selectivity and affinity. Furthermore, peptides can disrupt protein-protein interactions, which has proven a difficult challenge for small molecules. And unlike proteins, peptides can be chemically synthesized, can penetrate deeper into tissues, and are generally less immunogenic because of their small size[19,20]. However, peptides generally suffer from short half-lives and limited delivery options. Unless specially designed (like our D-peptides), peptides are susceptible to proteases and are rapidly degraded, often with half-lives on the order of minutes[19]. Furthermore, their small size leads to rapid clearance (e.g., by renal filtration). Moreover, peptides do not easily cross cell membranes, which not only limits access to potential cytoplasmic targets, but also prevents absorption from the GI tract. As a result, peptides are generally delivered parenterally.

Fuzeon is an FDA-approved HIV entry inhibitor that exemplifies many of the challenges associated with peptide therapeutics. For instance, Fuzeon is rapidly degraded by proteases. Therefore, very large doses must be given to make up for its rapid clearance (90 mg subcutaneously injections twice each day). Such large doses drive up the cost of the therapy (~$30,000/year) and require formulations that are irritating to the skin leading to severe injection site reactions. Moreover, Fuzeon binds the mutation-prone groove region of the gp41 N-Trimer, leading to rapid development of resistance. Although approved, these challenges limit Fuzeon to salvage therapy in patients with treatment-resistant HIV.

By overcoming the common limitations of peptides, our work aims to simplify patient dosing by enabling once-weekly or once-monthly subcutaneous injection. Having already overcome protease susceptibility by developing D-peptides, avoiding additional routes of clearance must be addressed to achieve suitable pharmacokinetics.

Pharmacokinetic Considerations

Because we recognized the general limitations of peptide therapeutics at an early stage, we developed our anti-HIV candidates to be protease stable from the very beginning by utilizing nondegradable D-peptides. However, rapid clearance is still a major concern; even nondegradable peptides can be quickly cleared by renal filtration or other metabolic process.

Numerous promising PK-enhancing strategies for peptides have emerged over the years, with several yielding FDA-approved products. And because insulin, glucagon-like peptide 1 (GLP-1), interferon (IFN-alpha2a), and HIV C-peptide-based entry inhibitors all have proven efficacy, it seems that every PK-enhancing strategy has been applied to at least one of them. PEGylation has yielded 11 approved products and is arguably the most successful strategy to date. Lipidation is a growing field with two approved products. Direct albumin conjugation is perhaps the next-most developed approach, demonstrating impressive gains in half-life. Chapter 5 focuses on utilizing the most promising of these techniques to improve the pharmacokinetics of our lead candidate, PIE12-trimer.

PEGylation

Conjugating peptides and proteins to polyethylene glycol (PEG), also known as polyethylene oxide (PEO), has an impressive track record of enhancing PK in approved-products (Table 1-1). PEGylation primarily enhances PK by reducing renal filtration, and because PEG is extensively hydrated by water, less PEG is required to reduce filtration than might be anticipated from molecular weight alone. While the molecular weight cutoff for globular proteins to avoid renal clearance is ~70 kDa, peptide and protein PEG conjugates need only acquire a combined molecular weight of 40-60 kDa. This can usually be accomplished by the addition of 20-40 kDa of PEG.

The PK-enhancing benefits of PEG are sigmoidal, so exceeding 40 kDa of PEG provides little additional PK benefit and appears to increase uptake into the reticuloendothelial system[21]. Moreover, adding less than 5 kDa of PEG appears to provide little PK benefit. Notably, PEGylation also diminishes clearance of susceptible therapeutics by reducing proteolysis (e.g., Omontys [peginesitide]) and immunogenicity (e.g., Krystexxa [PEG-uricase]).

Important challenges are associated with PEGylation. PEGylation usually reduces activity of the protein/peptide conjugate, and the polydispersity of PEG complicates quantitation, essentially necessitating ELISA-based quantitation. Viscosity must also be considered. We attached a 40 kDa Y-branched PEG to PIE12 and found that viscosity limits its solubility to about 10 mM in 50 mM HEPES, pH 7.4. Hydroxyethylene starch conjugation (HESylation) is an alternative strategy based on the same principles of PEGylation, but HES is less viscous than PEG[22].

Table 1-1. FDA-Approved PEGylated Peptides and Proteins.

Year of FDA-approval	Trade-name	Generic name(s)	Companies involved in manufacturing	Size before PEGylation (number of amino acids, m.w.)	Size, number, geometry of PEG chains	Total molecular weight	Indication	Route	Non-PEGylated half-life	PEGylated half-life
1990	Adagen	Pegademase bovine; PEG-adenosine deaminase	Enzon	bovine adenosine deaminase [ADA EC 3.5.4.4] (336 aa, 42 kDa)	11-17 linear 5 kDa PEG chains	~100 kDa	ADA-associated SCIDS	IM, weekly	< 30 min IV	3-6 days
1994	Oncaspar	Pegasparaginase; Pegaspargase	Enzon	L-asparaginase [type EC-2, EC 3.5.1.1] (326 aa, 34 kDa)	Multiple linear 5 kDa PEG chains	~100 kDa	Acute Lymphoblastic Leukemia	IM, no more than every 14 days	8-30 hours IV	5.8 days
2000	PEG-INTRON	peginterferon alfa-2b	Enzon	Interferon-alpha2b (165 aa, 19.3 kDa)	A single linear 12 kDa PEG	31 kDa	HCV, cancer, MS, HIV	Subcut., weekly	8 hours IM	40 hours
2002	PEGASYS	peginterferon alfa-2a	Roche; Nektar	Interferon-alpha2a (165 aa, 19.3 kDa)	A single branched 40 kDa PEG	60 kDa	HCV	Subcut., weekly	3-4 hours IV	160 hours
2002	Somavert	Pegvisomant	Pfizer; Nektar	An analog of hGH (191 aa, 22 kDa)	4-6 linear 5 kDa PEG chains	42-52 kDa	Acromegaly	Subcut., daily	15-30 hours IV	6 days
2002	Neulasta; PEG-filgrastim	PEG-filgrastim	Amgen; Nektar	G-CSF (175 aa, 19 kDa)	A single linear 20 kDa PEG chain	39 kDa	Neutropenia during chemotherapy	Subcut., given once per chemo cycle	1.3-7.2 hours IV	15-80 hours

Table 1-1 continued. FDA-Approved PEGylated Peptides and Proteins.

2004	Macugen; Pegaptinib	PEG-anti-VEGF-aptamer (oligonucleotide)	Pfizer; Eyetech Pharm.; Nektar	A 28-mer oligonucleotide aptamer, ~10 kDa	A single branched 40 kDa PEG	~50 kDa	Wet age-related Macular degeneration	Intravitreous injection into eye, once every 6 wks.	ND	10 day plasma half-life
2005	Cimzia; CD870	PEG-anti-TNF-Fab; certolizumab pegol	UCB; Nektar	Anti-TNF-Fab (light chain 214 aa, heavy chain 229 aa; 51 kDa)	A single branched 40 kDa PEG	91 kDa	Crohn's Disease	Subcut., once every 4 weeks		14 days
2007	MIRCERA	PEG-Epoetin-beta	Roche; Nektar	Epoetin-beta glycoprotein (165 aa, 30 kDa)	A single linear 30 kDa PEG chain	60 kDa	Anemia in chronic kidney disease (CKD)	IV or Subcut., once every 2-4 weeks	~7 hours	134 hours
2010	Krystexxa	Pegloticase (previously Puricase/PEG-Uricase)	Savient Pharmaceuticals; Nektar	Tetrameric enzyme uricase; 34 kDa/monomer = 136 kDa tetra.	8-10 10 kDa mPEG chains per monomer	~497-540 kDa	Gout	8 mg IV every 2 weeks.	4 hours	154-331 hours
2012	Omontys (formerly Hematide)	PEG-EPO-mimic	Affymax, Nektar	EPO-mimicking peptide (14 aa dimer, 28 aa total, ~4 kDa)	A single branched 40 kDa PEG	~44 kDa	Dialysis and non-dialysis CKD patients with PRCA	Subcut. once every 3-4 weeks	Minutes	Up to 60 hours

Lipid Conjugation

Lipid conjugation is another validated approach for improving half-life. Endogenous free fatty acids (FFAs) bind strongly (mid to low nM K_D[23-25]) to human serum albumin (HSA), which circulates with an impressive 19 day half-life[26]. Thus, conjugating a fatty acid (acylation) to a peptide reduces clearance by promoting HSA association. The approved products Victoza (liraglutide) and Levemir (insulin detemir) utilize this strategy, employing palmitate and myristate respectively.

Cholesterol conjugation is an alternative lipidation strategy. Cholesterol is reported to have a 25-435 μM affinity for albumin[27,28] and a strong but reversible affinity for cell membranes[9]. Cholesterol conjugation has been show to significantly improve PK properties, as well as localize antiviral peptides to lipid rafts, greatly enhancing their antiviral potency[29]. However, PK studies of cholesterol conjugates have not been done in humans who possess a unique circulating lipid profile, so there may be a significant difference in the way cholesterol conjugates are shuttled and interact with circulating lipid carriers in humans compared to rodents.

Albumin Binding Peptides and Molecules

Since acylation has demonstrated reliable PK-enhancement through albumin interaction, albumin-binding peptides and molecules have emerged as alternative PK-enhancing techniques. Genentech's SA21 is the best studied of this group. SA21 is an 18 amino acid disulfide-constrained peptide (Ac-RLIEDI**C**LPRWG**C**LWEDD-NH2) with 467 nM affinity for HSA and exhibits a 2.3 hour terminal half-life after IV injection in rabbits[30]. A similar disulfide-bonded peptide with micromolar affinity has been

identified by Dyax after screening a $CX_{10}C$ phage library[31], while an extremely high affinity (50 fM) albumin-binding protein has been engineered by optimizing (also by phage display) a bacterially-derived nanomolar affinity 46-residue three-helix bundle[32]. Finally, "Albu tag" is a unique small molecule that displays a high affinity for albumin (330 nM at 37 °C) and a maleimide moiety for thiol-mediated peptide conjugation[33].

Direct Albumin Conjugation

As mentioned, albumin circulates with an impressive 19-day half-life in humans. Albumin enjoys this half-life by avoiding renal filtration. For globular proteins, the size limitation for avoiding glomerular filtration is ~70 kDa, and although albumin is slightly below this size threshold (66.5 kDa), it avoids filtration because it is highly negatively charged and experiences electrostatic repulsion from the highly negatively charged glomerular basement membrane of the kidney. By comparison, IgG (150 kDa), one of the largest circulating proteins, circulates with a half-life of 21-27 days (subclasses 1, 2 and 4; subclass 3 has a half-life of only 7 hours)[34].

Rationally, if albumin-binding moieties increase half-life, direct conjugation to albumin should increase half-life even further. To this end, three strategies have been described. Two strategies involve thiol-mediated conjugation to the uniquely exposed Cys-34 in the Ia subdomain of albumin. The difference between them is whether conjugation is completed *in vitro* to purified HSA or a thiol-reactive prodrug is delivered for conjugation *in vivo* to circulating HSA. The accessibility of albumin's Cys-34 thiol both *in vitro* and *in vivo* is discussed by Katz et al., who note that physiologically free thiols are fairly rare such that side-reactions are expected to be uncommon[35]. The third

reported strategy involves genetically linking a peptide to HSA such that a fusion protein can be expressed[36], though such a strategy depends on recombinant expression and would not be suitable for D-peptides.

Other PK-Enhancers

A variety of other PK-enhancing moieties can be found in the literature. Fc conjugation is a validated strategy with several approved products (e.g., Orencia, Enbrel). The Fc domain derived from human IgG1 increases half-life by utilizing cellular Fc receptors. These receptors mediate endocytosis of Fc domains followed by a return to circulation[37]. Moreover, Fc receptors in the lung are thought to provide an opportunity for trans-pulmonary delivery of peptides into circulation[38]. Fc domains require mammalian cell-line expression in order to achieve appropriate folding and glycosylation, although recent work has focused on mutated Fc variants to simplify production.[39] PK-enhancing transferrin and GCSF conjugations are also reported in the literature but have not yet been extensively utilized. Like Fc domains, these conjugations are thought to improve half-life by utilizing receptors that mediate endocytosis and recycling[37].

Fuzeon has been found to contain a critical 8 amino-acid hydrophobic foot, WASLWNWF, which is necessary for its potency (through membrane localization) and half-life[40]. The sequence is derived from the gp41 MPER region (Fig. 1-2). This moiety is attractive as a potential PK-booster because of its short length, and because its generally hydrophobic sequence may enable it to function equally well in D, making it nondegradable.

Our lab has also considered multimerization as a strategy for PK-enhancement. As mentioned previously, globular proteins are efficiently filtered by the kidney until they exceed ~70 kDa in size. Each PIE12 peptide is ~2 kDa, and each PIE12-trimer is ~7 kDa. To approach 70 kDa of molecular weight, strings of monomers or trimers could be linked together through any number of possible geometries. PEG linkers with multiple reactive groups are readily available, although their polydispersity may complicate studies that utilize them. Alternatively, multimerization could be achieved using controlled linkages, such as poly-Lys or poly(Lys-Gly-Gly) peptide scaffolds.

Depots and Drug Formulation

Depots are an attractive and validated PK-enhancing strategy that slowly releases compounds over a prolonged period of time, reducing clearance, increasing drug exposure, and prolonging the time between doses. For example, in the GLP-1 analog field, Byetta (exenatide) exhibits a 2.4 hour terminal half-life (SC) and must be administered twice per day, while Victoza (liraglutide) is a PK-enhanced acylated homologue with an improved terminal half-life of 13 hours (SC) that allows for once-daily subcutaneous administration[41,42]. However, even without the aid of PK-enhancing conjugations, Alkermes has co-developed Bydureon (extended release exenatide) utilizing their biodegradable depot formulation (50:50 poly(D,L-lactide-co-glycolide) polymer and sucrose), enabling an impressive once-weekly subcutaneous administration. It is likely that PK-enhancing conjugations (e.g., acylation or cholesterol conjugation) would be readily compatible with extended release depot formulations resulting in additive PK improvements.

Furthermore, drug formulation technology provides another means for improving half-life and bioavailability. Cyclosporine is a classic example of peptide drug formulation where excipients enabled ~30% oral bioavailability[43,44], although its success has not proven general for most peptides. Instead, a relatively new field has emerged that utilizes gut permeabilizers and protease inhibitors to improve the oral bioavailability of peptides. Gut permeability enhancers transiently reduce tight-junctions in the GI tract, allowing peptides to be absorbed paracellularly[45,46]. A primary concern with these agents is the potential for bacterial transmission into the bloodstream. For this reason, Unigene's technology is perhaps the most promising; using a gentle and naturally occurring gut permeabilizer common in goat milk (acylated carnitine), peptides can become absorbed in the duodenum immediately following stomach evacuation, a relatively microbe-free environment[47,48]. Other permeabilizing agents have been extensively reviewed[45,46].

Analytical Assay Development

As we prepared for investigational new drug (IND)-enabling studies involving pharmacokinetics and toxicity, it was apparent that we would need a robust quantitative assay for plasma and tissue samples. Pilot PK and toxicity studies are required to rank and select PIE12-trimer conjugates for advancement to expensive IND-enabling preclinical studies. Our original approach was to develop an assay that could accommodate a variety of PIE12 candidates, independent of what we had conjugated to them (i.e., an assay based on function/binding events). Further, we had hoped to develop a "homogenous" assay that required little or no sample preparation. We wanted an assay

where the addition of a few reagents to a sample could produce a detectable readout. We initially explored fluorescence-based assays like FRET and ELISA that have extraordinary sensitivity, with lower-limits of detection often below 10 nM.

Unfortunately, we encountered a variety of unanticipated barriers, some of which were insurmountable. The key problem was that unknown plasma component(s) interfered with our fluorescent assays and could not be removed. The interference also varied from animal to animal, preventing our ability to predict or account for it. Details and ideas for future troubleshooting are discussed in the Appendix. Given these problems, we developed an LC/MS/MS bioanalytical assay. Method development for each of our conjugates has been straightforward, allowing us to achieve lower-limits-of-detection below 10 nM. The PK studies conducted in Chapter 5 utilize this assay.

It is helpful to discuss briefly some basic principles behind a triple-quad mass spectrometer and the general MRM (Multiple Reaction Monitoring) method (Fig. 1-5). The triple-quad is comprised of three quadrupoles dubbed Q1, Q2, and Q3. Each quadrupole functions independently such that each can be set to allow only a chosen set of molecular weight/charge ratios to pass. Preceding Q1 is the source, which ionizes molecules that pass through it. Peptides usually pick up multiple charges in the source (e.g., each PIE12 prefers a +2 charge state, though +3 is also produced). Q1 then filters the influx to allow only selected parent ions to pass. The molecular weight range that is selected for Q1 is based on mass (m) per charge (z) ratios. The Q1-selected m/z parent(s) then enter Q2. Q2 is filled with a collision gas that breaks the parent ion into fragments, termed daughter ions, while Q3 is set to capture selected daughter ions. The MRM method utilizes all three quadrupoles; Q1 to select for a parent mass, Q2 to break the

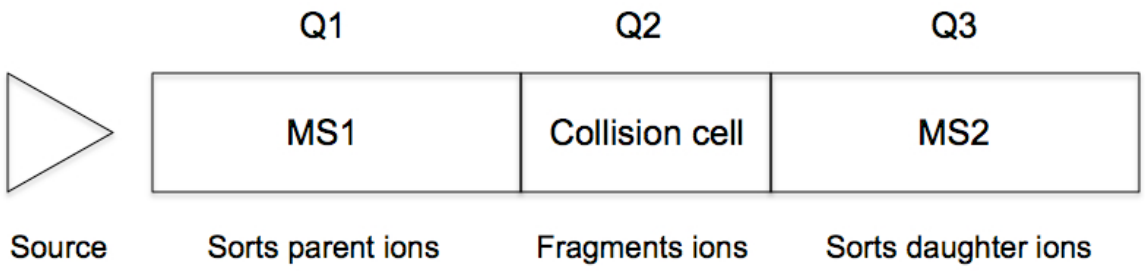

Figure 1-5. General Function of an LC/MS/MS Triple-Quad Mass Spectrometer. A source sends ionized particles into the first quadrupole Q1. One or more specified m/z ions are selected in Q1 and passed into Q2 where these parent ions collide with gas to produce daughter ion fragments. Q3 passes selected daughter ions to the detector. An MRM method monitors the number of counts produced by a pair of selected parent/daughter ions.

parent into fragments, and Q3 to select for a daughter mass. Notably, the process of breaking a parent ion and selecting a daughter ion reduces sensitivity by ~10-fold, but the signal-to-noise ratio improves dramatically, making the MRM method ideal for removing potentially confounding signals (e.g., from plasma samples). In general, triple-quads are considered "unit" resolution instruments (i.e., 1 m/z resolution).

FDA Approval Considerations

Precedent is an obvious benefit when pursuing FDA approval. As such, it is worth mentioning two IND's that have been filed for full-D peptide therapeutics. Genzyme's orally-administered Delmitide (NH2-D-Arg-D-Nle-D-Nle-D-Nle-D-Arg-D-Nle-D-Nle-D-Nle-D-Gly-D-Tyr-CONH2)[49,50], currently under investigation for ulcerative colitis, and Allelix's IV-administered CXCR4 inhibitor ALX40-4C (N-acetyl-nona-D-arginine amide)[51] have both been tested and found to be well tolerated in human trials. These precedents reduce concerns over a possible generalized innate toxicity from D-peptides.

Summary

Chapter 2 reviews the peptide therapeutics field with special emphasis on utilizing protease-resistant design for the discovery of HIV inhibitors. Chapter 3 describes how mirror-image phage display and structure-assisted design were utilized in the discovery of PIE12. Early oligomerization efforts are also described. Chapter 4 recounts the development of our powerful scaffold-based design for rapid synthesis of PIE12-trimer with membrane-tethering cargoes. PK-enhancing designs and related PK studies are portrayed in Chapter 5. Studies underway and immediately pending are discussed in the future directions in Chapter 6. Finally, efforts and lessons involving development of a FRET and ELISA bioanalytical assay are illustrated in the Appendix.

References

1 Cooper, D. A., R. T. Steigbigel, J. M. Gatell, J. K. Rockstroh, C. Katlama, P. Yeni, A. Lazzarin, B. Clotet, P. N. Kumar, J. R. Eron, M. Schechter, M. Markowitz, M. R. Loutfy, J. L. Lennox, J. Zhao, J. Chen, D. M. Ryan, R. R. Rhodes, J. A. Killar, L. R. Gilde, K. M. Strohmaier, A. R. Meibohm, M. D. Miller, D. J. Hazuda, M. L. Nessly, M. J. DiNubile, R. D. Isaacs, H. Teppler, B. Y. Nguyen, and BENCHMRK Study Teams. Subgroup and resistance analysis of raltegravir for resistant HIV-1 infection. *New England Journal of Medicine* **359**, 355-365 (2008).

2 Welch, B. D., Andrew P. VanDemark, Annie Heroux, Christopher P. Hill, and Michael S. Kay. Potent D-peptide inhibitors of HIV-1 entry. *Proceedings of the National Academy of Sciences* **104**, 16828-16833 (2007).

3 Mild, M., Joakim Esbjornsson, Eva Maria Fenyo, Patrik Medstrand. Frequent intrapatient recombination between human immunodeficiency virus type 1 R5 and X4 envelopes: implications for coreceptor switch. *Journal of Virology* **81**, 3369-3376 (2007).

4 Steger, H. K., Michael J. Root. Kinetic dependence to HIV-1 entry inhibition. *Journal of Biological Chemistry* **281**, 25813-25821 (Sept. 2006).

5 Welch, B. D., J. Nicholas Francis, Joseph S. Redman, Suparna Paul, Matthew T. Weinstock, Jacqueline D. Reeves, Yolanda S. Lie, Frank G. Whitby, Debra M. Eckert, Christopher P. Hill, Michael J. Root, and Michael S. Kay. Design of a potent D-peptide HIV-1 entry inhibitor with a strong barrier to resistance. *Journal of Virology* **84**, 11235-11244 (Nov. 2010).

6 Wild, C. T., Diane C. Shugars, Teresa K. Greenwell, Charlene B. McDanal, Thomas J. Matthews. Peptides corresponding to a predictive alpha-helical domain of human immunodeficiency virus type 1 gp41 are potent inhibitors of virus infection. *Proc Natl Acad Sci* **91**, 9770-9774 (1994).

7 Luo, C., K. Wang , Liu de Q, Y. Li, Q. S. Zhao. The functional roles of lipid rafts in T cell activation, immune diseases and HIV infection and prevention. *Cellular & Molecular Immunology* **5**, 1-7 (2008).

8 Waheed, A. A., and E. O. Freed. The role of lipids in retrovirus replication. *Viruses* **2**, 1146-1180 (2010).

9 Francis, J. N., Joseph S. Redman, Debra M. Eckert, and Michael S. Kay. Design of a modular tetrameric scaffold for the synthesis of membrane-localized D-peptide inhibitors of HIV-1 entry. *Bioconjugate Chemistry* (2012).

10 Uchil, P. D., and Walther Mothes. HIV entry revisited. *Cell* **137**, 402-404 (2009).

11 Chan, D. C., Christine T. Chutkowski, Peter S. Kim. Evidence that a prominent cavity in the coiled coil of HIV type 1 gp41 is an attractive drug target. *Proc. Natl. Acad. Sci. USA* **95**, 15613-15617 (1998).

12 Malim, M. H., L. S. Tiley, D. F. McCarn, J. R. Rusche, J. Hauber, B. R. Cullen. HIV-1 structural gene expression requires binding of the rev trans-activator to its RNA target sequence. *Cell* **60**, 675-683 (1990).

13 Bartel, D. P., Maria L. Zapp, Michael R. Green, Jack W. Szostak. HIV-1 rev regulation involves recognition of non-Watson-Crick base pairs in viral RNA. *Cell* **67**, 529-536 (1991).

14 FDA. Guidance for industry; biosimilars: questions and answers regarding implementation of the biologics price competition and innovation act of 2009. 1-18 (Feb 2012).

15 Brzezinski, M. R., B. J. Spink, R. A. Dean, C. E. Berkman, J. R. Cashman, W. F. Bosron. Humer liver carboxylesterase hCE-1: binding specificity for cocaine, heroin, and their metabolites and analogs. *Drug Metab Dispos.* **25**, 1089-1096 (1997).

16 Huang, H., C. D. Fleming, K. Nishi, M. R. Redinbo, B. D. Hammock. Stereoselective hydrolysis of pyrethoid-like fluorescent substrates by human and other mammalian liver carboxylesterases. *Chem Res Toxicol* **18**, 1381-1377 (2005).

17 Barbas, C. F., Dennis R Burton, Gregg J Silverman. *Phage Display: A Laboratory Manual*. (Cold Springs Harber Laboratory Press, 2001).

18 Schumacher, T., LM Mayr, DL Minor, MA Milhollen, MW Burgess, PS Kim. Identification of D-peptide ligands through mirror-image phage display. *Science* **271**, 1854-1857 (1996).

19 McGregor, D. P. Discovering and improving novel peptide therapeutics. *Current Opinion in Pharmacology* **8**, 616-619 (2008).

20 Pierce, T. S. Antibody Production and Purification Technical Handbook; Version 2. p. 5 (2010).

21 Yamaoka, T., Yasuhiko Tabata, and Yoshito Ikada. Distribution and tissue uptake of poly(ethylene glycol) with different molecular weights after intravenous administration to mice. *Journal of Pharmaceutical Sciences* **83**, 601-606 (1994).

22 Besheer, A., T. C. Hertel, J. Kressler, K. Mader, M. Pietzsch. Enzymatically catalyzed conjugation of a biodegradable polymer to proteins and small molecules using microbial transglutaminase. *Methods Mol Biol.* **751**, 17-27 (2011).

23 Spector, A. A. Fatty acid binding to plasma albumin. *Journal of Lipid Research* **16**, 165-179 (1975).

24 Richieri, G. V., Alberto Anel, and Alan M. Kleinfeld. Interactions of long-chain fatty acids and albumin: determination of free fatty acid levels using the fluorescent probe ADIFAB. *Biochemistry* **32**, 7574-7580 (1993).

25 Richieri, G. V., and Alan M. Kleinfeld. Unbound free fatty acid levels in human serum. *Journal of Lipid Research* **36**, 229-240 (1995).

26 Nguyen, A., Arthur E. Reyes II, Min Zhang, Paul McDonald, Wai Lee T. Wong, Lisa A. Damico and Mark S. Dennis. The pharmacokinetics of an albumin-binding Fab (AB.Fab) can be modulated as a function of affinity for albumin. *Protein Engineering, Design & Selection* **19**, 291-297 (2006).

27 Charbonneau, D. M., and Heider-Ali Tajmir-Riahi. Study on the interaction of cationic lipids with bovine serum albumin. *The Journal of Physical Chemistry B* **114**, 1148-1155 (2010).

28 Peng, L., He Minbo, Chen Fang, Li Xi and Zhang Chaocan. The interaction between cholesterol and human serum albumin. *Protein & Peptide Letters* **15**, 360-364 (2008).

29 Ingallinella, P., Elisabetta Bianchi, Neal A. Ladwa, Ying-Jie Wang, Renee Hrin, Maria Veneziano, Fabio Bonelli, Thomas J. Ketas, John P. Morre, Michael D. Miller, and Antonello Pessi. Addition of a cholesterol group to an HIV-1 peptide fusion inhibitor dramatically increases its antiviral potency. *Proceedings of the National Academy of Sciences* **106**, 5801-5806 (April 2009).

30 Dennis, M. S., Min Zhang, Y. Gloria Meng, Miryam Kadkodayan, Daniel Kirchhofer, Dam Combs, Lisa A. Damico. Albumin binding as a general strategy for improving the pharmacokinetics of proteins. *Journal of Biological Chemistry* **277**, 35035-35043 (2002).

31 Sato, A. K., D. J. Sexton, L. A. Morganelli, E. H. Cohen, Q. L. Wu, G. P. Conley, Z. Streltsova, S. W. Lee, M. Devlin, D. B. DeOliveira, J. Enright, R. B. Kent, C. R. Wescott, T. C. Ransohoff, A. C. Ley, R. C. Ladner. Development of mammalian serum albumin affinity purification media by peptide phage display. *Biotechnol Prog.* **18**, 182-192 (2002).

32 Jonsson, A., Jakob Dogan, Nina Herne, Lars Abrahmsen, Per-Ake Nygren. Engineering of a femtomolar affinity binding protein to human serum albumin. *Protein Eng Des Sel.* **21**, 515-527 (2008).

33 Trussel, S., Christoph Dumelin, Katharina Frey, Alessandra Villa, Fabian Buller, Dario Neri. New strategy for the extension of the serum half-life of antibody fragments. *Bioconjugate Chem.* **20**, 2286-2292 (2009).

34 Meulenbroek, A. J. in *Human IgG subclasses: useful diagnostic markers for immunocompetence; Third Edition* (ed Sanquin) (Sanquin, Amsterdam, The Netherlands, 2008).

35 Kratz, F., A. Warnecke, K. Scheuermann, C. Stockmar, J. Schwab, P. Lazar, P. Druckes, N. Esser, J. Drevs, D. Rognan, C. Bissantz, C. Hindergling, G. Folkers, I. Fichtner, C. Unger. Probing the cysteine-34 position of endogenous serum albumin with thiol-binding doxorubicin derivatives. Improved efficacy of an acid-sensitive doxorubicin derivative with specific albumin-binding properties compared to that of the parent compound. *J. Med. Chem.* **45**, 5523-5533 (2002).

36 Subramanian, G. M., M. Fiscella, A. Lamouse-Smith, S. Zeuzem, J. G. McHutchison. Albinterferon alpha-2b: a genetic fusion protein for the treatment of chronic hepatitis C. *Nat Biotechnol.* **25**, 1411-1419 (2007).

37 Lao, B. J., Daniel T. Kamei. Improving therapeutic properties of protein drugs through alteration of intracellular trafficking pathways. *Biotechnol. Prog.* **24**, 2-7 (2008).

38 Bitonti, A. J., J. A. Dumont. Pulmonary administration of therapeutic proteins using an immunoglobulin transport pathway. *Adv Drug Deliv Rev.* **58**, 1106-1118 (2006).

39 Beck, A., Thierry Wurch, Christian Bailly, Nathalie Corvaia. Strategies and challenges for the next generation of therapeutic antibodies. *Nat Rev Immunol.* **10**, 345-352 (2010).

40 Pan, C., Shuwen Liu, Shibo Jiang. HIV-1 gp41 fusion intermediate: a target for HIV therapeutics. *J Formos Med Assoc.* **109**, 94-105 (2010).

41 Pharmaceuticals, A. 1-30 (Amylin Pharmaceuticals, http://byetta.com, 2011).

42 Nordisk, N. 1-12 (Novo Nordisk, http://www.victozaPro.com, 2012).

43 Tan, K. K., A. K. Trull, J. A. Uttridge, J. Wallwork. Relative bioavailability of cyclosporin from conventional and microemulsion formulations in heart-lung transplant candidates with cystic fibrosis. *Eur J Clin Pharmacol.* **48**, 285-289 (1995).

44 Drewe, J., Christoph Beglinger, Thomas Kissel. The absorption site of cyclosporin in the human gastrointestinal tract. *Br. J. clin. Pharmac.* **33**, 39-43 (1992).

45 Park, K., Ick Chan Kwon, Kinam Park. Oral protein delivery: current status and future prospect. *Reactive & Functional Polymers* **71**, 280-287 (2011).

46 Peppas, N. A., Nikhil J. Kavimandan. Nanoscale analysis of protein and peptide absorption: insulin absorption using complexation and pH-sensitive hydrogels as delivery vehicles. *Eur J Pharm Sci.* **29**, 183-197 (2006).

47 Unigene Laboratories, I. *Proprietary Delivery Technologies*, <http://www.unigene.com/proprietary-delivery-technologies> (2012).

48 Weinstock, L. B. Gastroenterology Board Review Manual; small intestinal bacterial overgrowth. *Hospital Physician* **14**, 2-12 (2008).

49 Travis, S., Lee Min Yap, Chris Hawkey, Bryan Warren, Mirella Lazarov, Tim Fong, R. J. Tesi, and RDP Investigators Study Group. RDP58 is a novel and potentially effective oral therapy for ulcerative colitis. *Inflamm Bowel Dis* **11**, 713-719 (2005).

50 Stevenson, C. L. Advances in peptide pharmaceuticals. *Curr Pharm Biotechnol.* **10**, 122-137 (2009).

51 Doranz, B. J., Lionel G. Filion, Francisco Diaz-Mitoma, Daniel S. Sitar, Jan Sahai, Frederic Baribaud, Michael J. Orsini, Jeffrey L. Benovic, William Cameron, Robert W. Doms. Safe use of the CXCR4 inhibitor ALX40-4C in humans. *AIDS Res Hum Retroviruses* **17**, 475-486 (2006).

CHAPTER 2

PROTEASE-RESISTANT PEPTIDE DESIGN – EMPOWERING NATURE'S FRAGILE WARRIORS AGAINST HIV

Reproduced with permission from Matthew T. Weinstock, J. Nicholas Francis, Joseph S. Redman, and Michael S. Kay. "Protease-Resistant Peptide Design – Empowering Nature's Fragile Warriors." Biopolymers: Peptide Science; Epub. ahead of print 4th April 2012; DOI: 10.1002/bip.22073

Invited Review
Protease-Resistant Peptide Design—Empowering Nature's Fragile Warriors Against HIV

Matthew T. Weinstock, J. Nicholas Francis, Joseph S. Redman, Michael S. Kay
Department of Biochemistry, University of Utah School of Medicine, Salt Lake City, UT 84112-5650

Received 23 December 2011; revised 5 March 2012; accepted 4 April 2012
Published online 14 April 2012 in Wiley Online Library (wileyonlinelibrary.com). DOI 10.1002/bip.22073

ABSTRACT:

Peptides have great potential as therapeutic agents, but their use is often limited by susceptibility to proteolysis and their resulting in vivo *fragility. In this review, we focus on peptidomimetic approaches to produce protease-resistant peptides with the potential for greatly improved clinical utility. We focus on the use of mirror-image (D-peptide) and ß-peptides as two leading approaches with distinct design principles and challenges. Application to the important and difficult problem of inhibiting HIV entry illustrates the current state-of-the-art in peptidomimetic technologies. We also summarize future directions for this field and highlight remaining obstacles to widespread use of protease-resistant peptides. © 2012 Wiley Periodicals, Inc. Biopolymers (Pept Sci) 98: 431–442, 2012.*

Keywords: peptidomimetics; HIV entry; peptide design

This article was originally published online as an accepted preprint. The "Published Online" date corresponds to the preprint version. You can request a copy of the preprint by emailing the Biopolymers editorial office at biopolymers@wiley. com

Correspondence to: Michael S. Kay, Department of Biochemistry, University of Utah School of Medicine, 15 N Medical Drive East Rm 4100, Salt Lake City, UT 84112-5650, USA; e-mail: kay@biochem.utah.edu
Matthew T. Weinstock and J. Nicholas Francis contributed equally to this work.
Contract grant sponsor: NIH (to M.S.K.)
Contract grant number: AI076168
Contract grant sponsor: NIH Microbial Pathogenesis Predoctoral Training Grant (to J.N.F.)
Contract grant number: AI055434

INTRODUCTION

In drug discovery and development, peptide therapeutics have many advantages. Their polymeric nature makes synthesis straightforward, especially when compared with the synthetic schemes typically utilized for small molecules. Peptides are generally easier and less expensive to produce than recombinant proteins. Peptide therapeutics can also be more specific (and less toxic) than small molecules and excel at the challenging problem of disrupting large protein–protein interaction interfaces (i.e., "undruggable" targets). Due to advancements in genomics and proteomics, a plethora of natural peptide ligand sequences for important drug targets are available and provide a sensible starting point for the rational development of therapeutic compounds. In addition, a host of mature and emerging library-based screening techniques provides a means to rapidly discover novel peptide sequences with specific binding properties.

Despite these enticing advantages, a major problem limiting development of peptide therapeutics is their proteolytic sensitivity and associated delivery challenges. Synthetic therapeutic peptides are typically relatively unstructured and are therefore rapidly degraded *in vivo*, often with half-lives on the order of minutes.[1] Proteolysis commonly occurs in the GI lumen, intestinal brush border, enterocytes, hepatocytes, antigen-presenting cells, and plasma. Because of this *in vivo* fragility, oral delivery is generally not possible, necessitating frequent dosing by injection. Even when delivered parenterally, degradation in the blood combined with rapid renal filtration often results in drugs that are expensive, inconvenient, and unpleasant to administer.

Protease-resistant peptides would address many of these limitations. One of the most promising approaches is to modify the chemical structure of the peptide backbone (peptidomimetics).[2] Modifications that have been shown to substantially decrease proteolysis include N-methylation, ester

linkages (α-hydroxy acids), insertion of additional methylene groups into the backbone (β-amino acids, γ-amino acids etc.), and the use of D-amino acids. More significant changes to the peptide backbone include peptoids, azapeptides, oligoureas, arylamides, and oligohydrazides.[2–4]

In this review, we describe how modified peptide backbones can be used to design protease-resistant inhibitors with a special focus on the high-priority problem of designing protease-resistant HIV entry inhibitors. Although these modified backbones effectively address protease sensitivity, each is associated with a set of design challenges using rational design or library screening techniques. This review will not cover traditional strategies to reduce protease sensitivity, e.g., peptide capping, sequence alteration at susceptible sites, cyclization, or stapling, which have been extensively reviewed elsewhere.[5]

INHIBITING HIV ENTRY

An estimated 34 million people worldwide are infected with HIV, the causative agent of AIDS, resulting in nearly 2 million deaths per year and over 25 million cumulative deaths (UNAIDS). Dramatic progress has been made in reducing mortality since the inception of antiretroviral therapy against HIV enzymes reverse transcriptase, protease, and recently integrase. However, the relentless development of drug resistance necessitates ongoing development of therapeutics that target other stages in the viral lifecycle. In particular, there have been extensive efforts to develop potent, broadly active, and economical entry inhibitors for the prevention and treatment of HIV/AIDS.[6]

The current HIV entry pathway model is shown in Figure 1. Viral entry into host cells is mediated by the trimeric HIV envelope (Env) glycoprotein. Env contains the noncovalently associated surface gp120 and transmembrane gp41 subunits. gp120's primary function is to interact with cell receptors that mark HIV's preferred target cells (e.g., T-cells and macrophages), while gp41 induces membrane fusion. Host cell interactions are mediated by gp120 through association with the primary cell receptor (CD4) and chemokine coreceptor (either CXCR4 or CCR5, depending on viral tropism). Upon gp120 engagement with cell receptors, a complex series of structural rearrangements in gp120 propagate to gp41, activating it for membrane fusion (reviewed by Ref. 7). At this stage, gp41 forms an extended prehairpin intermediate containing an N-terminal trimeric coiled coil (N-trimer) and C-terminal region (C-peptides) of unknown structure. Fusion is driven by collapse of this intermediate as three helical C-peptides pack anti-parallel to the N-trimer (trimer-of-hairpins formation), drawing the viral and host cell membranes into close proximity.

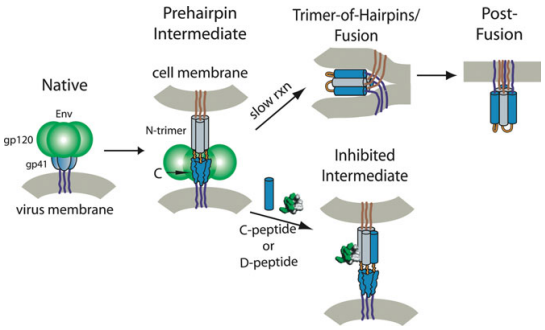

FIGURE 1 HIV entry pathway. HIV Env is composed of surface (gp120, green) and transmembrane (gp41, blue) subunits. Fusion is initiated by binding to CD4 and a chemokine coreceptor, which activates gp41 and induces formation of the prehairpin intermediate. In this intermediate, the gp41 N-terminal region forms a trimeric coiled coil (N-trimer, gray), which is separated from the C-peptide region (dark blue). This intermediate slowly collapses to form a trimer-of-hairpins structure that brings the viral and cell membranes into close apposition, leading to fusion. C-peptide and D-peptide inhibitors bind to the N-trimer, preventing trimer-of-hairpins formation and membrane fusion.

A similar fusion mechanism is utilized by many other enveloped viruses, including influenza, Ebola, and paramyxoviruses.[7]

C-Peptide Inhibitors

This mechanism suggests that peptides derived from the N- and C-peptide regions of gp41 could prevent viral membrane fusion in a dominant-negative manner by preventing trimer-of-hairpins formation. Indeed, both N-and C-peptides inhibit HIV entry.[8–14] The N-trimer/C-peptide interaction is predominantly mediated by conserved interactions between the hydrophobic face of helical C-peptides and a hydrophobic groove formed between helices in the N-trimer. C-peptide inhibitors are more promising drug candidates because of their higher potency and better solubility compared with N-peptide inhibitors.

C-peptide inhibitors were first identified through screens of gp41-derived peptides.[9,11] Fuzeon (Enfuvirtide, T-20) is a 36 amino acid L-peptide taken from the gp41 C-peptide region. Fuzeon inhibits HIV entry with nM potency and reduces viral loads by 2 logs,[15] leading to its approval as the first HIV entry inhibitor in 2003. Unfortunately, Fuzeon's clinical use has been limited by its short half-life. Fuzeon requires injection at very high doses (90 mg, twice daily) to overcome its proteolysis and rapid renal filtration. These practical problems result in a drug that is expensive (~$30,000 per year), can cause painful injection site reactions, and is only approved for patients experiencing treat-

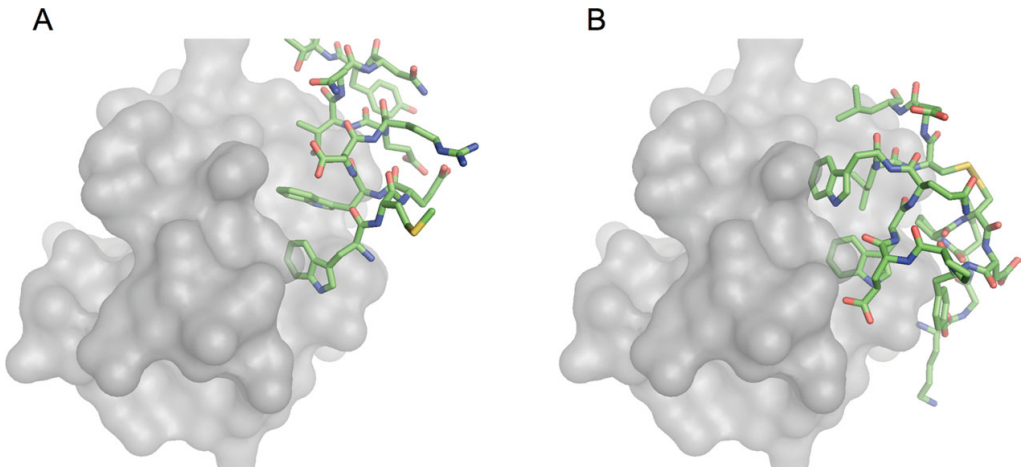

FIGURE 2 One pocket, two binding solutions. The gp41 pocket (from pdb code 3L35) is shown with (A) the natural gp41 C-peptide (pdb code 1AIK) and (B) D-peptide PIE12 (pdb code 3L35). Structures were aligned on the 17 pocket-forming residues from gp41 and rendered using Pymol.

ment failure due to multi-drug resistance ("salvage therapy"). Fuzeon's high dosing requirements and *in vivo* fragility also limit options for less frequent dosing via depot formulation.

The gp41 "Pocket" Region

At the N-trimer's C-terminus lie three symmetry-related deep hydrophobic pockets. Each pocket has a volume of $\sim$400 Å^3 that is filled primarily by three C-peptide residues (Trp628, Trp631, and Ile635)[16,17] (Figure 2). The pocket is a promising inhibitory target because of its critical importance in membrane fusion and very high level of conservation across diverse HIV strains.[16,18] Mutations in the pocket are often not well tolerated due to the requirement for compensatory mutations in the C-peptide region to restore binding. In addition, the pocket region is encoded by the structured RNA region of the Rev-responsive element (RRE), which contains a signal critical for nuclear export of viral RNA.[18] Interestingly, extensive efforts by numerous groups to discover small molecule pocket-binding inhibitors have had limited success, generally producing inhibitors with modest potency and/or significant toxicity.[19–23] Based on this body of work, the gp41 pocket appears to be "undruggable" by small molecule inhibitors, a common problem for extended protein–protein interaction interfaces.

Fuzeon was discovered before the gp41 6-helix bundle crystal structure and does not bind to the gp41 pocket. However, next generation C-peptide inhibitors (e.g., C34, T-1249) do include pocket-binding residues and enjoy superior potencies and resistance profiles.[24–26] The follow-on compound to Fuzeon, T-1249, performed very well in clinical trials, but was not developed further due to unspecified formulation problems, which we speculate includes challenges in the economic synthesis of this 39-residue peptide and a requirement for four 1 mL injections, once per day, as used in a phase I/II trial.[25]

Fuzeon and T-1249 show that a peptide fusion inhibitor can be very effective against HIV, but the impact of such drugs will be limited until the problems of short half-life and high dosing (and the resulting high cost) can be overcome. In this review, we focus on two distinct strategies that have yielded promising protease-resistant peptide fusion inhibitors with the potential to overcome Fuzeon's *in vivo* fragility.

RATIONAL DRUG DESIGN WITH MODIFIED PEPTIDE BACKBONES

While there is much interest in the *de novo* development of peptides with defined structural and functional characteristics, this work is hampered by limitations in currently available modeling strategies. Thus, as illustrated below, most successful rational designs of protease-resistant peptides start from sequence and structural information from existing peptide ligands.

In the realm of rational design of modified peptide therapeutics, β-peptides and mixed α/β-peptides are among the most promising. β-peptides are composed of β-amino acids, which contain an extra backbone methylene group (between

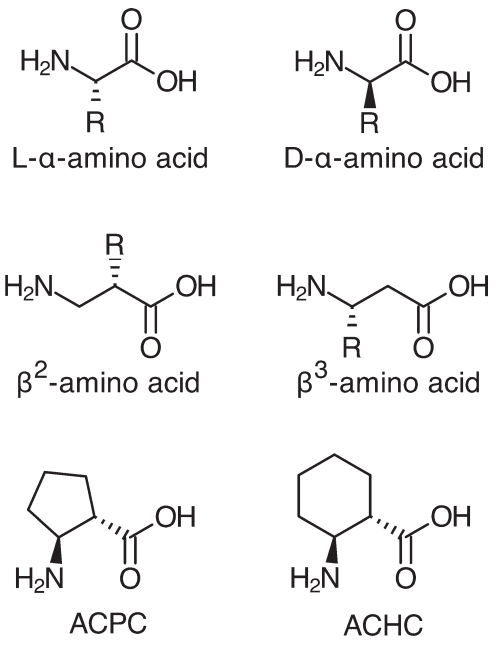

FIGURE 3 Peptidomimetic structures.

the amino and α-carbon, specified as a β^2-amino acid, or between the carboxylate and α-carbon, specified as a β^3-amino acid) (Figure 3). Short β-peptide sequences can adopt robust secondary structures analogous to α-helices formed by α-amino acids. If a natural helical peptide ligand is known, a β-peptide mimic can be generated by the precise placement in three dimensions of key side chains onto a β-peptide scaffold. Two β-peptide scaffolds that have been extensively utilized are the 12-helix and 14-helix, named after the number of atoms between hydrogen bonding groups (these and other β-residue-containing scaffolds are reviewed elsewhere[3,27–30]). The specific structural motif adopted by a particular β-peptide is dictated by the nature of the substituent β-amino acids.[31] β-peptides composed of monosubstituted, acyclic β-amino acids or cyclic six-member ring β-amino acids preferentially adopt the 14-helix structure, while the 12-helix structure is favored by peptides composed of cyclic five-member ring β-amino acids. The helical parameters of the 12- and 14-helices are discussed and compared with α-helices in Refs. 27 and 31.

In a 14-helix composed of β^3-amino acids, side chains at residues *i*, *i*+3, and *i*+6 are presented along the same face of the helix, and are reasonably superimposable with side chains at residues *i*, *i*+4, and *i*+7 of an α-helix.[32] This property can be exploited to display epitopes that mimic an α-helical face and has been applied to the development of low-mid μM HIV entry inhibitors that bind to the gp41 pocket region.[33,34] In an analogous approach, β-peptide inhibitors of HCMV entry were developed using the 12-helix scaffold.[35] To map an α-helix epitope onto the 12-helix, side chains at positions *i*, *i*+4, and *i*+7 on the α-helix are placed at positions *i*, *i*+3, and *i*+5 on the 12-helix. Although acyclic residues diminish 12-helix propensity, they provide the easiest avenue for side chain attachment, so a minimum number of acyclic β^2 or β^3 residues were introduced into the structure at specific points to mimic side chain presentation of the native α-helix. This approach enabled the rapid discovery of inhibitors with modest potency, but its main challenge is the lack of a route forward, by rational design or high-throughput screening, to optimize these initial hits.

A sequence-based approach utilizing mixed α/β-peptides has been applied to develop an HIV entry inhibitor that structurally and functionally mimics C-peptides (~10 turn α-helix).[36] In this approach, a subset of C-peptide residues were strategically replaced with homologous β^3-amino acids following an ααβααβ pattern, which, despite the additional methylene units, does not significantly alter secondary structure of the helix.[37] On folding, this pattern generates an α-helix-like conformation with a β-residue stripe that runs down the side of the helix distal to the interaction surface, minimizing disruption of the binding interface. On replacing 11 of the 38 residues with β^3-amino acids, the resulting α/β-peptide had >10,000-fold diminished affinity for its binding target relative to the α-peptide counterpart.

As a second step in the design, specific β^3-residues were replaced by cyclic β-residue homologues. The cyclic residues were incorporated to reduce the entropic penalty associated with helix formation due to the inherent torsional flexibility of β^3-residues. β^3 analogues of alanine in the α/β-peptide were replaced with a nonpolar, five-member ring constrained β-residue (ACPC), while β^3 analogues of arginine were replaced with a polar, heterocyclic analogue of ACPC (APC). These replacements improved affinity by ~400-fold over the peptide with acyclic residues. Although the binding affinity never recovers to that of the original α-peptide ligand, the resulting α/β-peptide was nearly as potent as the α-peptide, but with the added advantage of being 280-fold more resistant to proteolytic degradation by proteinase K. The apparent discrepancy of having diminished binding affinity, yet α-peptide-like potency is likely due to the potency plateau observed for many HIV entry inhibitors (see the discussion of the "resistance capacitor" below).

The original report indicated that the N-terminal Trp-Trp-Ile motif of the α/β-peptide does not engage the C-terminal hydrophobic pocket of gp41, but subsequent crystallographic analysis indicated that that the pocket-binding motif

on the α/β-peptide is indeed able to engage the pocket. The authors suggest that the lack of engagement in the original structure was an artifact caused by crystal packing, and that the newer structure more faithfully portrays the binding of the α/β-peptide (see discussion in supplementary materials of Ref. 38).

GENETICALLY ENCODED LIBRARY-BASED SCREENS

An alternative to rational design is screening of random peptide libraries. These high-throughput methods identify novel peptides with a desired function (typically binding to an immobilized target). Commonly used screening techniques include phage, ribosome, and mRNA display, but these methods all rely on cellular translation machinery and are therefore not yet fully compatible with peptidomimetics in their standard forms. Though there have been many advances and refinements in the field of synthetic peptidomimetic library generation (e.g., split and pool synthesis, physically addressable synthesis by photolithography), these synthetic libraries are typically limited to $<10^6$ members[39] compared with the billion to trillion member libraries that can be generated with genetically encoded libraries.

D-Peptides

D-peptides are entirely composed of D-amino acids, which are mirror-image stereoisomers of the L-amino acids found in naturally occurring L-peptides. D-Peptides are a promising therapeutic platform because they are highly resistant to natural proteases.[40] In elegant work by the Kent group,[41] D-HIV protease was shown to cleave only D-peptide substrates, showing that proteases exhibit highly stereospecific substrate discrimination.

The symmetry relationship between L- and D-peptides can be exploited in mirror-image display techniques[42] in which a mirror-image version of the target molecule is generated by solid-phase synthesis using D-amino acids. Randomized genetically encoded L-peptide libraries are then screened against this D-target. The winning L-peptides are identified by DNA sequencing and then the corresponding D-peptides are synthesized. By symmetry, the D-peptide will have the same activity toward the natural L-target as the L-peptide had against the mirror-image D-target (Figure 4).

A major limitation of mirror-image display is the requirement for chemical synthesis of the D-target. Synthesis of D-peptides is currently done using traditional solid phase peptide synthesis (SPPS).[43] Routine use of SPPS chemistries for the production of peptides is limited to ~50 residues,

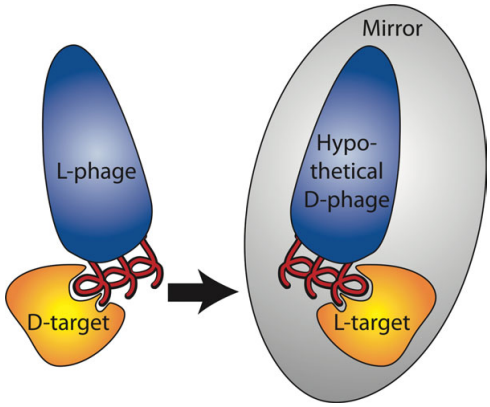

FIGURE 4 Mirror-image phage display. Phage bearing L-peptides are panned against a mirror-image protein (D-target). By symmetry, D-versions of binding peptides will bind to the natural L-targets.

though this limit varies widely depending on the required purity and sequence/structure properties of the peptide in question (e.g., extended beta-strand peptides can aggregate during SPPS). Despite these challenges, syntheses of very long peptides have been reported (e.g., the synthesis of the 140-residue IL-3 protein[44]).

Larger D-peptide targets can be obtained using peptide ligation techniques to link multiple synthesized peptide fragments. A variety of ligation chemistries have been developed (see Ref. 45 for a very thorough review), but the most common technique is cysteine-mediated native chemical ligation (NCL). NCL requires the presence of an N-terminal cysteine on one peptide fragment and a C-terminal thioester on the other (see Ref. 46 for a summary of popular recombinant and synthetic methods for the generation of peptides bearing a C-terminal thioester) and results in the ligation of the two segments via a native peptide bond. SPPS of thioester-containing peptides has traditionally been carried out via Boc chemistry, but recent advances have enabled the robust synthesis of thioesters using the easier and more popular Fmoc chemistry[47] and commercially available Dawson Dbz resin (Novabiochem). Other means of accessing peptide thioesters via Fmoc chemistry have been recently reviewed.[48]

By strategically utilizing masked N-terminal cysteines (e.g., thioproline), multiple peptide fragments can be joined together sequentially or in a single-pot reaction.[49–53] This strategy has been used in the D-peptide synthesis of the 81-residue snow flea antifreeze protein.[54] NCL leaves a Cys residue at each ligation site, but this "scar" can be removed by desulphurization of the cysteine residue to alanine.[55,56] Furthermore, several creative adaptions of NCL allow residues other than an N-terminal cysteine to be present at the liga-

tion junction, such as N-terminal, thiol-containing auxiliary groups that can be removed via reduction,[57] UV irradiation,[58,59] or treatment with acid[60,61] after they have facilitated peptide bond formation. In another approach, modified versions of phenylalanine,[62] valine,[63] or lysine[64] bearing a thiol substituent were incorporated at the N-terminus of a peptide fragment and yielded the respective native amino acid at the ligation site following NCL/desulfurization.

Once a D-target has been synthesized, it can be used in conjunction with mirror-image display to screen peptide libraries for novel sequences of interest (see our work on HIV below and Ref. 65). The unifying feature that underlies all of the library-based display techniques discussed here is the physical linkage of a peptide to its corresponding genotype (RNA or DNA). This linkage allows the library to be subjected to multiple rounds of interrogation/library amplification leading to enrichment of sequences that bind to a target of interest. In these techniques, library diversity is generated in the nucleotide coding sequence, and cellular machinery efficiently translates this information into a peptide library. The display techniques most suitable for screening high-diversity libraries can be broken down into two broad categories: viral display and cell-free display systems (briefly described here, but for a more extensive review see Refs. 66–70).

Viral Display

Phage display continues to be the workhorse of the viral display techniques because of its ease of use, versatility, and low cost. Since phage display requires a bacterial transformation step, library size is typically limited to $\sim 10^9$–10^{10}. The most commonly utilized phage display system is the nonlytic M13-family filamentous phage, in which the peptide library is expressed as an N-terminal fusion with the pIII minor coat protein. Up to five copies of pIII are present on the phage surface, making both polyvalent and monovalent display techniques possible. Polyvalent display provides a strong avidity effect, which is highly advantageous for screening naïve peptide libraries containing only rare low affinity binders. In contrast, monovalent display reduces avidity and allows for more stringent selection of peptides with high affinity. In an early round of phage display, library diversity is high, but each sequence is represented by only a few phage. As with any library display method, the application of selection pressure must be sufficient to drive selection for tighter binders, but not so severe as to eliminate rare tight binding sequences due to stochastic factors. In later rounds, as phage library diversity drops and each remaining sequence is represented by numerous phage, selection pressure can be steadily increased. Insufficient selection pressure can select for "cheater" phage that do not bear authentic tight binding peptides (e.g., phage with growth advantages).

Besides filamentous phage display, techniques employing various eukaryotic viruses, including retroviruses, baculovirus, Adeno-associated virus, and Adenovirus have been or are currently being developed for displaying peptide libraries.[67] Other display techniques (e.g., bacterial, yeast, or mammalian cell display) have several advantages over phage display (e.g., more sophisticated folding machinery, post-translational modifications, ability to use FACS sorting), but are more complex and typically limited to less diverse libraries (reviewed by Refs. 66, 67, 71, 72).

Cell-Free Display

One of the major advantages of cell-free techniques (reviewed by Ref. 73) is that they are carried out *in vitro*. Because a transformation step is not required, library diversities $>10^{12}$ can be generated.[69] Due to the proposed correlation between library diversity and the affinity of selected ligands, this large increase in library diversity over typical viral or cell surface display systems provides a distinct advantage.

Ribosome display[74,75] capitalizes on the fact that it is possible to stall the *in vitro* translation of a polypeptide so that the ribosome remains assembled and attached to the mRNA transcript and the nascent translated polypeptide. This mRNA-ribosome-polypeptide ternary complex serves to link genotype to phenotype and can be panned against a target to isolate sequences of interest. The ternary complex can then be eluted and dissociated with EDTA, allowing for the isolation of the original mRNA transcript.

Alternatively, RNA display[76] links phenotype to genotype by connecting an mRNA sequence directly to the peptide it encodes. This linkage is accomplished by chemically attaching the antibiotic puromycin to the 3' end of the RNA via a DNA linker. As the mRNA is being translated, the ribosome will stall once it reaches the DNA linker, allowing puromycin to enter the ribosomal A site, where the ribosome catalyzes covalent attachment to the recently translated polypeptide. This peptide–RNA complex can then be subjected to panning against a specific target.

While *in vitro* display techniques that link the peptide phenotype to an RNA genotype overcome many of the limitations of phage display, the instability of RNA molecules along with other technical challenges fundamental to these techniques has limited their application to a relatively small number of expert laboratories. To address these challenges, techniques that link the library peptides directly to their encoding DNA have recently been developed.

CIS display (Isogenica) exploits the unique activity of RepA, a bacterial plasmid DNA-replication initiation protein.[77] RepA is a cis-acting protein that tightly binds to the origin of replication (*ori*) on the plasmid from which it was expressed. A stretch of DNA between the sequence that encodes RepA and the *ori* known as the CIS element contains a rho-dependent transcriptional terminator that is thought to stall the RNA polymerase during transcription of RepA. The current model holds that this delay allows the newly synthesized RepA protein emerging from the ribosome to interact with the CIS element, which subsequently directs RepA to the *ori* DNA. Peptide libraries can be fused to the N-terminus of RepA, thereby creating a link between phenotype and the DNA genotype. Like other *in vitro* techniques, CIS display has the capability to accommodate peptide libraries much larger than those possible for phage display. In one example,[77] a library of $>10^{12}$ randomized 18-mer peptides was constructed and was used to isolate sequences that bound to disparate targets. In a similar approach, DNA sequences encoding randomized peptide libraries are fused to the bacteriophage P2A gene. P2A is an endonuclease involved in the rolling circle replication of bacteriophage P2 DNA. P2A becomes covalently attached to the same DNA molecule from which it was expressed, linking phenotype to genotype. This technique has been used in a pilot study to select single-chain antibodies from a 10^7-member library and may be suitable for screening much larger libraries.[78]

D-PEPTIDE INHIBITORS OF HIV ENTRY

Here we describe the history of our potent D-peptide inhibitors of HIV entry, developed in the Kim and Kay laboratories. Initially, mirror-image polyvalent phage display was used to screen naïve peptide libraries of various lengths and geometries for binding to an HIV N-trimer pocket mimic (IQN17).[18] Pocket-specific binding was only observed in disulfide-constrained 10-mer sequences ($CX_{10}C$) containing an EWXWL consensus sequence. An initial group of ~10 winning sequences were validated by measuring their binding to the desired target and several negative control targets (mutated or missing pockets) to demonstrate pocket-specific binding.

Validated D-peptides inhibited HIV entry (lab strain HXB2) with IC_{50} values ranging from 11 to 270 μM.[18] A co-crystal structure of one of the higher affinity D-peptides (D10-p1) in complex with IQN17 shows that D10-p1 contains two short left handed α-helical segments flanking a turn imposed by the disulfide constraint. The binding interface between the hydrophobic pocket of IQN17 and D10-p1 is mediated by residues in the C-terminal α-helix, with residues in the EWXWL consensus motif making the largest contributions. Comparison of the D10-p1/IQN17 crystal structure to the native post-fusion gp41 structure[17] reveals that critical residues for binding in D10-p1 are very similar in chemical character to those of the natural C-peptide ligand (primarily W628, W631, and I635), but adopt distinct conformations due to their opposite chirality.

Due to library diversity limitations, the first-generation library only surveyed about one in a million possible sequences.[18] The identification of a strong EWXWL consensus sequence allowed us to fix these four residues to produce a "constrained" library with only six randomized residues (~10^9 possible sequences). Panning this library produced ~4-fold more potent inhibitors.[79]

Surprisingly, an 8-mer (CX_8C) was also among the winning sequences. Since 8-mers were not part of the library design and likely arose from rare replication errors, their relative success suggested that the 8-mer geometry might provide a better pocket-binding solution. Our crystal structure of the first identified 8-mer, PIE1 (pocket-specific inhibitor of entry), bound to IQN17 reveals that the key pocket-binding residues (WXWL) adopt nearly identical positions within the pocket as seen with D10-p1, leading to very similar binding interfaces despite PIE1's reduced length.[79] The key difference between PIE1 and D10-p1 is a more compact D-peptide structure with a tighter hydrophobic core devoid of water. PIE1 has a D-Pro at position 8 that likely aids making the tighter turn necessary for circularization forced by the shorter disulfide-constrained loop.[79]

To completely explore 8-mer sequence space, a new library was generated with the core consensus sequence WXWL fixed (CX_4WXWLC). While screening this library using traditional solid-phase phage display, we observed that polyvalency made it difficult to distinguish modest (μM) and tight (nM) binders. Solid-phase target presentation is advantageous for selection of weak initial binders from a naïve library, but problematic for identifying strong binders in a sea of modest binders since all binders are strongly retained on the high-density target surface. Moving the binding reaction into solution (solution-phase phage display) reduces inter-target avidity and allows additional selection pressure by reducing target concentration through rounds of panning.[80] Despite reduced inter-molecular avidity, solution-phase phage were still found to have dramatically higher binding affinities in the context of the panning than expected based on K_D values of the derived D-peptides, likely due to intra-molecular avidity on the trimeric target. To overcome this barrier, an L-peptide version of PIE2[79] (identified during earlier rounds of solution-phase phage display) was employed as a soluble competitor for subsequent rounds of

panning. Increased selection pressure was applied by escalating PIE2 concentrations, leading to the discovery of PIE7, which is ~15-fold more potent than D10-p1 (IC_{50} = 620 nM, HXB2 strain).

Our co-crystal structure of PIE7 in complex with IQN17 suggested that further gains in binding affinity could be made through optimization of the residues outside the disulfide bond, which make significant gp41 contacts.[79] Initially, these four "flanking" residues outside the disulfide bond (Gly–Ala on the N-terminus and Ala–Ala on the C-terminus) were not varied due to library cloning restrictions. We redesigned the phage display vector to relocate the cloning sites and allow randomization of the flank residues. After four rounds, PIE12 (HP-[PIE7 core]-EL) was identified with ~20-fold improved potency over PIE7. The PIE12/IQN17 crystal structure (Figure 2) reveals that PIE12's improved binding is likely due to ring-stacking interactions of D-His1 and D-Pro2 with the pocket residue Trp571 and burial of an additional 50 Å^2 hydrophobic of surface area by D-Leu15.[81] Beyond the changes in the flanking regions, the central core structure is unchanged from PIE7.

Crosslinking and the Resistance Capacitor

After battling the confounding effects of avidity throughout our phage display screens, we hoped to re-introduce avidity to boost the potency of our D-peptides. Our D-peptide/N-trimer crystal structures reveal the precise relationship between neighboring D-peptides binding to the three symmetry-related pockets. Using this information, we used discrete polyethylene glycol (PEG) crosslinkers to generate dimeric and trimeric D-peptides,[79] which showed dramatically improved antiviral potency (up to 2000-fold) over monomeric D-peptides.[79,81] PIE12-trimer, our lead inhibitor, is ~30-fold more potent than Fuzeon and inhibits a diverse panel of the most common circulating HIV strain subtypes worldwide in the high pM—low n*M* range.[81]

Interestingly, we encountered a limit to the potency gains that could be achieved by monomer affinity optimization and crosslinking. We hypothesized that this potency plateau was imposed by the limited time window available for inhibitor binding (target is only available in the transient pre-hairpin intermediate) and the inhibitor association rate (limited by diffusion), as previously observed for the pre-hairpin intermediate inhibitor 5-helix.[82] Although this potency limit would prevent us from designing more potent inhibitors, we hypothesized that "over-engineering" our inhibitors (i.e., continuing to improve inhibitor binding despite a lack of corresponding improvement in potency) would endow them with a reserve of binding energy that would stall the development of resistance mutations. We predict that this "resistance capacitor" would also greatly delay the emergence of resistance by eliminating the selective advantage conferred by these mutations (i.e., severing the link between affinity and potency). Only a profoundly disruptive mutation would escape the resistance capacitor. In support of this hypothesis, we were only able to identify high-level PIE12-trimer resistance after 65 weeks of viral passaging in the presence of inhibitor, compared with ~3 weeks for Fuzeon.[81] As predicted, PIE12-trimer was also able to absorb the impact of earlier-generation D-peptide resistance mutations.

PROTEASE-RESISTANT PEPTIDES FACE OTHER PHARMACOKINETIC CHALLENGES

Reduction of peptide susceptibility to proteases increases peptide longevity, but another major threat to serum half-life is rapid clearance via renal filtration. For globular proteins, the glomerular filtration size limit is ~70 kDa. Although albumin is slightly smaller, it avoids filtration because of electrostatic repulsion from the highly negatively charged glomerular basement membrane. Albumin is the smallest major unfiltered protein, efficiently circulating in the bloodstream with a half-life of approximately 19 days in humans.[83] The small size of peptide therapeutics means that an additional level of design is required to reduce renal filtration and realize the full benefits of protease resistance. Several common PK optimization strategies suitable for peptides are briefly described below.

PEG is a hydrophilic polymer commonly used for protein conjugation. Adding PEG to a protein has been one of the most clinically successful strategies for improving pharmacokinetics.[84] Early studies on the effects of PEG size on biodistribution revealed that good serum retention is achieved between 40 and 60 kDa, while exceeding this range resulted in increased uptake and accumulation within the reticuloendothelial system.[85] Thus, the PEGylation field has largely adopted the strategy of adding ~40 kDa of PEG weight to peptide and small protein therapeutics. PEG is extensively hydrated such that its hydrodynamic radius is much larger than expected from its molecular weight. Furthermore, distributing the weight of the PEG polymer in a branched geometry improves half-life and reduces steric interference.[86] PEG conjugation can also be reversible (e.g., an ester linkage), creating a circulating depot from which the therapeutic is cleaved over time (e.g., in case drug activity is adversely affected by PEG conjugation).[87,88] Limitations of PEGylation include steric interference with binding, long-lived accumulation in renal tubule cells, viscosity, and polydispersity. An alternative approach uses a hydroxyethyl starch polymer (HESylation) to reduce renal filtration.[89]

Albumin binding (covalent or noncovalent) is another recently validated approach for prolonging serum half-life (reviewed by Ref. 90). Promising albumin-binding strategies include covalent albumin-peptide conjugation, as well as reversible binding to circulating albumin via albumin-binding peptides, small molecules, or fatty acids.[90–92] As an example, albumin conjugation of an HIV C-peptide inhibitor (either *in vitro* or *in vivo*) dramatically improves serum half-life,[93] as does cholesterol conjugation to a lesser extent, presumably via weak reversible interactions with albumin and/or cell membranes.[94]

FUTURE DIRECTIONS

Recombinant Production of Peptidomimetics

Although robust recombinant production of peptidomimetics is not yet possible, significant recent advances in synthetic biology may enable routine production of diverse peptidomimetic libraries in the near future. One promising approach is *in vitro* codon reprogramming for the synthesis of unnatural polymers. This approach relies on cell-free translation systems to reconstitute ribosomal peptide synthesis using a minimal set of purified protein components.[95–100] By chemically or enzymatically charging tRNA molecules with novel amino acid analogues, the genetic code can be effectively reprogrammed *in vitro*. When these cell-free systems with genetic code modifications are used in conjunction with a display technology, peptides with novel amino acids can be screened for a desired property. For example, ribosome display was used in conjunction with *in vitro* codon reprogramming to isolate peptide sequences from an mRNA library that encoded an unnatural, selectable amino acid.[101–103]

Along these lines, it has been demonstrated that tRNAs can be charged with a variety of amino acid analogues that will modify the peptide backbone, including α-hydroxy acids, N-methyl amino acids, α,α-disubstituted amino acids, β-amino acids, and D-amino acids.[104] However, the efficiency of ribosomal incorporation of Ala/Phe analogues varies greatly from fairly robust (α-hydroxy acid and N-methyl) to weak (α,α-disubstituted amino acids) to undetectable (β- and D-amino acids).[104] Subsequent work has described the ability of the translation machinery to accommodate amino acid analogues with novel side chains and backbones.[105]

In one example, seven codons were each reassigned to encode a unique α-hydroxy acid, and polymers as long as 12 consecutive α-hydroxy acids could be synthesized.[106] In another report, the incorporation efficiencies of 23 N-methyl amino acids, 19 of which bore naturally occurring side chains, were determined. Eight of these 19 N-methyl amino acids were incorporated at specific points in a polypeptide with >30% efficiency as compared with wild type. A peptide up to 10 residues long could be synthesized from three unique N-methyl amino acids.[107]

While less success has been reported with ribosomal incorporation of D-amino acids, modifications to the ribosomal peptidyltransferase center and helix 89 of the 23S rRNA can relax the ribosome's natural substrate specificity, thereby enhancing the incorporation of D-amino acid residues into a growing polypeptide chain.[108,109] Although these techniques have not yet been employed as such, in principle cell-free translation systems coupled with *in vitro* display techniques could be used to screen libraries of polymers with novel backbones. As an advance in this direction, genetic code reprogramming has already been used in conjunction with mRNA display technology to generate mRNA-peptide fusions containing N-methyl amino acids.[110]

Another approach to recombinantly produce peptidomimetics relies on the ability to expand the genetic code *in vivo* via the generation of evolved tRNA/aminoacyl-tRNA synthetase pairs. In these systems, the foreign tRNA functions as an amber suppressor, effectively allowing the amber nonsense codon to be reprogrammed to encode a non-natural amino acid.[111,112] It has been demonstrated that genetic code expansion can be used in conjunction with phage display to incorporate a non-natural amino acid into a pIII fusion peptide.[113] In the future, multiple codons could be reassigned, permitting the incorporation of multiple unnatural residues *in vivo*. Several advances have been made toward this end. In a recent publication describing a technique for rapid, genome-wide engineering, the authors show progress toward replacing all 314 TAG stop codons in *E. coli* with the TAA stop codon.[114] This type of genome manipulation could be used for the removal of redundancy from the genetic code, freeing up codons for potential reprogramming. In another approach involving evolved tRNA/aminoacyl-tRNA synthetase pairs, an evolved orthogonal ribosome able to read both 3- and 4-base codons was able to efficiently incorporate two different non-natural amino acids into a single polypeptide chain *in vivo*.[115,116] These approaches present tantalizing possibilities for the production of peptide libraries with unnatural side chains and backbones, but the technology is not yet sufficiently robust to allow for widespread application. Additional engineering of tRNA molecules, elongation factors, and the ribosome itself will likely be required for use with certain diverse peptidomimetics.[109,117,118]

D-Peptides present a unique opportunity for designing an artificial recombinant production system. Because of their symmetry relationship with natural peptides, an *in vitro*

translation system composed of all opposite-chirality components (D-proteins and nucleotides containing L-ribose) would function equivalently to natural translation, when provided with mirror-image DNA substrates. Synthesis of all ribosomal components presents an enormous synthetic challenge, but recent advances in SPPS and peptide ligation may now make this approach feasible. A mirror-image *in vitro* translation system would provide a useful tool for D-peptide drug discovery and production, but may not be ideal for large-scale production, especially of complex D-proteins (e.g., those requiring chaperones or post-translational modifications). The ultimate goal is to produce D-peptides using a synthetic mirror-image organism, a strategy we dub the "D. coli" project. The key to this project is synthesizing the minimal set of RNAs and proteins necessary to allow enzymatic production of other larger components and ultimately all components needed for a self-replicating organism. It is also not yet clear how to "start up" such an organism.[119,120]

Cost and Toxicity of Peptidomimetics

In addition to achieving their biological objectives, peptidomimetics will need to overcome concerns about cost and toxicity to succeed as therapeutics. Currently there are no FDA-approved fully peptidomimetic peptides, so information on their *in vivo* toxicity is extremely limited. Initial data from two D-peptides that have advanced to clinical trials (Genzyme's Delmitide[121] and Allelix's ALX40-4C[122]) showed that both D-peptides (one orally administered, one systemically delivered) were well tolerated in humans. Further comfort is provided by over a dozen approved D-amino acid-containing peptides, as well as two approved ß-amino acid-containing peptides.[123] These data suggest that these amino acids are not intrinsically toxic, but more rigorous animal toxicology studies on different classes of fully protease-resistant peptides will be required for a definitive determination. Such studies will also determine whether these peptidomimetics induce significant immunogenicity upon chronic administration. Finally, the cost of D-, *β*-, and other uncommon amino acids is currently significantly higher than the corresponding common L-amino acids, largely because of their current status as specialty reagents. However, we anticipate the cost of these amino acids will drop dramatically as they are adopted in high-volume production of therapeutic peptides, as has already occurred with several D-amino acids in large-scale peptide production.

The authors thank Debra Eckert for critical review of the article and figures preparation. M.S.K. is a Scientific Director and consultant of the D-peptide Research Division of Navigen, which is commercializing D-peptide inhibitors of viral entry.

REFERENCES

1. McGregor, D. P. Curr Opin Pharmacol 2008, 8, 616–619.
2. Patch, J. A.; Barron, A. E. Curr Opin Chem Biol 2002, 6, 872–877.
3. Goodman, C. M.; Choi, S.; Shandler, S.; DeGrado, W. F. Nat Chem Biol 2007, 3, 252–262.
4. Hill, D. J.; Mio, M. J.; Prince, R. B.; Hughes, T. S.; Moore, J. S. Chem Rev 2001, 101, 3893–4012.
5. Stevenson, C. L. Curr Pharm Biotechnol 2009, 10, 122–137.
6. Tilton, J. C.; Doms, R. W. Antiviral Res 2010, 85, 91–100.
7. Eckert, D. M.; Kim, P. S. Annu Rev Biochem 2001, 70, 777–810.
8. Chan, D. C.; Kim, P. S. Cell 1998, 93, 681–684.
9. Jiang, S.; Lin, K.; Strick, N.; Neurath, A. R. Nature 1993, 365, 113.
10. Wild, C.; Oas, T.; McDanal, C.; Bolognesi, D.; Matthews, T. Proc Natl Acad Sci U S A 1992, 89, 10537–10541.
11. Wild, C. T.; Shugars, D. C.; Greenwell, T. K.; McDanal, C. B.; Matthews, T. J. Proc Natl Acad Sci U S A 1994, 91, 9770–9774.
12. Lu, M.; Blacklow, S. C.; Kim, P. S. Nat Struct Biol 1995, 2, 1075–1082.
13. Eckert, D. M.; Kim, P. S. Proc Natl Acad Sci U S A 2001, 98, 11187–11192.
14. Root, M. J.; Kay, M. S.; Kim, P. S. Science 2001, 291, 884–888.
15. Kilby, J. M.; Hopkins, S.; Venetta, T. M.; DiMassimo, B.; Cloud, G. A.; Lee, J. Y.; Alldredge, L.; Hunter, E.; Lambert, D.; Bolognesi, D.; Matthews, T.; Johnson, M. R.; Nowak, M. A.; Shaw, G. M.; Saag, M. S. Nat Med 1998, 4, 1302–1307.
16. Chan, D. C.; Chutkowski, C. T.; Kim, P. S. Proc Natl Acad Sci U S A 1998, 95, 15613–15617.
17. Chan, D. C.; Fass, D.; Berger, J. M.; Kim, P. S. Cell 1997, 89, 263–273.
18. Eckert, D. M.; Malashkevich, V. N.; Hong, L. H.; Carr, P. A.; Kim, P. S. Cell 1999, 99, 103–115.
19. Frey, G.; Rits-Volloch, S.; Zhang, X. Q.; Schooley, R. T.; Chen, B.; Harrison, S. C. Proc Natl Acad Sci U S A 2006, 103, 13938–13943.
20. Ferrer, M.; Kapoor, T. M.; Strassmaier, T.; Weissenhorn, W.; Skehel, J. J.; Oprian, D.; Schreiber, S. L.; Wiley, D. C.; Harrison, S. C. Nat Struct Biol 1999, 6, 953–960.
21. Debnath, A. K.; Radigan, L.; Jiang, S. J Med Chem 1999, 42, 3203–3209.
22. Jin, B. S.; Ryu, J. R.; Ahn, K.; Yu, Y. G. AIDS Res Hum Retroviruses 2000, 16, 1797–1804.
23. Jiang, S.; Lu, H.; Liu, S.; Zhao, Q.; He, Y.; Debnath, A. K. Antimicrob Agents Chemother 2004, 48, 4349–4359.
24. Dwyer, J. J.; Wilson, K. L.; Davison, D. K.; Freel, S. A.; Seedorff, J. E.; Wring, S. A.; Tvermoes, N. A.; Matthews, T. J.; Greenberg, M. L.; Delmedico, M. K. Proc Natl Acad Sci U S A 2007, 104, 12772–12777.
25. Lalezari, J. P.; Bellos, N. C.; Sathasivam, K.; Richmond, G. J.; Cohen, C. J.; Myers, R. A.; , Jr.Henry, D. H.; Raskino, C.; Melby, T.; Murchison, H.; Zhang, Y.; Spence, R.; Greenberg, M. L.; Demasi, R. A.; Miralles, G. D. J Infect Dis 2005, 191, 1155–1163.
26. Ray, N.; Harrison, J. E.; Blackburn, L. A.; Martin, J. N.; Deeks, S. G.; Doms, R. W. J Virol 2007, 81, 3240–3250.
27. Cheng, R. P.; Gellman, S. H.; DeGrado, W. F. Chem Rev 2001, 101, 3219–3232.

28. Pilsl, L. K.; Reiser, O. Amino acids 2011, 41, 709–718.
29. Horne, W. S.; Gellman, S. H. Acc Chem Res 2008, 41, 1399–1408.
30. Seebach, D.; Gardiner, J. Acc Chem Res 2008, 41, 1366–1375.
31. Kritzer, J. A.; Stephens, O. M.; Guarracino, D. A.; Reznik, S. K.; Schepartz, A. Biorg Med Chem 2005, 13, 11–16.
32. Harker, E. A.; Daniels, D. S.; Guarracino, D. A.; Schepartz, A. Biorg Med Chem 2009, 17, 2038–2046.
33. Stephens, O. M.; Kim, S.; Welch, B. D.; Hodsdon, M. E.; Kay, M. S.; Schepartz, A. J Am Chem Soc 2005, 127, 13126–13127.
34. Bautista, A. D.; Stephens, O. M.; Wang, L.; Domaoal, R. A.; Anderson, K. S.; Schepartz, A. Bioorg Med Chem Lett 2009, 19, 3736–3738.
35. English, E. P.; Chumanov, R. S.; Gellman, S. H.; Compton, T. J Biol Chem 2006, 281, 2661–2667.
36. Horne, W. S.; Johnson, L. M.; Ketas, T. J.; Klasse, P. J.; Lu, M.; Moore, J. P.; Gellman, S. H. Proc Natl Acad Sci U S A 2009, 106, 14751–14756.
37. Horne, W. S.; Price, J. L.; Keck, J. L.; Gellman, S. H. J Am Chem Soc 2007, 129, 4178–4180.
38. Johnson, L. M.; Horne, W. S.; Gellman, S. H. J Am Chem Soc 2011, 133, 10038–10041.
39. Lam, K. S.; Lehman, A. L.; Song, A.; Doan, N.; Enstrom, A. M.; Maxwell, J.; Liu, R. Methods Enzymol 2003, 369, 298–322.
40. Zawadzke, L. E.; Berg, J. M. J Am Chem Soc 1992, 114, 4002–4003.
41. Milton, R. C.; Milton, S. C.; Kent, S. B. Science 1992, 256, 1445–1448.
42. Schumacher, T. N.; Mayr, L. M.; Minor, D. L.; Jr. Milhollen, M. A.; Burgess, M. W.; Kim, P. S. Science 1996, 271, 1854–1857.
43. Kent, S. B. Chem Soc Rev 2009, 38, 338–351.
44. Clark-Lewis, I.; Aebersold, R.; Ziltener, H.; Schrader, J. W.; Hood, L. E.; Kent, S. B. Science 1986, 231, 134–139.
45. Hackenberger, C. P.; Schwarzer, D. Angew Chem Int Ed 2008, 47, 10030–10074.
46. Muralidharan, V.; Muir, T. W. Nat Methods 2006, 3, 429–438.
47. Blanco-Canosa, J. B.; Dawson, P. E. Angew Chem Int Ed 2008, 47, 6851–6855.
48. Mende, F.; Seitz, O. Angew Chem Int Ed 2011, 50, 1232–1240.
49. Bang, D.; Chopra, N.; Kent, S. B. H. J Am Chem Soc 2004, 126, 1377–1383.
50. Bang, D.; Kent, S. B. H. Agnew Chem Int Ed 2004, 43, 2534–2538.
51. Boerema, D. J.; Tereshko, V. A.; Kent, S. B. H. Biopolymers 2008, 90, 278–286.
52. Mandal, K.; Kent, S. B. Angew Chem Int Ed 2011, 50, 8029–8033.
53. Kumar, K. S.; Bavikar, S. N.; Spasser, L.; Moyal, T.; Ohayon, S.; Brik, A. Angew Chem Int Ed 2011, 50, 6137–6141.
54. Pentelute, B. L.; Gates, Z. P.; Dashnau, J. L.; Vanderkooi, J. M.; Kent, S. B. H. J Am Chem Soc 2008, 130, 9702–9707.
55. Wan, Q.; Danishefsky, S. J. Angew Chem 2007, 46, 9248–9252.
56. Rohde, H.; Seitz, O. Biopolymers 2010, 94, 551–559.
57. Canne, L. E.; Bark, S. J.; Kent, S. B. H. J Am Chem Soc 1996, 118, 5891–5896.
58. Kawakami, T.; Aimoto, S. Tetrahedron Lett 2003, 44, 6059–6061.
59. Marinzi, C.; Offer, J.; Longhi, R.; Dawson, P. E. Biorg Med Chem 2004, 12, 2749–2757.
60. Botti, P.; Carrasco, M. R.; Kent, S. B. H. Tetrahedron Lett 2001, 42, 1831–1833.
61. Offer, J.; Boddy, C. N.; Dawson, P. E. J Am Chem Soc 2002, 124, 4642–4646.
62. Crich, D.; Banerjee, A. J Am Chem Soc 2007, 129, 10064–10065.
63. Haase, C.; Rohde, H.; Seitz, O. Angew Chem 2008, 47, 6807–6810.
64. Yang, R.; Pasunooti, K. K.; Li, F.; Liu, X. W.; Liu, C. F. Chem Commun (Camb) 2010, 46, 7199–7201.
65. Liu, M.; Pazgier, M.; Li, C.; Yuan, W.; Lu, W. Angew Chem Int Ed 2010, 49, 3649–3652.
66. Gronwall, C.; Stahl, S. J Biotechnol 2009, 140, 254–269.
67. Sergeeva, A.; Kolonin, M. G.; Molldrem, J. J.; Pasqualini, R.; Arap, W. Adv Drug Deliv Rev 2006, 58, 1622–1654.
68. Kehoe, J. W.; Kay, B. K. Chem Rev 2005, 105, 4056–4072.
69. FitzGerald, K. Drug Discovery Today 2000, 5, 253–258.
70. Ullman, C. G.; Frigotto, L.; Cooley, R. N. Brief Funct Genomics 2011, 10, 125–134.
71. Lee, S. Y.; Choi, J. H.; Xu, Z. H. Trends Biotechnol 2003, 21, 45–52.
72. Daugherty, P. S. Curr Opin Struct Biol 2007, 17, 474–480.
73. Barendt, P. A.; Sarkar, C. A. In Protein Engineering and Design; Park, S. F.; Cochran, J. R., Eds.; CRC Press, 2009; pp 51–82.
74. Mattheakis, L. C.; Bhatt, R. R.; Dower, W. J. Proc Natl Acad Sci U S A 1994, 91, 9022–9026.
75. Hanes, J.; Pluckthun, A. Proc Natl Acad Sci U S A 1997, 94, 4937–4942.
76. Roberts, R. W.; Szostak, J. W. Proc Natl Acad Sci U S A 1997, 94, 12297–12302.
77. Odegrip, R.; Coomber, D.; Eldridge, B.; Hederer, R.; Kuhlman, P. A.; Ullman, C.; FitzGerald, K.; McGregor, D. Proc Natl Acad Sci U S A 2004, 101, 2806–2810.
78. Reiersen, H.; Lobersli, I.; Loset, G. A.; Hvattum, E.; Simonsen, B.; Stacy, J. E.; McGregor, D.; FitzGerald, K.; Welschof, M.; Brekke, O. H.; Marvik, O. J. Nucleic Acids Res 2005, 33, e10.
79. Welch, B. D.; VanDemark, A. P.; Heroux, A.; Hill, C. P.; Kay, M. S. Proc Natl Acad Sci U S A 2007, 104, 16828–16833.
80. Barbas, C. F. Phage Display: A Laboratory Manual; Cold Springs Harbor Laboratory Press: New York, 2001.
81. Welch, B. D.; Francis, J. N.; Redman, J. S.; Paul, S.; Weinstock, M. T.; Reeves, J. D.; Lie, Y. S.; Whitby, F. G.; Eckert, D. M.; Hill, C. P.; Root, M. J.; Kay, M. S. J Virol 2010, 84, 11235–11244.
82. Steger, H. K.; Root, M. J. J Biol Chem 2006, 281, 25813–25821.
83. Dennis, M. S.; Zhang, M.; Meng, Y. G.; Kadkhodayan, M.; Kirchhofer, D.; Combs, D.; Damico, L. A. J Biol Chem 2002, 277, 35035–35043.
84. Fishburn, C. S. J Pharm Sci 2008, 97, 4167–4183.
85. Yamaoka, T.; Tabata, Y.; Ikada, Y. J Pharm Sci 1994, 83, 601–606.
86. Fee, C. J. Biotechnol Bioeng 2007, 98, 725–731.
87. Greenwald, R. B. J Control Release 2001, 74, 159–171.
88. Tong, R.; Cheng, J. Polym Rev 2007, 47, 345–381.
89. Besheer, A.; Hertel, T. C.; Kressler, J.; Mader, K.; Pietzsch, M. Methods Mol Biol 2011, 751, 17–27.
90. Kratz, F. J Control Release 2008, 132, 171–183.

91. Madsen, K.; Knudsen, L. B.; Agersoe, H.; Nielsen, P. F.; Thogersen, H.; Wilken, M.; Johansen, N. L. J Med Chem 2007, 50, 6126–6132.
92. Trussel, S.; Dumelin, C.; Frey, K.; Villa, A.; Buller, F.; Neri, D. Bioconjug Chem 2009, 20, 2286–2292.
93. Stoddart, C. A.; Nault, G.; Galkina, S. A.; Thibaudeau, K.; Bakis, P.; Bousquet-Gagnon, N.; Robitaille, M.; Bellomo, M.; Paradis, V.; Liscourt, P.; Lobach, A.; Rivard, M. E.; Ptak, R. G.; Mankowski, M. K.; Bridon, D.; Quraishi, O. J Biol Chem 2008, 283, 34045–34052.
94. Ingallinella, P.; Bianchi, E.; Ladwa, N. A.; Wang, Y. J.; Hrin, R.; Veneziano, M.; Bonelli, F.; Ketas, T. J.; Moore, J. P.; Miller, M. D.; Pessi, A. Proc Natl Acad Sci U S A 2009, 106, 5801–5806.
95. Forster, A. C.; Weissbach, H.; Blacklow, S. C. Anal Biochem 2001, 297, 60–70.
96. Forster, A. C.; Tan, Z. P.; Nalam, M. N. L.; Lin, H. N.; Qu, H.; Cornish, V. W.; Blacklow, S. C. Proc Natl Acad Sci U S A 2003, 100, 6353–6357.
97. Shimizu, Y.; Kanamori, T.; Ueda, T. Methods 2005, 36, 299–304.
98. Shimizu, Y.; Kuruma, Y.; Ying, B. W.; Umekage, S.; Ueda, T. FEBS J 2006, 273, 4133–4140.
99. Ohta, A.; Yamagishi, Y.; Suga, H. Curr Opin Chem Biol 2008, 12, 159–167.
100. Shimizu, Y.; Inoue, A.; Tomari, Y.; Suzuki, T.; Yokogawa, T.; Nishikawa, K.; Ueda, T. Nat Biotechnol 2001, 19, 751–755.
101. Tan, Z. P.; Blacklow, S. C.; Cornish, V. W.; Forster, A. C. Methods 2005, 36, 279–290.
102. Forster, A. C.; Cornish, V. W.; Blacklow, S. C. Anal Biochem 2004, 333, 358–364.
103. Watts, R. E.; Forster, A. C. Methods Mol Biol 2012, 805, 349–365.
104. Tan, Z. P.; Forster, A. C.; Blacklow, S. C.; Cornish, V. W. J Am Chem Soc 2004, 126, 12752–12753.
105. Hartman, M. C.; Josephson, K.; Lin, C. W.; Szostak, J. W. PloS One 2007, 2, e972.
106. Ohta, A.; Murakami, H.; Suga, H. Chembiochem 2008, 9, 2773–2778.
107. Kawakami, T.; Murakami, H.; Suga, H. Chem Biol 2008, 15, 32–42.
108. Dedkova, L. M.; Fahmi, N. E.; Golovine, S. Y.; Hecht, S. M. J Am Chem Soc 2003, 125, 6616–6617.
109. Dedkova, L. M.; Fahmi, N. E.; Golovine, S. Y.; Hecht, S. M. Biochemistry 2006, 45, 15541–15551.
110. Frankel, A.; Millward, S. W.; Roberts, R. W. Chem Biol 2003, 10, 1043–1050.
111. Wang, L.; Brock, A.; Herberich, B.; Schultz, P. G. Science 2001, 292, 498–500.
112. Wang, Q.; Parrish, A. R.; Wang, L. Chem Biol 2009, 16, 323–336.
113. Feng, T.; Tsao, M. L.; Schultz, P. G. J Am Chem Soc 2004, 126, 15962–15963.
114. Isaacs, F. J.; Carr, P. A.; Wang, H. H.; Lajoie, M. J.; Sterling, B.; Kraal, L.; Tolonen, A. C.; Gianoulis, T. A.; Goodman, D. B.; Reppas, N. B.; Emig, C. J.; Bang, D.; Hwang, S. J.; Jewett, M. C.; Jacobson, J. M.; Church, G. M. Science 2011, 333, 348–353.
115. Neumann, H.; Wang, K.; Davis, L.; Garcia-Alai, M.; Chin, J. W. Nature 2010, 464, 441–444.
116. Wang, K.; Schmied, W. H.; Chin, J. W. Angew Chem Int Ed 2012, 51, 2288–2297.
117. Doi, Y.; Ohtsuki, T.; Shimizu, Y.; Ueda, T.; Sisido, M. J Am Chem Soc 2007, 129, 14458–14462.
118. Dale, T.; Uhlenbeck, O. C. Trends Biochem Sci 2005, 30, 659–665.
119. Jewett, M. C.; Forster, A. C. Curr Opin Biotechnol 2010, 21, 697–703.
120. Forster, A. C.; Church, G. M. Mol Syst Biol 2006, 2, 45.
121. Travis, S.; Yap, L. M.; Hawkey, C.; Warren, B.; Lazarov, M.; Fong, T.; Tesi, R. J. Inflamm Bowel Dis 2005, 11, 713–719.
122. Doranz, B. J.; Filion, L. G.; Diaz-Mitoma, F.; Sitar, D. S.; Sahai, J.; Baribaud, F.; Orsini, M. J.; Benovic, J. L.; Cameron, W.; Doms, R. W. AIDS Res Hum Retroviruses 2001, 17, 475–486.
123. Vlieghe, P.; Lisowski, V.; Martinez, J.; Khrestchatisky, M. Drug Discov Today 2010, 15, 40–56.

CHAPTER 3

DESIGN OF A POTENT D-PEPTIDE HIV-1 ENTRY INHIBITOR WITH A STRONG BARRIER TO RESISTANCE

Reproduced with permission from Brett D. Welch*, J. Nicholas Francis*, Joseph S. Redman, Suparna Paul, Matthew T. Weinstock, Jacqueline D. Reeves, Yolanda S. Lie, Frank G. Whitby, Debra M. Eckert, Christopher P. Hill, Michael J. Root, and Michael S. Kay. "Design of a Potent D-Peptide HIV-1 Entry Inhibitor with a Strong Barrier to Resistance." Journal of Virology, Vol. 84, No. 21, pp. 11235-11244; Nov. 2010, DOI: 10.1128/JVI.01339-10

* These authors contributed equally to this work.

JOURNAL OF VIROLOGY, Nov. 2010, p. 11235–11244 Vol. 84, No. 21
0022-538X/10/$12.00 doi:10.1128/JVI.01339-10

Design of a Potent D-Peptide HIV-1 Entry Inhibitor with a Strong Barrier to Resistance▽

Brett D. Welch,[1]† J. Nicholas Francis,[1]† Joseph S. Redman,[1] Suparna Paul,[2] Matthew T. Weinstock,[1] Jacqueline D. Reeves,[3] Yolanda S. Lie,[3] Frank G. Whitby,[1] Debra M. Eckert,[1] Christopher P. Hill,[1] Michael J. Root,[2] and Michael S. Kay[1]*

Department of Biochemistry, University of Utah School of Medicine, Salt Lake City, Utah 84112[1]; Department of Biochemistry and Molecular Biology, Thomas Jefferson University, Philadelphia, Pennsylvania 19107[2]; and Monogram Biosciences, 345 Oyster Point Blvd., South San Francisco, California 94080[3]

Received 23 June 2010/Accepted 6 August 2010

The HIV gp41 N-trimer pocket region is an ideal viral target because it is extracellular, highly conserved, and essential for viral entry. Here, we report on the design of a pocket-specific D-peptide, PIE12-trimer, that is extraordinarily elusive to resistance and characterize its inhibitory and structural properties. D-Peptides (peptides composed of D-amino acids) are promising therapeutic agents due to their insensitivity to protease degradation. PIE12-trimer was designed using structure-guided mirror-image phage display and linker optimization and is the first D-peptide HIV entry inhibitor with the breadth and potency required for clinical use. PIE12-trimer has an ultrahigh affinity for the gp41 pocket, providing it with a reserve of binding energy (resistance capacitor) that yields a dramatically improved resistance profile compared to those of other fusion inhibitors. These results demonstrate that the gp41 pocket is an ideal drug target and establish PIE12-trimer as a leading anti-HIV antiviral candidate.

The HIV envelope protein (Env) mediates viral entry into cells (11). Env is cleaved into surface (gp120) and transmembrane (gp41) subunits that remain noncovalently associated to form trimeric spikes on the virion surface (16). gp120 recognizes target cells by interacting with cellular receptors, while gp41 mediates membrane fusion. Peptides derived from heptad repeats near the N and C termini of the gp41 ectodomain (N and C peptides) interact in solution to form a six-helix bundle, representing the postfusion structure (3, 55, 56). In this structure, N peptides form a central trimeric coiled coil (N trimer), creating grooves into which C peptides bind. This structure, in conjunction with the dominant-negative inhibitory properties of exogenous N and C peptides, suggests a mechanism for Env-mediated entry (10, 22, 58–60).

During entry, gp41 forms an extended prehairpin intermediate that leaves the exposed N-trimer region vulnerable to inhibition for several minutes (18, 35). This intermediate ultimately collapses as the C-peptide regions bind to the N-trimer grooves to form a trimer of hairpins (six-helix bundle), juxtaposing viral and cellular membranes and inducing fusion. Enfuvirtide (Fuzeon), the only clinically approved HIV fusion inhibitor, is a C peptide that binds to part of the N-trimer groove and prevents six-helix bundle formation in a dominant-negative manner (61). Enfuvirtide is active in patients with multidrug resistance to other classes of inhibitors and is a life-prolonging option for these patients (30, 31). However, enfuvirtide use is restricted to salvage therapy due to several limitations, including (i) high dosing requirements (90 mg, twice-daily injections), (ii) high cost (~$30,000/year/patient in the United States), and (iii) the rapid emergence of resistant strains (21, 47).

A deep hydrophobic pocket at the base of the N-trimer groove is an especially attractive inhibitory target because of its high degree of conservation (3, 12, 48), poor tolerance to substitution (4, 34), and critical role in membrane fusion (2). Indeed, this region is conserved at both the amino acid level (for gp41 function in membrane fusion) and the nucleotide level (for the structured RNA region of the Rev-responsive element). Enfuvirtide binds to the N-trimer groove just N terminal to the pocket and is significantly more susceptible to resistance mutations than 2nd-generation C-peptide inhibitors, such as T-1249, that also bind to the pocket (8, 13, 29, 44, 46, 47, 58).

Peptide design, molecular modeling, and small-molecule screening have produced a diverse set of compounds that interact with the gp41 pocket and inhibit HIV-1 entry with modest potency, but often with significant cytotoxicity (7, 14, 15, 17, 23, 24, 26, 34, 51, 54). The first direct evidence that pocket-specific binders are sufficient to inhibit HIV entry came with the discovery of protease-resistant D-peptides identified using mirror-image phage display (12). In this technique, a phage library is screened against a mirror-image version of the target protein (synthesized using D-amino acids) (50). By symmetry, mirror images (D-peptides) of the discovered sequences will bind to the natural L-peptide target. As the mirror images of naturally occurring L-peptides, D-peptides cannot be digested by natural proteases. Protease resistance provides D-peptides theoretical treatment advantages of extended survival in the body and possible oral bioavailability (41, 42, 49).

* Corresponding author. Mailing address: Department of Biochemistry, University of Utah School of Medicine, 15 N. Medical Drive East, Rm. 4100, Salt Lake City, UT 84112-5650. Phone: (801) 585-5021. Fax: (801) 581-7959. E-mail: kay@biochem.utah.edu.
† These authors contributed equally to this work.
▽ Published ahead of print on 18 August 2010.

These 1st-generation D-peptide entry inhibitors possess potency against a laboratory-adapted isolate (HXB2) at low to mid-μM concentrations (12). We previously reported an affinity-matured 2nd-generation D-peptide called PIE7, *p*ocket-specific *i*nhibitor of *e*ntry 7 (57). A trimeric version of PIE7 is the first high-affinity pocket-specific HIV-1 inhibitor and has potency against X4-tropic (HXB2) and R5-tropic (BaL) strains at sub-nM concentrations. However, significant further optimization is required to create a robust clinical candidate for two reasons. First, this D-peptide is much less potent (requiring high nM concentrations) against JRFL, a primary R5-tropic strain. Therefore, improved PIE potency is necessary to combat diverse primary strains. Second, by improving the affinity of our inhibitors for the pocket target, we hope to provide a reserve of binding energy that will delay the emergence of drug resistance, as described below.

We and others have reported a potency plateau for some gp41-based fusion inhibitors that is likely imposed by the transient exposure of the prehairpin intermediate (9, 27, 53, 57). For very high-affinity inhibitors, association kinetics (rather than affinity) limits potency so that two inhibitors with significantly different affinities for the prehairpin intermediate can have similar antiviral potencies. We proposed that overengineering our D-peptides with substantial affinity beyond this potency plateau would provide a reserve of binding energy that would combat affinity-disrupting resistance mutations (57). Such a resistance capacitor should also prevent the stepwise accumulation of subtle resistance mutations in Env by eliminating the selective advantage that such mutants would otherwise confer.

Here, we report on the design and characterization of a 3rd-generation pocket-specific D-peptide, PIE12-trimer, with ~100,000-fold improved target binding compared to that of the best previous D-peptide, significantly broadened inhibitory potency, and an enhanced resistance capacitor that provides a strong barrier to viral resistance. We achieved this increased potency via structure-guided phage display and crosslinker optimization. PIE12-trimer has a dramatically improved resistance profile compared to the profiles of earlier D-peptides, as well as those of enfuvirtide and T-1249. These results validate the resistance capacitor hypothesis and establish PIE12-trimer as a leading anti-HIV therapeutic candidate.

MATERIALS AND METHODS

Peptide synthesis. All peptides were synthesized as described previously (57). All dimers and trimers except PIE12-trimer were made essentially as described using bis-dPEG$_5$ NHS ester (where PEG is polyethylene glycol and NHS is *N*-hydroxysuccinimide; catalog no. 10224; Quanta BioDesign); PIE12-trimer was synthesized using the following higher-yield protocol. PIE12-GK (2 mM) was reacted with bis-dPEG$_5$ NHS ester crosslinker (1 M stock in dimethylacetamide) at a 1:20 (peptide/PEG) molar ratio in 100 mM HEPES (pH 7.8 to 8) for 90 s at room temperature (RT). The reaction was stopped by addition of acetic acid to 5% and 3 M guanidine HCl (GuHCl) and purified by reverse-phase high-pressure liquid chromatography (RP-HPLC; C_{18} column; Vydac). This product (~3 to 5 mM) was reacted at a 2:1 molar excess with PIE12-GKK in dimethylacetamide buffered by triethylamine (pH 7.5) for 75 min and purified by RP-HPLC (C_{18} column; Vydac).

Phage display vector design. Use of a commercially available phage library cloning system (NEB) allowed us to relocate cloning sites away from the flanking regions (38). We redesigned the regions immediately outside the flanking residues in our cloning vector in order to structurally isolate them and minimize any bias caused by flanking sequence randomization. Our library peptides are displayed as fusions to the phage p3 protein, which contains an N-terminal leader sequence that is cleaved by *Escherichia coli* secretion signal peptidases. In the original vector, the N-terminal flanking residues of the library peptides are immediately adjacent to the secretion signal. Due to proximity to the secretion signal cleavage site, it is likely that randomization of these residues would differentially affect library-p3 protein secretion and peptide presentation on the phage surface. This bias would confound the selection of N-terminal flanking sequences solely on the basis of their affinity for the N trimer. To avoid this bias, we introduced a five-amino-acid spacer to structurally isolate the cleavage site from the randomized N-terminal flanking residues. We choose the N-terminal residues (KIEEG) from maltose binding protein (MBP) as the spacer sequence, since MBP is very efficiently cleaved during secretion from *E. coli*.

We have observed that mutations in the C-terminal sequence that links the peptide to the phage p3 protein can also create undesirable selection bias (presumably by allowing the C terminus of the D-peptides to form a continuous helix with the N terminus of p3, thus enhancing peptide presentation to the target) (57). Therefore, a flexible GGGS spacer was inserted after the C-terminal flanking residues to structurally isolate them from the N terminus of p3.

To validate this new phage display vector, we used it to clone an earlier PIE (PIE2) along with a mutant (PIE2-AAA) which had previously been observed to enhance phage affinity for the pocket target via mutation of the linker between the library peptide and p3, although this mutation did not enhance inhibitor potency when incorporated into a D-peptide (57). We assayed the target binding affinity of the resultant phage (Φ) and compared it to that of phage produced with the previous phage vector. In the previous phage vector, PIE2-AAA-Φ "cheated" in order to bind to the target with an ~70-fold more affinity than PIE2-Φ, but this difference was abolished in the modified vector (data not shown). Furthermore, sequencing revealed that N-terminal flanking residues from the amplified phage library prior to selection were random, indicating a lack of bias due to signal peptidase cleavage efficiency.

Phage display. An 8-mer flanking library phage display was performed essentially as described previously (57). Four rounds of mirror-image solution-phase phage display were performed by incubating (for 2 h at RT) 10^{10} phage (amplified from the previous round) with 10 nM biotinylated D-IZN17 (a mimic of the D-peptide gp41 pocket target) in the presence of escalating soluble competitor (L-2K-PIE2) (10, 30, 90, and 360 μM for rounds 1 to 4, respectively) (57). Phage-bound D-IZN17 was rapidly captured from solution using Dynal T1 streptavidin-coated magnetic beads (Invitrogen) and briefly washed 3 times with 500 μl of 0.1% Tween 20 in Tris-buffered saline (wash buffer contained 100 μM D-biotin for the 1st wash). Phage was eluted in 50 μl of glycine (pH 2.2) elution buffer (10 min at RT) and neutralized with 7.5 μl of 1 M Tris, pH 9.1. The amplified phage library was sequenced prior to the first round of selection to confirm randomization, and preamplified eluted phage was sequenced following each round. All phage binding experiments were performed using the same protocol described above using 270 μM L-PIE2 soluble competitor. A 7-mer phage display was performed using a similar protocol.

Crystal growth and data collection. The original form of PIE12 (see Table 1) contains a C-terminal GK extension and did not yield highly diffracting crystals in complex with IQN17, a gp41 pocket mimic. Variants of PIE12 instead containing an N-terminal K or KG extension (K-PIE12, KHPCDYPEWQWLCEL; KG-PIE12, KGHPCDYPEWQWLCEL) crystallized in complex with IQN17 under a variety of conditions. In each case, the reservoir (850 μl) comprised a solution from a commercially available crystallization screen, and the crystallization drop was prepared by mixing 0.3 or 0.5 μl of the IQN17-PIE12 or IQN17-PIE71 protein solution (1:1.1 molar ratio, 10 mg/ml total in water) with 0.3 μl of the reservoir solution. Crystals typically grew in 1 to 10 days. All crystals were grown by sitting-drop vapor diffusion. IQN17-PIE12 form I crystals (KG-PIE12) were grown at 21°C in Hampton Scientific condition Screen II 48 (10% PEG 20,000, 0.1 M bicine, pH 9.0, 2% dioxane). IQN17-PIE12 form II crystals (KG-PIE12) were grown at 21°C in Emerald Biosystems condition Cryo-II 37 (50% ethylene glycol, 0.1 M imidazole, pH 8.0). IQN17-PIE12 form III crystals (K-PIE12) were grown at 4°C in Emerald Biosystems condition Cryo-II 25 (40% 2-methyl-2,4-pentanediol (MPD), 0.1 M *N*-cyclohexyl-3-aminopropanesulfonic acid (CAPS) [pH 10.5]). IQN17-PIE71 crystals were grown at 21°C in Qiagen PACT crystallization condition G4 (20% PEG 3350, 0.2 M potassium thiocyanate, 0.1 M bis-Tris propane, pH 7.5).

Crystals were mounted in a nylon loop and either directly cryocooled by plunging them into liquid nitrogen or cryocooled following brief (20 s) immersion in 20 μl crystallization buffer with 30% (IQN17-PIE12) or 15% (IQN17-PIE71) added glycerol. Crystals were maintained at 100 K during data collection. Data were collected either in the laboratory using a rotating copper anode X-ray generator or at a synchrotron beam line. Data were processed using the DENZO and SCALEPACK programs (40). All structures were determined by molecular replacement using the PHASER program (33) with IQN17-PIE7 as the search

model. The models were rebuilt using the O program (25) and refined against a maximum-likelihood target function using the REFMAC program (36). Structures were checked using the MolProbity program (6) (see Table 2 for data and refinement statistics).

Explanation of Lys placement. We were concerned that direct C-terminal addition of Lys would not be well tolerated because the D-peptide C-terminal region forms an α helix critically involved in the pocket-binding interface, with the C terminus itself being amidated for helix stability. Therefore, we inserted a Gly between the original C terminus of PIE7 and the C-terminal Lys, both to cap the helix and to separate the Lys from the binding interface. Unexpectedly, PIE7-GK-monomer is slightly more potent than PIE7 (see Table 1). A version of PIE7 containing an N- and C-terminal Lys (K-PIE7-GK) has the same potency as PIE7-GK (data not shown), indicating a beneficial effect imposed by the C-terminal Gly-Lys, as opposed to a deleterious effect created by a single Lys at the N terminus. This benefit is likely the reason that the linkage consisting of an ~22-Å cross-linker at the C terminus whose spacer arm consists of 5 PEGs (C_5C) results in a potency slightly superior to that of the N_5C linkage (see Table 1).

Viral infectivity assays. Pseudovirion infectivity assays were performed as described previously (57). Purified lyophilized inhibitors were dissolved in water (monomers) or 50 mM HEPES, pH 7.5 (dimers and trimers), to make high-concentration stocks. For HEPES-containing samples, all media were adjusted so that the HEPES content matched that in the sample with the highest HEPES concentration (typically, ~1 mM). HEPES at higher concentrations (e.g., 3 mM) enhanced infectivity up to ~15% but had minimal effect at ≤0.5 mM. The Monogram Biosciences PhenoSense Entry and peripheral blood mononuclear cell (PBMC) assays were performed as described previously (43, 52).

CD studies. Samples were prepared with 2 μM IZN17, a 1.1× molar ratio of inhibitor to target binding sites, phosphate-buffered saline (PBS; 50 mM sodium phosphate, 150 mM NaCl, pH 7.4), and 2 M GuHCl in a total volume of 2.5 ml. Thermal melts were performed by melting the sample in a square 1-cm cuvette from 25°C to 90°C (or 93°C for PIE12-trimer) in 2°C increments with 2 min of equilibration. To show reversibility, reverse melts were performed on each sample from 90°C to 30°C in 10°C increments with 5 min of equilibration. Data were averaged from a 30-s collection on an Aviv model 410 circular dichroism (CD) spectrapolarimeter.

For each sample, the CD data followed a smooth sigmoid transition as the sample was heated or cooled. The data were smoothed in the Kaleidagraph program (Synergy Software) using 2 points from both sides. The derivative value of the smoothed data was used to determine the point with the steepest rate of change on the melt curve, which is the melting temperature (T_m).

Passaging studies. Laboratory-adapted HIV-1 strain NL4-3 was generated by transient transfection of proviral DNA (pNL4-3) into 293T cells using Lipofectamine (Invitrogen). Cell-free supernatants containing virus were collected 48 h posttransfection and used to infect 5×10^5 CEM-1 cells in RPMI 1640 medium (0.5 ml). Virus was serially propagated once a week by 1:5 dilution of cell-free viral supernatants into fresh CEM-1 cells (5×10^5 cells, 0.5 ml) in the absence or presence of inhibitor (PIE7-dimer, PIE12-dimer, or PIE12-trimer). Viral titers were monitored biweekly by p24 antigen enzyme-linked immunosorbent assay (PerkinElmer). The inhibitor concentration started at approximately the 50% inhibitory concentrations (IC_{50}s; 20 nM for PIE7-dimer; 1 nM for PIE12-dimer, and PIE12-trimer) and was raised 1.5- to 2-fold when p24 antigen levels in inhibitor-containing cultures approached that in inhibitor-free cultures (usually 2 to 3 weeks for PIE7-dimer). PIE12-dimer and PIE12-trimer required a slower escalation strategy with prolonged incubation at a fixed inhibitor concentration for 5 to 15 weeks before escalation.

To identify PIE7-dimer escape mutations, viral RNA was isolated from cell-free supernatants of at least two cultures independently propagated in either the presence (resistant virus) or absence (control virus) of inhibitor (Qiagen RNA purification kit). Env cDNA was generated by reverse transcription (Eppendorf cMaster RTplus system and cMaster reverse transcription kit), amplified by PCR, and sequenced in five stretches (Thomas Jefferson University Nucleic Acid Facility). To confirm selected mutations in the gp41 N-peptide region, the cDNA segment encoding the gp41 ectodomain was reamplified by PCR and subcloned into the pAED4 vector, and the plasmid DNA from three or more individual clones was sequenced. The substitutions E560K and V570I were observed in all sequences from PIE7-dimer-resistant virus but were not observed in any sequence from control virus. An expression plasmid for HXB2 Env (pEBB_HXB2 Env) incorporating these substitutions was generated using site-directed mutagenesis (QuikChange; Stratagene) and was utilized in the pseudoviral infectivity assay described above.

Protein Data Bank accession numbers. The Protein Data Bank (PDB) accession numbers for the PIE12-IQN17 complex are 3L35, 3L36, and 3L37 for crystal forms I, II, and III, respectively, and 3MGN for the PIE71-IQN17 complex.

TABLE 1. D-peptide inhibition data[c]

Sample	Sequence	IC_{50} (nM)[a]	
		HXB2	JRFL
PIE7	KGA[PIE7]AA	620[b]	24,000[b]
PIE7-GK	GA[PIE7]AAGK	390	16,000
PIE7-GKK	GA[PIE7]AAGKK	380	19,000
PIE12	HP[PIE7]ELGK	37	580
PIE13[c]	HP[PIE7]KL	41	1,500
PIE14	HP[PIE7]RLGK	33	1,100
PIE15	HA[PIE7]ELGK	67	1,400
$N_9N(PIE7)_2$	$(KGA[PIE7]AA)_2$	1.9[b]	2,300[b]
$N_5C(PIE7)_2$	GA[PIE7]AAGKKGA[PIE7]AA	0.6	300
$C_5C(PIE7)_2$	$(GA[PIE7]AAGK)_2$	0.5	200
$C_5C(PIE12)_2$	$(HP[PIE7]ELGK)_2$	0.4	14
$N_9N(PIE7)_3$	$(KGA[PIE7]AA)_3$[d]	0.3[b]	220[b]
$C_5C(PIE7)_3$	$(GA[PIE7]AAGK)_3$[d]	0.1	6.7
$C_5C(PIE12)_3$	$(HP[PIE7]ELGK)_3$[d]	0.5	2.8
C37		1.4[b]	13[b]
Enfuvirtide		3.7[b]	5.0[b]

[a] The IC_{50} standard error of the mean is <25% for duplicate assays for all values.
[b] Values are from reference 57.
[c] PIE13 does not include a C-terminal GK extension because its C-terminal flanking sequence contains a Lys residue.
[d] The central peptide of each trimer has two tandem Lys residues (not shown).
[e] PIE7, CDYPEWQWLC, or PIE7 core motif.

RESULTS

Structure-guided phage display to optimize flanking residues. PIE inhibitors consist of a short core sequence surrounded by a disulfide bond that imparts structural rigidity required for binding (Table 1) (12). The large jump in affinity between our 1st-generation (12) and 2nd-generation (57) inhibitors was accomplished by optimizing this core sequence. There were also four fixed flanking residues outside the disulfide that arose from phage library cloning restrictions, Gly-Ala on the N terminus and Ala-Ala on the C terminus. Interestingly, our cocrystal structures of D-peptides in complex with a mimic of its gp41 pocket target (IQN17) reveal significant contacts between these presumed inert flanking residues and the pocket (12, 57). Thus, we reasoned that their optimization would likely lead to improved D-peptide affinity for the pocket.

To optimize these flanking residues, we used a commercially available phage library cloning system (NEB) that allowed us to relocate cloning sites away from the flanking regions (38). We redesigned the regions immediately outside the flanking residues in our cloning vector in order to structurally isolate them and minimize any bias caused by flanking sequence randomization. Using this vector, we constructed a phage library that varied only these four residues in the context of our previously optimized PIE7 core sequence (XXCDYPEWQW LCXX). After four rounds of panning, our phage library showed ~100-fold improved binding to a gp41 pocket mimic (D-IZN17) compared to that of clonal PIE7 phage with the original GA/AA flanking sequence. We extensively sequenced this phage pool to identify a consensus sequence, H(A/P)-[PIE7 core]-(R/K/E)L, as well as five dominant individual sequences. Using a phage clone binding assay, we found that these sequences bound the gp41 pocket 70- to 900-fold more tightly than PIE7, with PIE12 (HP-[PIE7 core]-EL) having the highest affinity (data not shown).

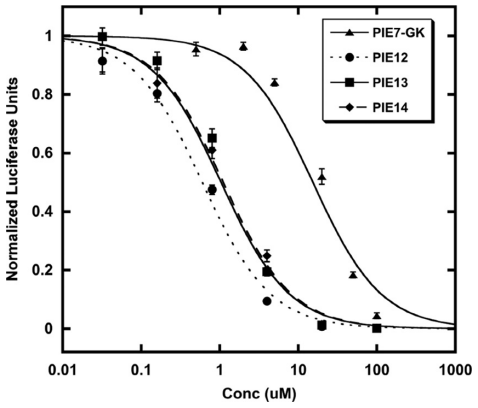

FIG. 1. Optimization of flanking residues enhances PIE potency. Each point represents the average of quadruplicate measurements from a representative pseudovirion entry inhibition assay (JRFL strain) normalized to the measurement for an uninhibited control. Error bars represent the standard errors of the means. PIE12 is ~2-fold more potent than PIE13 or PIE14 and is ~25-fold more potent than PIE7-GK.

Enhanced potency of 3rd-generation D-peptides. We synthesized D-peptides corresponding to the top three phage sequences in the binding assay (PIE12, PIE13, and PIE14) and tested their antiviral potencies in a pseudovirion entry assay (Table 1 and Fig. 1). Pairwise comparisons of both phage binding and inhibitor potency indicate that Pro is preferred over Ala at position 2 and Glu is preferred over Arg or Lys at position 13. As predicted from the phage binding assay, PIE12 has the best potency and is ~40-fold more potent than PIE7 (our best previously reported monomer) against strain JRFL.

Crystal structure of PIE12. To better understand the sources of PIE12's improved binding and potency, we crystallized PIE12 in complex with the N-trimer pocket mimic IQN17. Data were collected from three crystal forms (Table 2) at between 1.45- and 1.55-Å resolution. Each IQN17 trimer from the three crystal forms reported here and from the PIE7 structure (PDB accession number 2R5D) agreed well with one another (root mean square deviation [RMSD], 0.6 to 1.2 Å) on the basis of the least-squares overlap on all C_α atoms (residues 1 to 45 of all three chains). The structures suggest two sources of the improved affinity of PIE12 for IQN17 compared to that of PIE7. First, the new N-terminal flank residues (His1 and Pro2) form favorable ring stacking interactions with the pocket (IQN17-Trp571) (Fig. 2). Second, the substitution of Leu for Ala in the C-terminal flank sequence buries an additional ~50-Å^2 hydrophobic surface area in the pocket. Neither of these new interactions with the flanking sequence perturbs the original pocket-binding structure of the core PIE7 residues. Importantly, the structures reveal that PIE12's improved affinity does not result from new interactions with less conserved

TABLE 2. PIE12 and PIE71 crystallographic data and refinement statistics

Data	Result for PIE12 crystal:			Result for PIE71 crystal
	Form I	Form II	Form III	
Space group	$P2_1$	R3	P321	$P2_1$
Resolution (Å)	30.0–1.55 (1.61–1.55)[a]	30.0–1.45 (1.50–1.45)	30.0–1.45 (1.50–1.45)	30.0–1.40 (1.45–1.40)
No. of reflections measured	113,335	98,687	186,351	468,599
No. of unique reflections	25,088	10,475	14,802	82,774
Redundancy	4.5	9.4	12.6	5.7
Completeness (%)	86.5 (66.8)	97.1 (80.1)	99.7 (96.6)	98.2 (97.6)
$<I/\sigma I>$[b]	18 (2.4)	19 (3.1)	17 (2.7)	15 (2.0)
Mosaicity (degree)	0.44	0.37	0.45	0.29
R_{sym}[c]	0.051 (0.250)	0.058 (0.102)	0.107 (0.235)	0.052 (0.316)
Refinement				
Resolution (Å)	30.0–1.55 (1.59–1.55)	30.0–1.45 (1.49–1.45)	30.0–1.45 (1.49–1.45)	30.0–1.40 (1.44–1.40)
No. of reflections used for refinement	23,765	9,448	13,629	80,532
No. of reflections in R_{free}[d] set	1,273	1,026	1,136	1,654
R_{cryst}[e]	0.232 (0.465)	0.234 (0.301)	0.243 (0.299)	0.261 (0.306)
R_{free}	0.288 (0.624)	0.264 (0.392)	0.278 (0.350)	0.288 (0.335)
RMSD bonds (Å)/angles (degrees)	0.012/1.440	0.013/1.693	0.010/1.530	0.009/1.094
<B>[g]				
All atoms (Å^2)/no. of atoms	23.7/1,172	31.9/384	29.2/384	Mol[f] 1, 24.3/1,555; mol 2, 36.0/1,491
PIE12 molecules only (Å^2)/no. of atoms	21.3/420	30.8/144	25.9/144	Mol 1, 18.3/368; mol 2, 39.9/322
Water molecules (Å^2)/no. of water atoms	32.0/197	38.0/36	40.6/49	39.9/389
ϕ/Ψ[h] most favored (%)	100	98.1	100	99.0

[a] Values in parentheses refer to data in the high-resolution shell.
[b] $<I/\sigma I>$, average intensity of a group of reflections divided by the average standard deviation (sigma) of the same group of reflections.
[c] $R_{sym} = \Sigma|I - <I>|/\Sigma I$, where I is the intensity of an individual measurement and $<I>$ is the corresponding mean value.
[d] R_{free} is the same as R_{cryst} calculated with a randomly selected test set of reflections that were never used in refinement calculations.
[e] $R_{cryst} = \Sigma||Fo| - |Fc||/\Sigma|Fo|$, where $|Fo|$ is the observed and $|Fc|$ is the calculated structure factor amplitude.
[f] Mol, molecule.
[g] <B>, temperature factor.
[h] ϕ/ψ, dihedral angles.

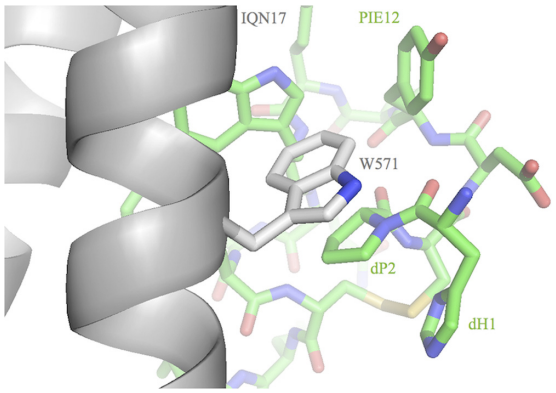

FIG. 2. Crystal structure of PIE12 binding to IQN17. Trp571 of the gp41 pocket (gray) and the N-terminal flank residues (dH1 and dP2) of PIE12 (green) appear to stabilize binding via ring-stacking interactions. The disulfide bond (yellow) is shown in the background.

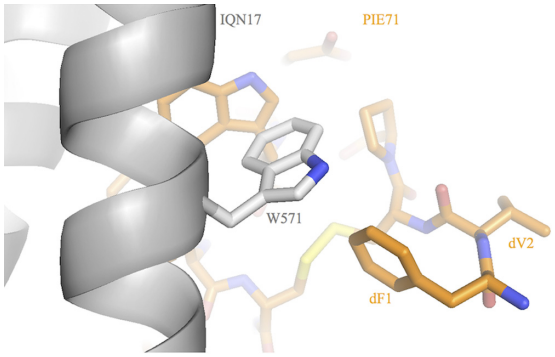

FIG. 3. Crystal structure of PIE71 binding to IQN17. The N-terminal flank residues (dF1 and dV2) of PIE71 (orange) are directed away from the pocket compared to the structure in PIE12 (Fig. 2). The disulfide bond (yellow) is shown in the background.

regions outside the pocket that might render PIE12 more vulnerable to resistance mutations.

Discovery and structure of a 7-mer D-peptide. The core sequence of PIE7 and PIE12 comprises 8 residues flanked by cysteines (8-mer). Modeling based on our 8-mer D-peptide/IQN17 crystal structures suggests that a 7-mer core is compatible with pocket binding of the WXWL consensus and formation of a disulfide bond (57). Previously, we saw that decreasing the size of the PIE core (from 10 to 8 residues) led to dramatically increased pocket binding (57), so we reasoned that further decreasing the size of the core might lead to additional potency gains. To explore this alternative geometry, we used a mirror-image discovery process similar to that employed with 8-mers to identify a 7-mer, PIE71 (FVCPPEWRWLCDL). PIE71 contains the same WXWL motif found in 8-mer and 10-mer pocket binders and inhibits strain HXB2 entry with an IC_{50} of 410 nM (data not shown), which is ~1.5 fold better than that of PIE7 but an order of magnitude worse than that of PIE12.

To gain a better understanding of the 7-mer binding solution, we determined a cocrystal structure of PIE71 in complex with IQN17 (Table 2). The key residues involved in the binding interface (WXWL) adopt nearly superposable conformations to those observed in PIE7 and PIE12, as do the C-terminal flank residues. However, the two structures deviate significantly at the N terminus (Fig. 2 and 3). Specifically, the 7-mer's disulfide bond is shifted much closer to the pocket, which directs the N-terminal flank residues away from the pocket region. As a result, the N-terminal flanking residues (Phe-Val) only graze the pocket, whereas PIE12's N-terminal flanking residues have an intimate interaction. So although the 7-mer is compatible with pocket binding, the smaller core is too constrained to allow optimal binding of the flank residues to the pocket. Due to this decreased binding interface and therefore decreased potency, we decided not to pursue the 7-mer geometry further.

Optimization of crosslinker length and geometry. We previously took advantage of the trimeric nature of the gp41 pocket target to geometrically increase the PIE7 binding affinity by cross-linking it into dimers and trimers (57). PIE7 has an N-terminal lysine, which furnishes a unique primary amino group (the N terminus is acetylated) and which was added for solubility. This lysine was used to produce dimers via reaction with a bis-PEG NHS ester crosslinker (NHS esters selectively react with primary amino groups). Trimers were produced by cross-linking two PIE7s to a central peptide with two lysines at the N terminus (2K-PIE7).

We hypothesized that the strength of the avidity effect is related to the length of the crosslinker and that shorter crosslinkers that still allow simultaneous binding to multiple pockets could strengthen potency. For the original N- to N-terminal linkage, we used a crosslinker with an ~35-Å spacer arm consisting of 9 PEG units (N_9N linkage). However, our crystal structures of D-peptides in complex with IQN17 reveal that C- to C-terminal or N- to C-terminal linkages could be significantly shorter and could be spanned by an ~22-Å crosslinker whose spacer arm consists of 5 PEGs (C_5C and N_5C linkages). Therefore, we relocated Lys to the C terminus of PIE7 (PIE7-GK) in order to make the N_5C heterodimers and C_5C homodimers (see Materials and Methods for additional details).

The resulting N_5C- and C_5C-PIE7-dimers have similar potencies that are significantly enhanced compared to the potency of our previous N_9N-PIE7-dimer (Table 1 and Fig. 4A). On the basis of these data, we chose C_5C connections as our standard linker, since they are simpler to produce than the hetero-N_5C linkage. Here, all dimers and trimers use the C_5C linkage unless otherwise specified. Combining our new optimized flanking residues and linkages, we produced PIE12-dimer and PIE12-trimer. Both are extremely potent against the difficult-to-inhibit primary strain JRFL (low-nanomolar IC_{50}s; Fig. 4B; Table 1), being up to 2 orders of magnitude more potent than our best previously described D-peptide (N_9N PIE7-trimer) (57).

Breadth against a diverse multiclade panel. HIV-1 has jumped from chimpanzees to humans at least three separate times, giving rise to groups M, N, and O (19). The main group (group M) accounts for >99% of all HIV-1 infections world-

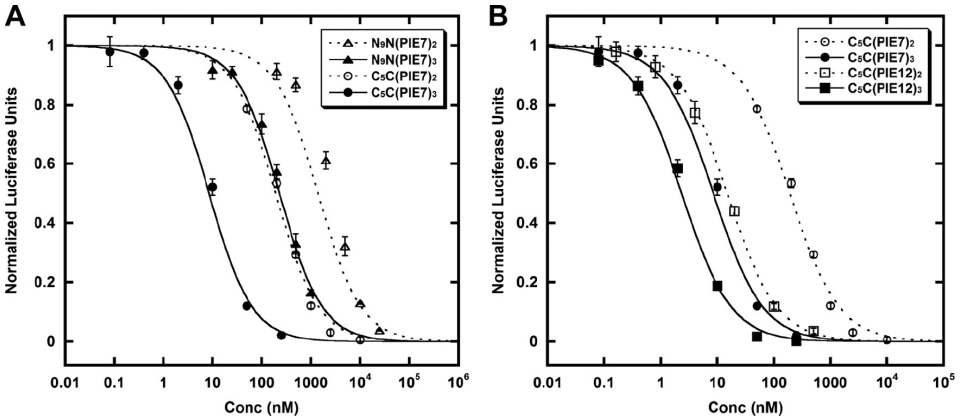

FIG. 4. Optimization of linkage geometry. Each point represents the average of quadruplicate measurements from a representative pseudovirion entry inhibition assay (JRFL strain) normalized to the measurement for the uninhibited control. Error bars represent the standard errors of the means. (A) Comparison of N_9N to C_5C linkages; (B) PIE7 versus PIE12-dimers and trimers (all C_5C linkages).

wide (32). HIV's high mutation rate has led to the emergence of diverse subtypes within group M that are categorized as clades A to D, F to H, J, and K and various circulating recombinant forms (CRFs; e.g., AE and BF). In 2000, clades A to D were estimated to represent >90% of HIV infections (39); however, in recent years CRFs have become more prevalent (1). Different subtypes contain up to 35% sequence diversity in Env, often causing antibodies raised against a particular strain to be ineffective against others (20).

To ensure that our pocket-specific D-peptides are potent and broadly neutralizing against the most common subtypes of HIV, we measured the potency of PIE7-trimer, PIE12-trimer, and PIE12 (with enfuvirtide as a control inhibitor) using the PhenoSense Entry pseudovirion assay (Monogram Biosciences) (Table 3) (43). The inhibitors were tested against a panel of 23 viruses pseudotyped with clonal and polyclonal envelopes representing clades A to D, several CRFs, and enfuvirtide-resistant strains. Both PIE7 and PIE12-trimers potently inhibited all strains tested, though PIE12-trimer was generally a superior inhibitor (and in all cases more potent than enfuvirtide). While PIE12-monomer is much less potent than PIE12-trimer, it is also broadly active. Interestingly, PIE12-trimer is ~10-fold more potent than PIE7-trimer against polyclonal virus from clades B and C (samples amplified from patient plasma), which is consistent with a resistance capacitor mechanism for maintaining potency in the presence of various Env sequences. All of the D-peptide inhibitors are unaffected by enfuvirtide resistance mutations. Additionally, lack of inhibition against a murine leukemia virus (MLV) control indicates that these inhibitors are specific and nontoxic in this assay.

Breadth against replication-competent primary viral isolates on PBMCs. To more closely mimic *in vivo* infection and further establish inhibitory breadth, we also tested the ability of PIE7-trimer, PIE12-trimer, and PIE12 to inhibit PBMC infection by replicating primary strains, again with enfuvirtide as a control (Table 4). These data confirm the potent and broad inhibitory activities of PIE7 and PIE12-trimer against all group M strains tested, including several CRFs. Toxicity was not observed on these cells at inhibitor concentrations up to 1 μM (the highest concentration tested), demonstrating a high therapeutic index for the trimers. Interestingly, the inhibitors are more potent in this assay than in the PhenoSense Entry assay, which may be due to differential receptor expression levels between the two cell types (45).

Notably, two group O strains were also tested in this assay and are much less sensitive to inhibition than group M strains. Group O contains several mutations (compared to the sequence of group M) in the pocket, including Q567R, T569S, K574R, Q577R, and V580L. The crystal structures of PIE7 and

TABLE 3. PhenoSense Entry assay data

HIV-1 isolate	Subtype	IC_{50} (nM)			
		PIE7-trimer	PIE12-trimer	PIE12-monomer	Enfuvirtide
A[a]	A	5.5	4.1	2,300	18
92RW008	A	2.0	1.0	1,400	7.2
92UG031	A	18	4.2	2,600	20
94KE105	AC	16	0.7	1,900	13
CMU02	AE	32	12	1,500	16
B[a]	B	140	13	3,300	30
1168	B	54	31	4,700	140.0
BaL	B	2.0	2.5	1,700	10
ENFr1[a]	B	2.0	0.8	790	760
ENFr2[a]	B	0.7	1.0	300	5,400
HXB2	B	0.1	0.3	50	2.6
JRCSF	B	13	3.4	1,100	14
JRFL	B	21	5.7	1,900	7.9
NL4.3	B	0.3	0.4	150	62
SF162	B	3.4	4.5	940	34
98CN009	BC	0.4	0.4	320	7.9
93BR029	BF	1.5	0.9	750	12
C[a]	C	220.0	26	5,100	71
97ZA012	C	2.0	0.7	1,500	10
98IN022	C	1.1	1.1	820	6.9
21068	C	6.6	5.0	1,800	47
D[a]	D	3.1	3.2	820	17
92UG005	D	3.9	2.5	2,000	10
aMLV		>10,000	>10,000	>500,000	>15,000

[a] Polyclonal viral envelopes amplified from patient plasma.

TABLE 4. PBMC assay data

HIV-1 isolate	Subtype	IC_{50} (nM)			
		PIE7-trimer	PIE12-trimer	PIE12-monomer	Enfuvirtide
92UG029	A	1.6	0.7	290	190
92UG037	A	0.1	0.2	36	41
93TH073	AE	0.6	0.8	270	200
CMU02	AE	0.2	0.4	300	44
CMU06	AE	0.3	0.4	210	5.7
IIIB	B	0.3	0.8	140	28
BaL	B	0.2	0.3	72	20
JRCSF	B	0.1	0.1	120	7.0
JRFL	B	0.5	0.3	110	1.7
93BR019	BF	1.7	4.7	170	>1,000
92BR025	C	15	5.2	>1,000	310
93IN101	C	0.4	0.4	160	22
92UG001	D	0.8	4.5	230	180
92UG046	D	0.1	1.2	170	130
93BR020	F	0.2	0.4	190	59
93BR029	F	0.2	0.8	86	19
G3	G	0.3	1.2	310	23
RU570	G	0.3	0.4	480	37
BCF01	Group O	>1,000	>1,000	>1,000	330
BCF02	Group O	>1,000	440	>1,000	0.4

PIE12 in complex with IQN17 reveal that, of these residues, the D-peptide directly interacts only with K574 (via a hydrophobic interaction) and Q577 (via hydrogen bonds). Group O gp41 has several other mutations in the groove just outside the pocket (i.e., H564E) that could also affect PIE potency (e.g., by slowing the association rate). It will be interesting to analyze the effects of these mutations in a group M (e.g., strain HXB2 or JRFL) background to see if they are responsible for the loss of potency.

Evidence for a charged resistance capacitor. With the design of PIE12-trimer, we now observe strong evidence for a highly charged resistance capacitor in which the PIE12-trimer pocket-binding affinity vastly exceeds the inhibitory potency. Comparing PIE7 and PIE12-trimers, we observe similar potencies against pseudovirion entry (Fig. 4B; Table 1), although we expect their target affinities to be extremely different.

Due to extraordinarily slow off rates, direct measurements of the pocket affinities for PIE7 and PIE12-trimers via surface plasmon resonance, used for earlier D-peptides (57), were not possible. Since the binding affinity of inhibitors correlates with the stability of inhibitor-target complexes, we used thermal denaturation monitored by CD to measure the relative stabilities of each IZN17-inhibitor complex and infer the relative affinities of our ultra-high-affinity binders. The melts were performed in 2 M GuHCl to destabilize the complexes and shift their melting points into an observable range (below 100°C).

The normalized thermal melts for each IZN17-inhibitor complex are plotted in Fig. 5, with T_m values being shown in the key. As expected, PIE12-trimer forms the most stable complex and has a T_m 8°C higher than that of the next most stable inhibitor complex (PIE7-trimer). PIE12 also forms a more stable complex than PIE7, as expected. Our previous experience showed that improvements in monomer affinity translated to approximately squared and cubed improvements in the corresponding dimers and trimers (57). On the basis of PIE12-trimer's optimized C_5C linkage (35-fold improved antiviral potency over that of the trimer with an N_9N linkage; strain JRFL data) and the ~25-fold difference in monomer potency between PIE7 and PIE12 (JRFL data), we estimate that PIE12-trimer binds to gp41 $>10^5$-fold (35×25^3) more tightly than N_9N PIE7-trimer. This predicted binding at subfemtomolar concentrations translates to a resistance capacitor charged to ~6 kcal/mol against strain JRFL. Interestingly, the potency plateau lies at a slightly better potency for trimers than for dimers, likely due to their faster association rates (i.e., three versus two opportunities for initial collision with the target).

Selection of resistant strains. To measure the resistance profile of our D-peptide inhibitors and test our resistance capacitor hypothesis, we conducted viral passaging studies with escalating inhibitor concentrations to select for resistant strains. These studies initially used PIE7-dimer, which was available from our previous study (57) and inhibits the parental strain, NL4-3, with an IC_{50} of ~20 nM. By doubling the PIE7-dimer concentration every 2 to 3 weeks, we obtained stable viral cultures in 2,000 nM inhibitor within 20 weeks of propagation. In comparison, we were able to obtain high-level enfuvirtide resistance (>1,000-fold) in only ~3 weeks using a similar protocol (H. K. Steger et al., submitted for publication).

Sequencing the N-peptide region of PIE7-dimer-resistant viruses revealed two selected mutations: E560K and V570I. These substitutions in the context of HXB2 pseudovirions conferred ~400-fold resistance to PIE7-dimer. These mutations also dramatically weaken the binding of D-peptides to the gp41 pocket but not the C-peptide inhibitor C37 (M. J. Root et al., unpublished data). It is not obvious from the PIE7 structure how these mutations weaken PIE7 binding. Despite this loss of affinity, the escape mutations had a minimal effect on the

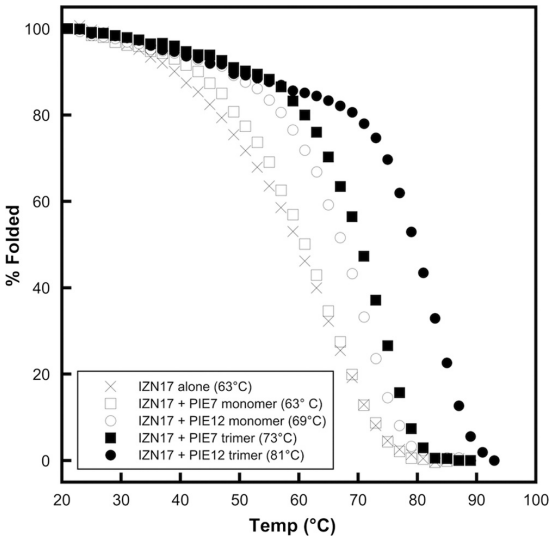

FIG. 5. Stability of D-peptide complexes. Normalized melting curves of IZN17 alone and with D-peptide inhibitors were monitored by CD in PBS–2 M GuHCl. T_m values are indicated in the key.

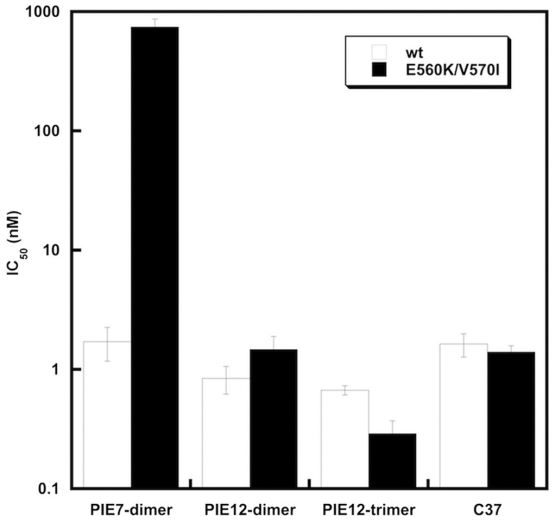

FIG. 6. Effect of PIE7-dimer resistance mutations on PIE7-dimer, PIE12-dimer, and PIE12-trimer potency. IC_{50}s against wild-type (wt) and PIE7-dimer-resistant (E560K/V570I) strain HXB2 pseudovirion entry are shown. The C-peptide inhibitor C37 is included as a control. Data represent the means from at least two independent experiments. Error bars represent the standard errors of the means.

potencies of PIE12-dimer and PIE12-trimer, as well as the C37 control inhibitor (Fig. 6). This result is predicted by the resistance capacitor hypothesis: affinity-disrupting escape mutations selected in the presence of weaker-binding inhibitors should be less disruptive to the potencies of tighter-binding inhibitors.

The rapid inhibitor escalation strategy utilized to generate PIE7-dimer resistance was not effective in generating HIV-1 resistant to PIE12-dimer or PIE12-trimer. Rather, the HIV-1 titer fell precipitously when inhibitor concentrations exceeded 20 nM (5 to 20 times the IC_{50}). Instead, we switched to a much slower escalation strategy with prolonged periods at stable inhibitor concentrations (5 to 15 weeks). Resistant virus emerged after 40 weeks of propagation in PIE12-dimer and after 65 weeks of propagation in PIE12-trimer. These observations suggest that a strong resistance capacitor profoundly delays selection of resistance mutations for these optimized fusion inhibitors.

Sequencing of the pocket region of PIE12-trimer-resistant viruses reveals only one mutation, Q577R. Interestingly, this substitution is present in nearly all group O isolates (including BCF01 and BCF02; Table 4) but is rare among group M isolates. Pseudovirions bearing Q577R confirm that this mutation confers substantial resistance to PIE12-trimer (data not shown). Examination of the PIE12 crystal structure shows that Q577 makes hydrogen bonds with Glu7 and Trp10 in PIE12, which may explain the disruptive effects of this mutation. Q577R's codon is predicted to disrupt the RRE stem-loop V structure, since it base pairs with the invariant W571 codon (Trp is encoded by only one codon).

DISCUSSION

PIE12-trimer is a D-peptide entry inhibitor with ~80-fold enhanced potency and an estimated >100,000-fold improved binding affinity compared to those of the best previously reported D-peptide. This dramatic improvement in affinity produces excellent breadth and a charged resistance capacitor to combat the emergence of resistance mutations. Indeed, PIE12-trimer was able to withstand the impact of resistance mutations to earlier D-peptides and required a much longer selection (65 weeks) to generate resistant strains. Ongoing work is exploring the mechanism of PIE7-dimer, PIE12-dimer, and PIE12-trimer resistance and its relationship to group O's insensitivity. A key question is whether HIV can develop resistance to these inhibitors independent of changes in affinity (e.g., kinetics) that are capable of maintaining viral fitness.

Viral escape affects even the newest class of FDA-approved HIV-1 drugs, integrase inhibitors. Resistance to raltegravir and corresponding treatment failure were observed in a significant subset of patients in both the phase II and III clinical studies (5), and corresponding resistance mutations can be seen within 4 weeks when resistant virus is selected in viral passaging studies (28). Our studies indicate that PIE12-trimer is a promising entry inhibitor that could overcome the limitations associated with the two currently approved entry inhibitors, enfuvirtide (high dosing, susceptibility to resistance) and maraviroc (Selzentry; effective only against R5 viruses) and may also prove to have a better resistance profile than even the newest class of HIV-1 inhibitors.

In addition to being a possible therapeutic agent, PIE12-trimer is an ideal candidate for a topical microbicide, as its protease resistance would allow it to withstand the protease-rich environment of the vaginal mucosa. In the absence of a safe and effective HIV vaccine, a topical microbicide to prevent the sexual transmission of HIV is an urgent unmet global health need. The ultimate utility of PIE12-trimer as a microbicide or therapeutic agent will be determined by advanced preclinical and clinical studies, including characterization of pharmacokinetics, *in vivo* toxicity, effectiveness in animal models of HIV infection (alone or in combination with other HIV inhibitors), and optimization of formulations for microbicide gels or vaginal rings.

More generally, the present work unequivocally shows that D-peptide inhibitors can be designed with high potency and specificity against natural L-protein targets. The D-peptide design methodology described here can be applied to diverse biomedical applications, particularly for the many viruses that share HIV's hairpin-closing entry mechanism (e.g., influenza virus, Ebola virus, respiratory syncytial virus, severe acute respiratory syndrome coronavirus, Dengue virus, and West Nile virus). Our resistance capacitor design strategy may also be generally applicable for treating other rapidly evolving diseases, especially when combined with recent advances in anticipating likely structural sources of drug resistance (37). Finally, the development of PIE12-trimer as a strong clinical candidate will allow D-peptide therapeutics to be evaluated *in vivo* to determine if their theoretical advantages warrant a prominent role as a new class of therapeutic agents.

ACKNOWLEDGMENTS

We thank Bob Schackmann and Scott Endicott (University of Utah Peptide Synthesis Core Facility) for peptide synthesis, Yu Shi for early 7-mer phage display, and Dong Han and Pham Phung (Monogram) for technical assistance with the PhenoSense Entry assay.

PBMC assays were performed by Southern Research Institute (principal investigator, Roger Ptak), funded by contract HHSN272200700041C (from the National Institute of Allergy and Infectious Diseases, National Institutes of Health [NIH], U.S. Department of Health and Human Services). This work was supported by grants from the NIH to M.S.K. (AI076168), M.J.R. (GM066682), and C.P.H. (GM082545), as well as a University of Utah Technology Commercialization Grant to M.S.K. Portions of this research were carried out at the Stanford Synchrotron Radiation Lightsource (SSRL), a national user facility operated by Stanford University on behalf of the Office of Basic Energy Sciences, U.S. Department of Energy. The SSRL Structural Molecular Biology Program is supported by the Office of Biological and Environmental Research, U.S. Department of Energy, and by the National Center for Research Resources, Biomedical Technology Program, NIH, and the National Institute of General Medical Sciences.

B.D.W., D.M.E., and M.S.K. are cofounders of Kayak Biosciences. This startup company is focused on advancing D-peptide inhibitors to the clinic.

REFERENCES

1. **Buonaguro, L., M. L. Tornesello, and F. M. Buonaguro.** 2007. Human immunodeficiency virus type 1 subtype distribution in the worldwide epidemic: pathogenetic and therapeutic implications. J. Virol. **81:**10209–10219.
2. **Chan, D. C., C. T. Chutkowski, and P. S. Kim.** 1998. Evidence that a prominent cavity in the coiled coil of HIV type 1 gp41 is an attractive drug target. Proc. Natl. Acad. Sci. U. S. A. **95:**15613–15617.
3. **Chan, D. C., D. Fass, J. M. Berger, and P. S. Kim.** 1997. Core structure of gp41 from the HIV envelope glycoprotein. Cell **89:**263–273.
4. **Chinnadurai, R., D. Rajan, J. Munch, and F. Kirchhoff.** 2007. Human immunodeficiency virus type 1 variants resistant to first- and second-version fusion inhibitors and cytopathic in ex vivo human lymphoid tissue. J. Virol. **81:**6563–6572.
5. **Cooper, D. A., R. T. Steigbigel, J. M. Gatell, J. K. Rockstroh, C. Katlama, P. Yeni, A. Lazzarin, B. Clotet, P. N. Kumar, J. E. Eron, M. Schechter, M. Markowitz, M. R. Loutfy, J. L. Lennox, J. Zhao, J. Chen, D. M. Ryan, R. R. Rhodes, J. A. Killar, L. R. Gilde, K. M. Strohmaier, A. R. Meibohm, M. D. Miller, D. J. Hazuda, M. L. Nessly, M. J. DiNubile, R. D. Isaacs, H. Teppler, and B. Y. Nguyen.** 2008. Subgroup and resistance analyses of raltegravir for resistant HIV-1 infection. N. Engl. J. Med. **359:**355–365.
6. **Davis, I. W., A. Leaver-Fay, V. B. Chen, J. N. Block, G. J. Kapral, X. Wang, L. W. Murray, W. B. Arendall III, J. Snoeyink, J. S. Richardson, and D. C. Richardson.** 2007. MolProbity: all-atom contacts and structure validation for proteins and nucleic acids. Nucleic Acids Res. **35:**W375–W383.
7. **Debnath, A. K., L. Radigan, and S. Jiang.** 1999. Structure-based identification of small molecule antiviral compounds targeted to the gp41 core structure of the human immunodeficiency virus type 1. J. Med. Chem. **42:**3203–3209.
8. **Derdeyn, C. A., J. M. Decker, J. N. Sfakianos, Z. Zhang, W. A. O'Brien, L. Ratner, G. M. Shaw, and E. Hunter.** 2001. Sensitivity of human immunodeficiency virus type 1 to fusion inhibitors targeted to the gp41 first heptad repeat involves distinct regions of gp41 and is consistently modulated by gp120 interactions with the coreceptor. J. Virol. **75:**8605–8614.
9. **Dwyer, J. J., K. L. Wilson, D. K. Davison, S. A. Freel, J. E. Seedorff, S. A. Wring, N. A. Tvermoes, T. J. Matthews, M. L. Greenberg, and M. K. Delmedico.** 2007. Design of helical, oligomeric HIV-1 fusion inhibitor peptides with potent activity against enfuvirtide-resistant virus. Proc. Natl. Acad. Sci. U. S. A. **104:**12772–12777.
10. **Eckert, D. M., and P. S. Kim.** 2001. Design of potent inhibitors of HIV-1 entry from the gp41 N-peptide region. Proc. Natl. Acad. Sci. U. S. A. **98:**11187–11192.
11. **Eckert, D. M., and P. S. Kim.** 2001. Mechanisms of viral membrane fusion and its inhibition. Annu. Rev. Biochem. **70:**777–810.
12. **Eckert, D. M., V. N. Malashkevich, L. H. Hong, P. A. Carr, and P. S. Kim.** 1999. Inhibiting HIV-1 entry: discovery of D-peptide inhibitors that target the gp41 coiled-coil pocket. Cell **99:**103–115.
13. **Eggink, D., C. E. Baldwin, Y. Deng, J. P. Langedijk, M. Lu, R. W. Sanders, and B. Berkhout.** 2008. Selection of T1249-resistant human immunodeficiency virus type 1 variants. J. Virol. **82:**6678–6688.
14. **Ernst, J. T., O. Kutzki, A. K. Debnath, S. Jiang, H. Lu, and A. D. Hamilton.** 2002. Design of a protein surface antagonist based on alpha-helix mimicry: inhibition of gp41 assembly and viral fusion. Angew. Chem. Int. ed. Engl. **41:**278–281.
15. **Ferrer, M., T. M. Kapoor, T. Strassmaier, W. Weissenhorn, J. J. Skehel, D. Oprian, S. L. Schreiber, D. C. Wiley, and S. C. Harrison.** 1999. Selection of gp41-mediated HIV-1 cell entry inhibitors from biased combinatorial libraries of non-natural binding elements. Nat. Struct. Biol. **6:**953–960.
16. **Freed, E. O., and M. A. Martin.** 1995. The role of human immunodeficiency virus type 1 envelope glycoproteins in virus infection. J. Biol. Chem. **270:**23883–23886.
17. **Frey, G., S. Rits-Volloch, X. Q. Zhang, R. T. Schooley, B. Chen, and S. C. Harrison.** 2006. Small molecules that bind the inner core of gp41 and inhibit HIV envelope-mediated fusion. Proc. Natl. Acad. Sci. U. S. A. **103:**13938–13943.
18. **Furuta, R. A., C. T. Wild, Y. Weng, and C. D. Weiss.** 1998. Capture of an early fusion-active conformation of HIV-1 gp41. Nat. Struct. Biol. **5:**276–279.
19. **Gao, F., E. Bailes, D. L. Robertson, Y. Chen, C. M. Rodenburg, S. F. Michael, L. B. Cummins, L. O. Arthur, M. Peeters, G. M. Shaw, P. M. Sharp, and B. H. Hahn.** 1999. Origin of HIV-1 in the chimpanzee Pan troglodytes troglodytes. Nature **397:**436–441.
20. **Gaschen, B., J. Taylor, K. Yusim, B. Foley, F. Gao, D. Lang, V. Novitsky, B. Haynes, B. H. Hahn, T. Bhattacharya, and B. Korber.** 2002. Diversity considerations in HIV-1 vaccine selection. Science **296:**2354–2360.
21. **Golding, H., M. Zaitseva, E. de Rosny, L. R. King, J. Manischewitz, I. Sidorov, M. K. Gorny, S. Zolla-Pazner, D. S. Dimitrov, and C. D. Weiss.** 2002. Dissection of human immunodeficiency virus type 1 entry with neutralizing antibodies to gp41 fusion intermediates. J. Virol. **76:**6780–6790.
22. **Jiang, S., K. Lin, N. Strick, and A. R. Neurath.** 1993. HIV-1 inhibition by a peptide. Nature **365:**113.
23. **Jiang, S., H. Lu, S. Liu, Q. Zhao, Y. He, and A. K. Debnath.** 2004. N-substituted pyrrole derivatives as novel human immunodeficiency virus type 1 entry inhibitors that interfere with the gp41 six-helix bundle formation and block virus fusion. Antimicrob. Agents Chemother. **48:**4349–4359.
24. **Jin, B. S., J. R. Ryu, K. Ahn, and Y. G. Yu.** 2000. Design of a peptide inhibitor that blocks the cell fusion mediated by glycoprotein 41 of human immunodeficiency virus type 1. AIDS Res. Hum. Retroviruses **16:**1797–1804.
25. **Jones, T. A., J. Y. Zou, S. W. Cowan, and M. Kjeldgaard.** 1991. Improved methods for building protein models in electron density maps and the location of errors in these models. Acta Crystallogr. A **47**(Pt 2)**:**110–119.
26. **Judice, J. K., J. Y. Tom, W. Huang, T. Wrin, J. Vennari, C. J. Petropoulos, and R. S. McDowell.** 1997. Inhibition of HIV type 1 infectivity by constrained alpha-helical peptides: implications for the viral fusion mechanism. Proc. Natl. Acad. Sci. U. S. A. **94:**13426–13430.
27. **Kahle, K. M., H. K. Steger, and M. J. Root.** 2009. Asymmetric deactivation of HIV-1 gp41 following fusion inhibitor binding. PLoS Pathog. **5:**e1000674.
28. **Kobayashi, M., K. Nakahara, T. Seki, S. Miki, S. Kawauchi, A. Suyama, C. Wakasa-Morimoto, M. Kodama, T. Endoh, E. Oosugi, Y. Matsushita, H. Murai, T. Fujishita, T. Yoshinaga, E. Garvey, S. Foster, M. Underwood, B. Johns, A. Sato, and T. Fujiwara.** 2008. Selection of diverse and clinically relevant integrase inhibitor-resistant human immunodeficiency virus type 1 mutants. Antiviral Res. **80:**213–222.
29. **Lalezari, J. P., N. C. Bellos, K. Sathasivam, G. J. Richmond, C. J. Cohen, R. A. Myers, Jr., D. H. Henry, C. Raskino, T. Melby, H. Murchison, Y. Zhang, R. Spence, M. L. Greenberg, R. A. Demasi, and G. D. Miralles.** 2005. T-1249 retains potent antiretroviral activity in patients who had experienced virological failure while on an enfuvirtide-containing treatment regimen. J. Infect. Dis. **191:**1155–1163.
30. **Lalezari, J. P., K. Henry, M. O'Hearn, J. S. Montaner, P. J. Piliero, B. Trottier, S. Walmsley, C. Cohen, D. R. Kuritzkes, J. J. Eron, Jr., J. Chung, R. DeMasi, L. Donatacci, C. Drobnes, J. Delehanty, and M. Salgo.** 2003. Enfuvirtide, an HIV-1 fusion inhibitor, for drug-resistant HIV infection in North and South America. N. Engl. J. Med. **348:**2175–2185.
31. **Lazzarin, A., B. Clotet, D. Cooper, J. Reynes, K. Arasteh, M. Nelson, C. Katlama, H. J. Stellbrink, J. F. Delfraissy, J. Lange, L. Huson, R. DeMasi, C. Wat, J. Delehanty, C. Drobnes, and M. Salgo.** 2003. Efficacy of enfuvirtide in patients infected with drug-resistant HIV-1 in Europe and Australia. N. Engl. J. Med. **348:**2186–2195.
32. **Marx, P. A.** 2005. Unsolved questions over the origin of HIV and AIDS. ASM News **71:**15–20.
33. **McCoy, A. J., R. W. Grosse-Kunstleve, P. D. Adams, M. D. Winn, L. C. Storoni, and R. J. Read.** 2007. Phaser crystallographic software. J. Appl. Crystallogr. **40:**658–674.
34. **Miller, M. D., R. Geleziunas, E. Bianchi, S. Lennard, R. Hrin, H. Zhang, M. Lu, Z. An, P. Ingallinella, M. Finotto, M. Mattu, A. C. Finnefrock, D. Bramhill, J. Cook, D. M. Eckert, R. Hampton, M. Patel, S. Jarantow, J. Joyce, G. Ciliberto, R. Cortese, P. Lu, W. Strohl, W. Schleif, M. McElhaugh, S. Lane, C. Lloyd, D. Lowe, J. Osbourn, T. Vaughan, E. Emini, G. Barbato, P. S. Kim, D. J. Hazuda, J. W. Shiver, and A. Pessi.** 2005. A human monoclonal antibody neutralizes diverse HIV-1 isolates by binding a critical gp41 epitope. Proc. Natl. Acad. Sci. U. S. A. **102:**14759–14764.
35. **Munoz-Barroso, I., S. Durell, K. Sakaguchi, E. Appella, and R. Blumenthal.** 1998. Dilation of the human immunodeficiency virus-1 envelope glycoprotein fusion pore revealed by the inhibitory action of a synthetic peptide from gp41. J. Cell Biol. **140:**315–323.
36. **Murshudov, G. N., A. A. Vagin, and E. J. Dodson.** 1997. Refinement of

macromolecular structures by the maximum-likelihood method. Acta Crystallogr. D Biol. Crystallogr. **53:**240–255.
37. **Nalam, M. N., A. Ali, M. D. Altman, G. S. Reddy, S. Chellappan, V. Kairys, A. Ozen, H. Cao, M. K. Gilson, B. Tidor, T. M. Rana, and C. A. Schiffer.** 2010. Evaluating the substrate-envelope hypothesis: structural analysis of novel HIV-1 protease inhibitors designed to be robust against drug resistance. J. Virol. **84:**5368–5378.
38. **Noren, K. A., and C. J. Noren.** 2001. Construction of high-complexity combinatorial phage display peptide libraries. Methods **23:**169–178.
39. **Osmanov, S., C. Pattou, N. Walker, B. Schwardlander, and J. Esparza.** 2002. Estimated global distribution and regional spread of HIV-1 genetic subtypes in the year 2000. J. Acquir. Immune Defic. Syndr. **29:**184–190.
40. **Otwinowski, Z., and W. Minor.** 1997. Processing of X-ray diffraction data collected in oscillation mode. Methods Enzymol. **276:**307–326.
41. **Pappenheimer, J. R., C. E. Dahl, M. L. Karnovsky, and J. E. Maggio.** 1994. Intestinal absorption and excretion of octapeptides composed of D amino acids. Proc. Natl. Acad. Sci. U. S. A. **91:**1942–1945.
42. **Pappenheimer, J. R., M. L. Karnovsky, and J. E. Maggio.** 1997. Absorption and excretion of undegradable peptides: role of lipid solubility and net charge. J. Pharmacol. Exp. Ther. **280:**292–300.
43. **Petropoulos, C. J., N. T. Parkin, K. L. Limoli, Y. S. Lie, T. Wrin, W. Huang, H. Tian, D. Smith, G. A. Winslow, D. J. Capon, and J. M. Whitcomb.** 2000. A novel phenotypic drug susceptibility assay for human immunodeficiency virus type 1. Antimicrob. Agents Chemother. **44:**920–928.
44. **Ray, N., J. E. Harrison, L. A. Blackburn, J. N. Martin, S. G. Deeks, and R. W. Doms.** 2007. Clinical resistance to enfuvirtide does not affect susceptibility of human immunodeficiency virus type 1 to other classes of entry inhibitors. J. Virol. **81:**3240–3250.
45. **Reeves, J. D., S. A. Gallo, N. Ahmad, J. L. Miamidian, P. E. Harvey, M. Sharron, S. Pohlmann, J. N. Sfakianos, C. A. Derdeyn, R. Blumenthal, E. Hunter, and R. W. Doms.** 2002. Sensitivity of HIV-1 to entry inhibitors correlates with envelope/coreceptor affinity, receptor density, and fusion kinetics. Proc. Natl. Acad. Sci. U. S. A. **99:**16249–16254.
46. **Reeves, J. D., F. H. Lee, J. L. Miamidian, C. B. Jabara, M. M. Juntilla, and R. W. Doms.** 2005. Enfuvirtide resistance mutations: impact on human immunodeficiency virus envelope function, entry inhibitor sensitivity, and virus neutralization. J. Virol. **79:**4991–4999.
47. **Rimsky, L. T., D. C. Shugars, and T. J. Matthews.** 1998. Determinants of human immunodeficiency virus type 1 resistance to gp41-derived inhibitory peptides. J. Virol. **72:**986–993.
48. **Root, M. J., M. S. Kay, and P. S. Kim.** 2001. Protein design of an HIV-1 entry inhibitor. Science **291:**884–888.
49. **Sadowski, M., J. Pankiewicz, H. Scholtzova, J. A. Ripellino, Y. Li, S. D. Schmidt, P. M. Mathews, J. D. Fryer, D. M. Holtzman, E. M. Sigurdsson, and T. Wisniewski.** 2004. A synthetic peptide blocking the apolipoprotein E/beta-amyloid binding mitigates beta-amyloid toxicity and fibril formation in vitro and reduces beta-amyloid plaques in transgenic mice. Am. J. Pathol. **165:**937–948.
50. **Schumacher, T. N., L. M. Mayr, D. L. Minor, Jr., M. A. Milhollen, M. W. Burgess, and P. S. Kim.** 1996. Identification of D-peptide ligands through mirror-image phage display. Science **271:**1854–1857.
51. **Sia, S. K., P. A. Carr, A. G. Cochran, V. N. Malashkevich, and P. S. Kim.** 2002. Short constrained peptides that inhibit HIV-1 entry. Proc. Natl. Acad. Sci. U. S. A. **99:**14664–14669.
52. **Southern Research Institute.** 2008, posting date. Anti-HIV evaluation assays in fresh human cells. Southern Research Institute, Birmingham, AL. http://www.southernresearch.org/contract-services/anti-hiv-evaluation-assays.html#fresh_human_cells.
53. **Steger, H. K., and M. J. Root.** 2006. Kinetic dependence to HIV-1 entry inhibition. J. Biol. Chem. **281:**25813–25821.
54. **Stephens, O. M., S. Kim, B. D. Welch, M. E. Hodsdon, M. S. Kay, and A. Schepartz.** 2005. Inhibiting HIV fusion with a beta-peptide foldamer. J. Am. Chem. Soc. **127:**13126–13127.
55. **Tan, K., J. Liu, J. Wang, S. Shen, and M. Lu.** 1997. Atomic structure of a thermostable subdomain of HIV-1 gp41. Proc. Natl. Acad. Sci. U. S. A. **94:**12303–12308.
56. **Weissenhorn, W., A. Dessen, S. C. Harrison, J. J. Skehel, and D. C. Wiley.** 1997. Atomic structure of the ectodomain from HIV-1 gp41. Nature **387:**426–430.
57. **Welch, B. D., A. P. VanDemark, A. Heroux, C. P. Hill, and M. S. Kay.** 2007. Potent D-peptide inhibitors of HIV-1 entry. Proc. Natl. Acad. Sci. U. S. A. **104:**16828–16833.
58. **Wild, C., J. W. Dubay, T. Greenwell, T. Baird, Jr., T. G. Oas, C. McDanal, E. Hunter, and T. Matthews.** 1994. Propensity for a leucine zipper-like domain of human immunodeficiency virus type 1 gp41 to form oligomers correlates with a role in virus-induced fusion rather than assembly of the glycoprotein complex. Proc. Natl. Acad. Sci. U. S. A. **91:**12676–12680.
59. **Wild, C., T. Greenwell, and T. Matthews.** 1993. A synthetic peptide from HIV-1 gp41 is a potent inhibitor of virus-mediated cell-cell fusion. AIDS Res. Hum. Retroviruses **9:**1051–1053.
60. **Wild, C., T. Oas, C. McDanal, D. Bolognesi, and T. Matthews.** 1992. A synthetic peptide inhibitor of human immunodeficiency virus replication: correlation between solution structure and viral inhibition. Proc. Natl. Acad. Sci. U. S. A. **89:**10537–10541.
61. **Wild, C. T., D. C. Shugars, T. K. Greenwell, C. B. McDanal, and T. J. Matthews.** 1994. Peptides corresponding to a predictive alpha-helical domain of human immunodeficiency virus type 1 gp41 are potent inhibitors of virus infection. Proc. Natl. Acad. Sci. U. S. A. **91:**9770–9774.

CHAPTER 4

DESIGN OF A MODULAR TETRAMERIC SCAFFOLD FOR THE SYNTHESIS OF MEMBRANE-LOCALIZED D-PEPTIDE INHIBITORS OF HIV-1 ENTRY

Reproduced with permission from J. Nicholas Francis, Joseph S. Redman, Debra M. Eckert, and Michael S. Kay. "Design of a Modular Tetrameric Scaffold for the Synthesis of Membrane-Localized D-Peptide Inhibitors of HIV-1 Entry."

Bioconjugate Chemistry, Vol. 23, No. 6, pp. 1252-1258;

1st May 2012; DOI: 10.1021/bc300076f

Bioconjugate Chemistry

Article

pubs.acs.org/bc

Design of a Modular Tetrameric Scaffold for the Synthesis of Membrane-Localized D-Peptide Inhibitors of HIV-1 Entry

J. Nicholas Francis, Joseph S. Redman, Debra M. Eckert, and Michael S. Kay*

Department of Biochemistry, University of Utah School of Medicine, 15 N Medical Drive East Room 4100, Salt Lake City, Utah 84112-5650, United States

ABSTRACT: The highly conserved HIV-1 gp41 "pocket" region is a promising target for inhibiting viral entry. PIE12-trimer is a protease-resistant trimeric D-peptide inhibitor that binds to this pocket and potently blocks HIV entry. PIE12-trimer also possesses a reserve of binding energy that provides it with a strong genetic barrier to resistance ("resistance capacitor"). Here, we report the design of a modular scaffold employing PEGs of discrete lengths for the efficient optimization and synthesis of PIE12-trimer. This scaffold also allows us to conjugate PIE12-trimer to several membrane-localizing cargoes, resulting in dramatically improved potency and retention of PIE12-trimer's ability to absorb the impact of resistance mutations. This scaffold design strategy should be of broad utility for the rapid prototyping of multimeric peptide inhibitors attached to potency- or pharmacokinetics-enhancing groups.

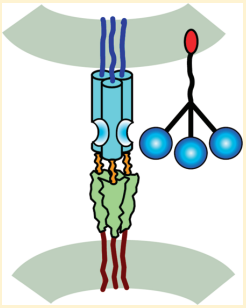

INTRODUCTION

HIV entry is mediated by the trimeric viral envelope glycoprotein (Env), which is cleaved into surface (gp120) and transmembrane (gp41) subunits.[1,2] Viral entry is triggered by binding of gp120 to a primary receptor (CD4) and subsequently a coreceptor (typically CXCR4 or CCR5), which induces large conformation changes in gp120 that activate gp41 for fusion.[3] gp41 then adopts an extended pre-hairpin conformation, embedding its N-terminal hydrophobic fusion peptide into the host cell membrane, bridging the virus and the host cell (Figure 1). In this state, the gp41 N-peptide region forms a trimeric coiled-coil (N-trimer), while the C-peptide region is in a structurally undefined state. This pre-hairpin intermediate then slowly collapses into a hairpin structure, with the C-peptide folding back upon the N-trimer to pack in an antiparallel orientation into the grooves of the N-trimer. The formation of this trimer-of-hairpins structure brings the viral and host membranes into close proximity and drives membrane fusion.[4,5]

In the pre-hairpin intermediate, gp41 is vulnerable to inhibitors that bind to either the N-trimer or C-peptide[2,6] and prevent hairpin formation.[7−9] This vulnerability has been exploited by the C-peptide-derived therapeutic Fuzeon (enfuvirtide). Fuzeon binds to a portion of the N-trimer groove, preventing fusion with nanomolar potency. Though effective, Fuzeon is currently utilized only as "salvage therapy" for patients with multidrug resistance because of its high cost (~$30 000/year/patient), dosing requirements (90 mg twice daily), injection site reactions, and the rapid emergence of resistant strains.[10,11]

The gp41 N-trimer contains a functionally critical and highly conserved deep hydrophobic pocket at its C-terminus.[4,12,13] The genomic region that encodes for the pocket also forms the structured RNA region of the Rev-responsive element (RRE), which is critical for the export of viral mRNA to the cytoplasm,[14] further constraining evolution of this region on

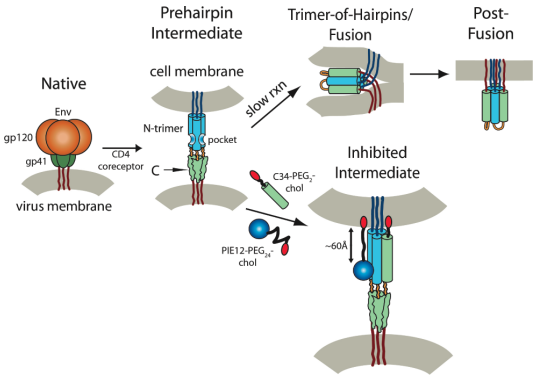

Figure 1. HIV entry pathway. Upon engagement with cellular receptor and coreceptor, gp120 and gp41 undergo a conformational change resulting in extension of gp41 into the pre-hairpin intermediate, exposing the hydrophobic pocket region of the N-trimer. gp41 collapses into the trimer-of-hairpins structure, juxtaposing the viral and host membranes and causing membrane fusion. The hydrophobic pocket targeted by PIE12 is an estimated 60 Å from the cell membrane, which can be bridged by a relaxed PEG24 linker. In contrast, the C-peptide C-terminus is directly adjacent to the membrane. Cholesterol (red) conjugated with PEG spacers (black lines) are shown.

Received: February 15, 2012
Revised: April 25, 2012
Published: May 1, 2012

the nucleotide level. Fuzeon binds to the N-trimer groove region just outside the pocket, an area that is more tolerant of resistance mutations. Second/third-generation C-peptide inhibitors (e.g, T1249, T2635) bind the groove and pocket and are much less susceptible to resistance.[10,15−20]

We have utilized structure-guided mirror-image phage display to generate D-peptide inhibitors that bind with high affinity to the pocket.[13,21,22] D-Peptides are protease resistant (as proteases have stereochemical specificity and generally only cleave L-substrates),[23] giving them the potential for a much longer lifetime in the body. PIE12, our most potent monomeric D-peptide, is a pocket-specific inhibitor of HIV-1 with high-nM potency against the difficult-to-inhibit primary HIV isolate JRFL. Since the N-trimer contains three symmetric pockets, we designed a trimeric version of PIE12 that uses PEG to link three monomers and greatly improves affinity and potency via avidity. PIE12-trimer inhibits all major HIV clades with high-pM to low-nM potency[21] and is a promising preclinical candidate for the treatment and prevention of HIV-1. Here, we describe a novel modular PEG scaffold used to optimize the production and the potency of PIE12-trimer.

While designing D-peptide inhibitors with progressively greater potency, we encountered a potency limit that could not be overcome by affinity optimization because the target is only available in the short-lived pre-hairpin intermediate. Due to the finite target exposure and the limits of diffusion, the potency of inhibitors with very high affinities (and on-rates) is limited by the diffusion-limited on-rate rather than binding affinity. For such diffusion-limited inhibitors, a potency plateau is reached beyond which further improvements in affinity do not improve potency. Similar potency plateaus have been observed for several inhibitors that target the transient pre-hairpin intermediate.[21,22,24−26] "Over-engineering" our inhibitors with improved affinity, but no corresponding improvement in potency, provides a reserve of binding energy and slows the evolution of resistance mutations. This "resistance capacitor" eliminates the selective advantage conferred by affinity-disrupting resistance mutations, since viruses bearing mutations that reduce affinity are still inhibited with equal potency, depriving HIV of an efficient evolutionary pathway to resistance. A profoundly disruptive mutation could escape the resistance capacitor, but such severe pocket mutations are discouraged due to the high cost to viral fitness. With high pM to low nM potency but sub-fM binding affinity, PIE12-trimer has a very strong resistance capacitor.[21]

We hypothesize that potency could be improved beyond the plateau by pre-positioning inhibitor on the cell surface, the site of viral entry, thus increasing the association rate beyond the diffusion limit. Using our novel modular PEG scaffold, we conjugate PIE12-trimer to membrane-localizing groups (cholesterol and alkyl chains) that improve potency up to ~160-fold. This approach greatly simplifies trimer synthesis and improves yield. Importantly, our data show that this gain in potency does not disrupt the resistance capacitor, leaving intact PIE12-trimer's strong barrier to resistance mutations. Using a discrete PEG scaffold with orthogonal reactive groups and defined geometry allows for rapid optimization of multimeric inhibitors and scouting of various potency-enhancing cargoes and should be of broad utility for the design of other multimeric peptide inhibitors.

EXPERIMENTAL PROCEDURES

Peptide Synthesis. Peptides were synthesized using a PTI PS3 peptide synthesizer or by RS Synthesis as previously described[21,22] to generate either PIE12-GK or ΔHP-PIE12-GK (lacks two N-terminal residues, D-His and D-Pro). PIE12-dPEG$_{4/5}$-NH$_2$ (the precursor to PIE12-trimer synthesis) was synthesized as follows: PIE12-GK (10 mM in dimethylacetamide, DMAC) was reacted with 250 mM stock solution of Fmoc-N-amido-dPEG$_{4/5}$-NHS ester (Quanta BioDesign 10994 and 10053) in dry DMAC (Acros Organics, septa sealed with molecular sieves) at a 1:1 molar ratio buffered by triethylamine (200 mM, pH 7.5) for 60 min at RT. This reaction was quenched by addition of acetic acid to 5% and purified by reverse-phase HPLC (water/acetonitrile gradient in 0.1% TFA) on a Waters BEH X-Bridge 10 μm, 300 Å C$_{18}$ column (RP-HPLC). Purified product was lyophilized, then resuspended in 20% piperidine in DMAC for 20 min to remove Fmoc and produce PIE12-PEG$_{4/5}$-NH$_2$, which was then purified by RP-HPLC.

Trimer Synthesis. PIE12-PEG$_{4/5}$-NH$_2$ (10 mM) was reacted with 250 mM stock solution trimethylolethane-triNHS ester (Figure 2A, Quanta BioDesign 10674) in DMAC at a 3.3:1 (peptide/scaffold) ratio in DMAC buffered by triethylamine (200 mM, pH 7.5) for 60 min at RT. Product was purified by RP-HPLC. All masses were confirmed by ESI-MS (AB Sciex API-3000).

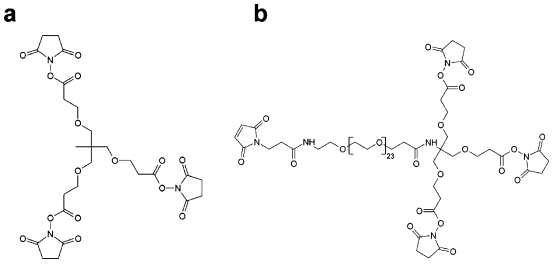

Figure 2. Trimeric and heterotetrameric PEG scaffolds and cargoes. A. Trimethoylethane-triNHS ester. B. Heterotetrameric PEG scaffold. The fourth maleimide arm is available for reaction with thiol-containing cargoes, such as 1-octadecanethiol (C18-SH) and thiocholesterol.

Cholesterol-PIE12-trimer and alkyl-PIE12-trimer were synthesized as follows: PIE12-PEG$_4$-NH$_2$ (10 mM) was reacted with Maleimide-PEG$_{12}$-triNHS ester (Quanta BioDesign 10676, 250 mM in DMAC) or Maleimide-PEG$_{24}$-triNHS ester (Figure 2B, Quanta BioDesign 10680, 250 mM in DMAC) at a 3.3:1 (peptide/scaffold) ratio in DMAC buffered by triethylamine (200 mM, pH 7.5) for 45 min at RT. Thiocholesterol (Sigma Aldrich, 136115, 250 mM in chloroform), 1-octanethiol (Sigma-Aldrich 471836), 1-hexadecanethiol (Sigma-Aldrich 52270), or 1-octadecanethiol (Sigma Aldrich 01858) were then added to a final concentration of 4.5 mM and reacted for an additional 60 min. For PEG$_{16}$, PIE12-PEG$_4$-NH$_2$ was first reacted with Mal-PEG$_{12}$-triNHS ester, followed by reaction with D-Cysteine (5 mM) to yield (PIE12-PEG$_4$)$_3$-PEG$_{12}$-Cys. This product was then purified by RP-HPLC before sequential reaction with Maleimide-PEG$_4$-NHS and thiocholesterol under conditions identical to those used to generate chol-PEG$_{24}$-PIE12-trimer. PEG$_{36}$, PEG$_{57}$, and PEG$_{132}$-trimer were produced through conjugation of PIE12-

dx.doi.org/10.1021/bc300076f | Bioconjugate Chem. 2012, 23, 1252−1258

PEG_4-NH_2 to Maleimide-PEG_{24}-triNHS ester, followed by addition of D-cysteine. This intermediate was then conjugated to Mal-PEG_{12}-NHS ester (Quanta Biodesign, 10284), Mal-PEG_{2K}-NHS ester (Creative PEGWorks, PHB-950, ~45 PEG units), or Mal-PEG_{5K}-NHS ester (Creative PEGWorks, PHB-952, ~120 PEG units) to yield Chol-PEG_{36}-PIE12-Trimer, Chol-PEG_{57}-PIE12-trimer, and Chol-PEG_{132}-PIE12-trimer, respectively. The reaction was quenched by addition of acetic acid to 5% before purification by RP-HPLC.

Viral Infectivity Assays. Pseudovirion infectivity assays were carried out as previously described[21,22] using HXB2 and JRFL luciferase reporter pseudovirions (NL4−3 strain) and HOS-CD4-CXCR4 (for HXB2) or HOS-CD4-CCR5 (for JRFL) target cells. Inhibitor curves were generated using six concentration points measured in quadruplicate, and luciferase counts were normalized to an uninhibited control. Inhibition curves were fit using a standard IC_{50} eq $[1 - c/(IC_{50} + c)]$ weighting each concentration point by its standard error in KaleidaGraph (*Synergy* software). Reported IC_{50} values are the average of at least 2 independent assays.

RESULTS

Our first goal was to simplify the synthesis of PIE12-trimer while also optimizing the linkages between PIE12 monomers. In our previous work, we synthesized PIE12-trimer by attaching bis-NHS ester PEG_5 spacers to PIE12-GK. After purification, two of these PEGylated monomers were reacted with a central PIE12-GKK monomer (two primary amines) to produce PIE12-trimer.[21] This method is cumbersome for large-scale production, because it requires the synthesis of two distinct D-peptides and a series of HPLC purifications to assemble the trimer, resulting in low yields. In addition, our PIE12 crystal structure suggested that shorter PEG linkers might adequately bridge the neighboring pockets and improve avidity. To address these goals, we redesigned the PIE12-trimer using a scaffold strategy. We designed a homotrimeric scaffold containing three NHS ester arms for conjugation to PIE12-GK (Figure 2a) in a single-pot reaction. PEG linkers of various lengths can be appended to the PIE12-GK peptide, allowing for the simple production of PIE12-trimers with varying PEG lengths.

PIE12-trimer's estimated sub-fM affinity for the N-trimer makes direct comparative K_D measurements (e.g., by surface plasmon resonance) very challenging. Although antiviral potency can be used as a surrogate for affinity, PIE12-trimer's potency plateau can mask even large changes in affinity. To overcome this problem, we designed a PIE12 variant with weakened affinity to allow comparative evaluation of different trimer geometries by measuring inhibitor potency. We previously observed that PIE12's two N-terminal residues make important contacts with the N-trimer and reasoned that deletion of these residues (D-His and D-Pro) would significantly reduce binding affinity without disrupting the overall orientation of PIE12 binding to the gp41 pocket or the local structure at the C-terminal PEG linkage site. ΔHP-PIE12 is 84-fold less potent than PIE12 (Table 1). In the context of the homotrimeric scaffold, ΔHP-PIE12 connected via our standard PEG_5 linkers has an IC_{50} of 380 nM against HXB2 (a standard lab-adapted strain) and is therefore well outside of the potency plateau (~500 pM for HXB2). Using ΔHP-PIE12-trimer, we can now detect changes in potency due to linker changes that subtly alter affinity.

Our initial exploration of PEG linker lengths in PIE12-trimer showed that PEG_2 and PEG_3 were slightly less potent than the original PEG_5. To determine whether PEG_4 or PEG_5 was the optimal arm length, both PEG_5 and PEG_4 ΔHP-PIE12 conjugates were attached to the homotrimeric scaffold, and we observed that a PEG_4 linker was slightly more optimal (Table 1). Therefore, PEG_4 was selected as the new standard linker for conjugating PIE12 to the scaffold. The scaffold synthesis strategy is dramatically simpler than our previous method for generating trimer since it requires only one peptide and a single purification. Additionally, the yields are considerably higher due to the reduced number of purification and lyophilization steps that led to loss of active NHS esters in the previous strategy. Finally, the high activity of the scaffold and single-pot reaction allow for near-stoichiometric concentrations of peptide and scaffold, further improving yield.

Table 1. D-Peptide Inhibition Data[a]

inhibitor	IC_{50} (nM) HXB2	JRFL
PIE12[b]	37 ± 2.3	580 ± 21.4
ΔHP-PIE12	3100 ± 783	nd
Chol-PEG_2-PIE12	69 ± 11	nd
Chol-PEG_{12}-PIE12	12 ± 3.6	nd
Chol-PEG_{24}-PIE12	0.64 ± 0.25	nd
C34	1.4 ± 0.3	13.4 ± 0.1
C34-PEG_2-Chol	0.044 ± 0.0004	0.05 ± 0.01
C34-PEG_{11}-Chol	0.021 ± 0.0014	0.024 ± 0.005
C34-PEG_{80}-Chol	0.022 ± 0.0004	0.1 ± 0.045
PEG_4-ΔHP-PIE12-trimer	300 ± 7.2	nd
PEG_5-ΔHP-PIE12-trimer	380 ± 13	nd
PEG_4-PIE12-trimer	0.72 ± 0.04	2.1 ± 0.28
Chol-PEG_{12}-PIE12-trimer	0.052 ± 0.02	0.06 ± 0.004
Chol-PEG_{16}-PIE12-trimer	0.02 ± 0.002	0.017 ± 0.0002
Chol-PEG_{24}-PIE12-trimer	0.013 ± 0.0013	0.019 ± 0.003
Chol-PEG_{36}-PIE12-trimer	0.011 ± 0.0015	0.015 ± 0.005
Chol-PEG_{57}-PIE12-trimer	0.007 ± 0.0013	0.013 ± 0.003
Chol-PEG_{132}-PIE12-trimer	0.012 ± 0.0015	0.025 ± 0.002
C8-PIE12-trimer	0.42 ± 0.01	nd
C16-PIE12-trimer	0.09 ± 0.014	0.11 ± 0.012
C18-PIE12-trimer	0.054 ± 0.018	0.087 ± 0.012

[a]Antiviral potency against HXB2 and JRFL HIV-1 strains. [b]From ref 21.

Heterotetrameric Scaffold. With the optimal PEG linker length in place, we next turned our attention to improving PIE12-trimer's potency via localization to sites of viral entry (the cell surface). To enable the conjugation of membrane-localizing groups to PIE12-trimer, we designed a heterotetrameric scaffold containing three short arms with NHS ester groups (for addition of PIE12-PEG_4-NH_2) and a fourth PEG arm of variable length functionalized with maleimide (an orthogonal reactive group for the addition of thiol-containing cargoes) (Figure 2b).

Our first cargo for the heterotetrameric scaffold was cholesterol. Several recent studies have shown that cholesterol conjugation improves both the potency and the circulating half-life of C-peptide inhibitors of HIV[27] and paramyxoviruses.[28,29] Cholesterol conjugation has also been shown to specifically localize dyes to the membrane surface.[30,31] A challenge of applying this approach to PIE12 is that, while the N-terminus of the C-peptide lies immediately adjacent to the membrane, PIE12 targets a pocket that we estimate is ~60 Å from the membrane (Figure 1). We used flexible PEG linkers of varying lengths to span this distance. PEG_{12} is sufficiently long if

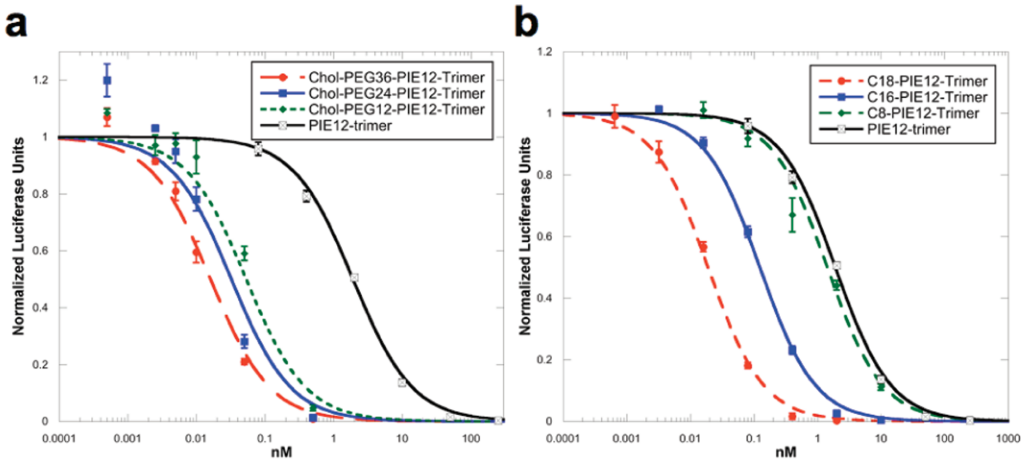

Figure 3. JRFL pseudovirion infectivity assay. A. Dependence of linker length on chol-PIE12-trimer potency. B. Thio-alkane-conjugated PIE12-trimer series with differing alkane lengths. Representative curves shown.

stretched taut, but PEG typically assumes an average length approximately half of its fully stretched distance.[32]

To study the potency effects of cholesterol (chol) conjugation to PIE12 and the length of the linker between chol and PIE12, we used monomeric PIE12, which is not in a potency plateau and therefore should be a sensitive reporter for optimal linker length. We began by generating chol-PIE12 conjugates using heterobifunctional PEG_2, PEG_{12}, and PEG_{24} NHS ester/maleimide cross-linkers to conjugate thiocholesterol (cholesterol with a thiol replacing its hydroxyl group) to PIE12's C-terminal Lys (its only primary amine). We observed that the PEG_2 conjugate, much too short to bridge the membrane to pocket distance, causes a 2-fold loss of potency (HXB2 strain) compared to unconjugated PIE12. In contrast, chol-PEG_{12}-PIE12 shows 3-fold improved potency, while PEG_{24} provides an even greater 58-fold increase in potency compared to PIE12. For comparison, we also synthesized C-peptide (C34) cholesterol conjugates of varying lengths (Table 1). We reproduce Ingalinella's finding of ~40-fold improved potency[27] using a short PEG_2 linker, but surprisingly, a longer linker (PEG_{11}) provides an additional 2-fold improvement in potency, and a much longer linker (PEG_{80}) maintains the same potency (HXB2 strain). A similar pattern is seen with the JRFL strain, but with significant attenuation at very long PEG linker lengths (4-fold worse than the optimal PEG length).

On the basis of these dramatic potency gains, we next conjugated cholesterol to PIE12-trimer using the heterotetrameric scaffold. Using the optimal PEG_4 linker determined earlier for the three NHS ester (PIE12) arms, we synthesized chol-PIE12-trimers with a variety of fourth arm (maleimide) lengths to confirm the relationship between PEG length and potency observed with the monomer. In the context of chol-PIE12-trimer, we did not need to utilize ΔHP-PIE12, as the cholesterol-mediated improvement in potency was discernible using PIE12. This sensitivity was expected because membrane localization affects the association rate rather than changing affinity (masked by the resistance capacitor). We varied the fourth arm from 12 to 132 PEG units, covering a distance range of ~60 to 480 Å (fully extended).

Cholesterol conjugation dramatically improves PEG_4-PIE12-trimer potency against both HXB2 and JRFL entry (up to 160-fold, Table 1 and Figure 3). Comparison of varying fourth arm lengths in chol-PIE12-trimer shows that inhibitor potency varies modestly in an optimal range between PEG_{24} and PEG_{57}. A shorter PEG_{12} linker is suboptimal, though it performs better than seen in the monomer series, likely due to the additional length provided by the PEG_4 arms. Only a slight decrease in potency is observed with the longest (PEG_{132}) linker. Despite being slightly less potent than Chol-PEG_{57}-PIE12-trimer, we have chosen Chol-PEG_{24}-PIE12-trimer as our lead candidate due to its ease of synthesis and the availability of monodisperse PEG_{24}. A monodisperse PEG scaffold will ease future preclinical studies of chol-PIE12-trimer purity, metabolism, pharmacokinetics, and stability. Importantly, cholesterol conjugates retain high (mM) aqueous solubility.

Another established strategy for localizing inhibitors to membranes is fatty acid conjugation.[33−37] Using the same heterotetramer scaffold strategy described above with cholesterol, we synthesized PIE12-trimers conjugated to aliphatic chains of 8, 16, and 18 carbons (C8/C16/C18-PIE12-trimer). While C8 conjugation has little effect on PIE12-trimer potency, C16 and C18 both provide substantial gains in potency, though to a lesser degree than seen with cholesterol (Table 1). C18-PIE12-trimer was slightly more potent than C16-PIE12-trimer.

Effect of Membrane Localization on the Resistance Capacitor. Drug resistance is a constant threat to the effectiveness of HIV inhibitors. PIE12-trimer is an attractive drug candidate in part because of its strong resistance capacitor, which provides a high genetic barrier to resistance.[21] The resistance capacitor depends on the diffusion-limited association rate for PIE12-trimer binding to gp41. The cholesterol and C16/18 conjugation strategies described here break through this kinetic barrier via inhibitor localization to viral entry sites (i.e., increasing effective inhibitor concentration and overcoming the diffusion rate limitation). In theory, this improvement in potency could come at the cost of weakening the resistance capacitor. To test for this possibility, we measured the potency of chol- and C16/C18-conjugated PIE12-trimer against resistance mutations we have previously identified.[21]

Previous selection for resistance to PIE7-dimer (an earlier-generation D-peptide inhibitor)[22] generated E560K/V570I, which minimally affects the potency of PIE12-trimer, but

dramatically reduces PIE7-dimer potency.[21] Selection of resistance to PIE12-trimer required more than a year of viral passaging, but ultimately resulted in the Q577R mutation, which decreases PIE12-trimer potency by >1000-fold.[21] The effect of these resistance mutations on chol- and C16/18-PIE12-trimer potency is shown in Table 2. The relative effects of both resistance mutations are similar for PIE12-trimer and the cholesterol/alkane-conjugated PIE12-trimers. However, because of the greatly improved potency of the conjugated PIE12-trimers, these inhibitors maintain nanomolar potency even against the severe Q577R resistance mutation. The impact of the less severe E560K/V570I resistance mutation is absorbed by all of the conjugated PIE12-trimers, as well as plain PIE12-trimer. These data suggest that the improvement in potency through C16/C18 and cholesterol conjugation retains enough excess binding energy to maintain an effective resistance capacitor.

Table 2. Antiviral Potency against Resistant Strains[a]

inhibitor	IC_{50} (nM)		
	WT HXB2	E560K/V570I	Q577R
PEG_4-PIE12-trimer	0.72	0.89	>3 μM
Chol-PEG_{24}-PIE12-trimer	0.013	0.01	10.1
C8-PIE12-trimer	0.42	0.86	452
C16-PIE12-trimer	0.09	0.045	39
C18-PIE12-trimer	0.054	0.035	32.5

[a]Antiviral potency against identified resistant strains (HXB2 background). The IC_{50} standard error of the mean values are <35% for all samples.

DISCUSSION

PIE12-trimer, our previously described D-peptide inhibitor, is a promising preclinical candidate for the treatment and prevention of HIV-1 due to its strong potency, wide breadth, and highly charged resistance capacitor that slows the emergence of resistance mutations. However, the transient nature of PIE12-trimer's target means that its potency is restricted by its diffusion-limited association rate with the gp41 pocket. In an attempt to break through this potency barrier, we designed a heterotetrameric scaffold to allow us to conjugate various membrane-localizing cargoes to PIE12-trimer. This scaffold also allows us to produce PIE12-trimer variants much more efficiently than previously reported. As hoped, conjugation of PIE12-trimer to cholesterol or C16/C18 reduces the kinetic limitation and greatly improves potency up to 160-fold.

We hypothesize that this increased potency is due to local concentration of inhibitor at membrane sites of viral entry. Cholesterol is specifically enriched at sites of viral entry (lipid rafts, where CD4 and coreceptor are localized).[38,39] The mechanism by which cholesterol improves potency is the focus of ongoing work. Preliminary evidence suggests that the interaction between cholesterol and the membrane is readily reversible, which may explain why there is a broad range of compatible linker lengths. It may also be the case that cholesterol-conjugated inhibitors interact directly with Env, as a cholesterol recognition/interaction amino acid consensus sequence (CRAC) has been identified in the membrane proximal region of gp41.[40]

By comparison, C16 and C18 conjugates are less potent than the cholesterol conjugate. Saturated fatty acids C16:0 (palmitate) and C18:0 (stearate) are also enriched in lipid rafts,[41] but are abundant in the general plasma membrane as well.[42] The reduced potency of alkylated PIE12-trimer compared to cholesterol may therefore be explained by a relatively lower affinity of alkyl chains for lipid rafts. Another possible explanation is fatty-acid sequestration by albumin, which is known to bind fatty acids with high affinity (compared to cholesterol),[43] though it is not known how loss of the acid group (leaving an alkane chain) affects this binding.

GPI anchors in lipid rafts contain C16 and C18 alkyl chains as well as acylated C16 and C18 fatty acids.[44] Originally, we synthesized alkyl conjugates, and noted that they improved potency through membrane association (overcoming the potency plateau). For completeness, we also synthesized an acylated C16 (fatty acid) conjugate. Surprisingly, the C16 acyl conjugate was much less potent than the C16 alkyl conjugate (data not shown), presumably because it does not associate as effectively with plasma membranes. This finding may explain why a recent study did not observe a potency enhancement with C16 acylation of C34.[27]

Importantly, we show that membrane localization does not impair the resistance capacitor. Both chol- and C16/C18-conjugated PIE12-trimer are able to absorb the affinity-disrupting impact of PIE7-dimer resistance mutations (E560K/V570I). For the more severe PIE12-trimer resistance mutation Q577R, the relative loss of potency for both conjugates is comparable to that seen with PIE12-trimer. The full resistance profile of these conjugates will be determined by ongoing viral passaging studies starting from both wild-type and PIE12-trimer resistant virus.

Although PIE12-trimer has ideal antiviral properties, its relatively small size (~8 kD) will likely lead to a short serum half-life due to renal filtration. In addition to their potency-boosting effects, we hypothesize that both cholesterol and alkyl conjugation will also lead to improvements in the pharmacokinetic (PK) properties of these inhibitors via interaction with cell membranes and albumin that slow renal clearance. Albumin serves as a carrier for both cholesterol[45] and fatty acids,[46] reducing the rate of renal filtration. Adherence to membrane surfaces may also slow the absorption of inhibitor from the subcutaneous space, enabling prolonged dosing via a slow-release depot effect. This type of depot would be especially attractive for nondegradable D-peptides.

This work demonstrates the successful application of modular PEG scaffold-based design to peptide drug optimization (both peptide geometry and localization to the site of action via conjugated localizing cargoes). This approach allows for alterations in the scaffold to accommodate a variety of cargoes and chemistries (e.g., "click" chemistry), as well as rapid optimization of PEG arm lengths. For viruses that undergo membrane fusion within the endosome, such as Ebola, this strategy could be employed to attach an endosome-targeting moiety to localize inhibitor to the site of entry and increase potency. Additionally, the scaffold allows for conjugation to a variety of cargoes to modulate PK properties (e.g., large branched PEGs, albumin, or albumin-binding peptides).[47,48] The scaffold itself is inexpensive to produce and can be used directly for cost-effective large-scale production.

PK and animal toxicity studies for chol- and C16/C18-PIE12-trimer are underway to determine how conjugation alters serum half-life and to determine if any specific toxicity arises as a result of conjugation. Fatty acid conjugation has been used to prolong serum half-life of a GLP-1 peptide (liraglutide,

C16) and insulin (detemir, C14). Alkane toxicity in the context of peptide conjugates has not been studied.

The *in vivo* efficacy of these conjugates will be determined in future studies of systemic treatment via subcutaneous injection or as a vaginally/rectally applied preventative (microbicide) in human tissue and animal models. Our D-peptide scaffold is especially advantageous for application as a microbicide due to its protease resistance, which should enable it to persist for extended periods in the vaginal/rectal mucosa's harsh protease-rich environment. The addition of membrane-binding groups may also improve microbicide tissue penetration and retention.

AUTHOR INFORMATION

Corresponding Author

*E-mail: kay@biochem.utah.edu. Phone: (801) 585-5021. Fax: (801) 581-7959.

Notes

The authors declare the following competing financial interest(s): DME and MSK are consultants and equity holders in Navigen, which is commercializing D-peptide inhibitors of HIV entry.

ACKNOWLEDGMENTS

We thank Paul Davis, James Guyo, and Robert Woodman of Quanta BioDesign for custom synthesis of the PEG scaffolds. This research was funded by an NIH grant AI076168 to M.S.K. J.N.F. is supported by an NIH Microbial Pathogenesis Predoctoral Training Grant (AI055434). Special thanks to Michael Root for providing cloned resistant strains and Brett Welch for critical review of the manuscript.

REFERENCES

(1) Freed, E. O., and Martin, M. A. (1995) The role of human immunodeficiency virus type 1 envelope glycoproteins in virus infection. *J. Biol. Chem. 270*, 23883−6.

(2) Eckert, D. M., and Kim, P. S. (2001) Mechanisms of viral membrane fusion and its inhibition. *Annu. Rev. Biochem. 70*, 777−810.

(3) Jones, P. L., Korte, T., and Blumenthal, R. (1998) Conformational changes in cell surface HIV-1 envelope glycoproteins are triggered by cooperation between cell surface CD4 and co-receptors. *J. Biol. Chem. 273*, 404−9.

(4) Chan, D. C., Fass, D., Berger, J. M., and Kim, P. S. (1997) Core structure of gp41 from the HIV envelope glycoprotein. *Cell 89*, 263−73.

(5) Weissenhorn, W., Dessen, A., Harrison, S. C., Skehel, J. J., and Wiley, D. C. (1997) Atomic structure of the ectodomain from HIV-1 gp41. *Nature 387*, 426−30.

(6) Root, M. J., Kay, M. S., and Kim, P. S. (2001) Protein design of an HIV-1 entry inhibitor. *Science 291*, 884−8.

(7) Jiang, S., Lin, K., Strick, N., and Neurath, A. R. (1993) HIV-1 inhibition by a peptide. *Nature 365*, 113.

(8) Wild, C., Oas, T., McDanal, C., Bolognesi, D., and Matthews, T. (1992) A synthetic peptide inhibitor of human immunodeficiency virus replication: correlation between solution structure and viral inhibition. *Proc. Natl. Acad. Sci. U. S. A. 89*, 10537−41.

(9) Wild, C. T., Shugars, D. C., Greenwell, T. K., McDanal, C. B., and Matthews, T. J. (1994) Peptides corresponding to a predictive alpha-helical domain of human immunodeficiency virus type 1 gp41 are potent inhibitors of virus infection. *Proc. Natl. Acad. Sci. U. S. A. 91*, 9770−4.

(10) Rimsky, L. T., Shugars, D. C., and Matthews, T. J. (1998) Determinants of human immunodeficiency virus type 1 resistance to gp41-derived inhibitory peptides. *J. Virol. 72*, 986−93.

(11) Golding, H., Zaitseva, M., de Rosny, E., King, L. R., Manischewitz, J., Sidorov, I., Gorny, M. K., Zolla-Pazner, S., Dimitrov, D. S., and Weiss, C. D. (2002) Dissection of human immunodeficiency virus type 1 entry with neutralizing antibodies to gp41 fusion intermediates. *J. Virol. 76*, 6780−90.

(12) Chan, D. C., Chutkowski, C. T., and Kim, P. S. (1998) Evidence that a prominent cavity in the coiled coil of HIV type 1 gp41 is an attractive drug target. *Proc. Natl. Acad. Sci. U. S. A. 95*, 15613−7.

(13) Eckert, D. M., Malashkevich, V. N., Hong, L. H., Carr, P. A., and Kim, P. S. (1999) Inhibiting HIV-1 entry: discovery of D-peptide inhibitors that target the gp41 coiled-coil pocket. *Cell 99*, 103−15.

(14) Pollard, V. W., and Malim, M. H. (1998) The HIV-1 Rev protein. *Annu. Rev. Microbiol. 52*, 491−532.

(15) Derdeyn, C. A., Decker, J. M., Sfakianos, J. N., Zhang, Z., O'Brien, W. A., Ratner, L., Shaw, G. M., and Hunter, E. (2001) Sensitivity of human immunodeficiency virus type 1 to fusion inhibitors targeted to the gp41 first heptad repeat involves distinct regions of gp41 and is consistently modulated by gp120 interactions with the coreceptor. *J. Virol. 75*, 8605−14.

(16) Eggink, D., Baldwin, C. E., Deng, Y., Langedijk, J. P., Lu, M., Sanders, R. W., and Berkhout, B. (2008) Selection of T1249-resistant human immunodeficiency virus type 1 variants. *J. Virol. 82*, 6678−88.

(17) Eggink, D., Bontjer, I., Langedijk, J. P., Berkhout, B., and Sanders, R. W. (2011) Resistance of human immunodeficiency virus type 1 to a third-generation fusion inhibitor requires multiple mutations in gp41 and is accompanied by a dramatic loss of gp41 function. *J. Virol. 85*, 10785−97.

(18) Ray, N., Harrison, J. E., Blackburn, L. A., Martin, J. N., Deeks, S. G., and Doms, R. W. (2007) Clinical resistance to enfuvirtide does not affect susceptibility of human immunodeficiency virus type 1 to other classes of entry inhibitors. *J. Virol. 81*, 3240−50.

(19) Reeves, J. D., Lee, F. H., Miamidian, J. L., Jabara, C. B., Juntilla, M. M., and Doms, R. W. (2005) Enfuvirtide resistance mutations: impact on human immunodeficiency virus envelope function, entry inhibitor sensitivity, and virus neutralization. *J. Virol. 79*, 4991−9.

(20) Lalezari, J. P., Bellos, N. C., Sathasivam, K., Richmond, G. J., Cohen, C. J., Myers, R. A., Jr., Henry, D. H., Raskino, C., Melby, T., Murchison, H., Zhang, Y., Spence, R., Greenberg, M. L., Demasi, R. A., and Miralles, G. D. (2005) T-1249 retains potent antiretroviral activity in patients who had experienced virological failure while on an enfuvirtide-containing treatment regimen. *J. Infect. Dis. 191*, 1155−63.

(21) Welch, B. D., Francis, J. N., Redman, J. S., Paul, S., Weinstock, M. T., Reeves, J. D., Lie, Y. S., Whitby, F. G., Eckert, D. M., Hill, C. P., Root, M. J., and Kay, M. S. (2010) Design of a potent D-peptide HIV-1 entry inhibitor with a strong barrier to resistance. *J. Virol. 84*, 11235−44.

(22) Welch, B. D., VanDemark, A. P., Heroux, A., Hill, C. P., and Kay, M. S. (2007) Potent D-peptide inhibitors of HIV-1 entry. *Proc. Natl. Acad. Sci. U. S. A. 104*, 16828−33.

(23) Milton, R. C., Milton, S. C., and Kent, S. B. (1992) Total chemical synthesis of a D-enzyme: the enantiomers of HIV-1 protease show reciprocal chiral substrate specificity. *Science 256*, 1445−8.

(24) Kahle, K. M., Steger, H. K., and Root, M. J. (2009) Asymmetric deactivation of HIV-1 gp41 following fusion inhibitor binding. *PLoS Pathog. 5*, e1000674.

(25) Platt, E. J., Durnin, J. P., and Kabat, D. (2005) Kinetic factors control efficiencies of cell entry, efficacies of entry inhibitors, and mechanisms of adaptation of human immunodeficiency virus. *J. Virol. 79*, 4347−56.

(26) Steger, H. K., and Root, M. J. (2006) Kinetic dependence to HIV-1 entry inhibition. *J. Biol. Chem. 281*, 25813−21.

(27) Ingallinella, P., Bianchi, E., Ladwa, N. A., Wang, Y. J., Hrin, R., Veneziano, M., Bonelli, F., Ketas, T. J., Moore, J. P., Miller, M. D., and Pessi, A. (2009) Addition of a cholesterol group to an HIV-1 peptide fusion inhibitor dramatically increases its antiviral potency. *Proc. Natl. Acad. Sci. U. S. A. 106*, 5801−6.

(28) Porotto, M., Rockx, B., Yokoyama, C. C., Talekar, A., Devito, I., Palermo, L. M., Liu, J., Cortese, R., Lu, M., Feldmann, H., Pessi, A., and Moscona, A. (2010) Inhibition of Nipah virus infection in vivo: targeting an early stage of paramyxovirus fusion activation during viral entry. *PLoS Pathog. 6*, e1001168.

(29) Porotto, M., Yokoyama, C. C., Palermo, L. M., Mungall, B., Aljofan, M., Cortese, R., Pessi, A., and Moscona, A. (2010) Viral entry inhibitors targeted to the membrane site of action. *J. Virol. 84*, 6760−8.
(30) Rajendran, L., Schneider, A., Schlechtingen, G., Weidlich, S., Ries, J., Braxmeier, T., Schwille, P., Schulz, J. B., Schroeder, C., Simons, M., Jennings, G., Knolker, H. J., and Simons, K. (2008) Efficient inhibition of the Alzheimer's disease beta-secretase by membrane targeting. *Science 320*, 520−3.
(31) Teruya, K., Nishizawa, K., and Doh-ura, K. (2010) Semisynthesis of a protein with cholesterol at the C-terminal, targeted to the cell membrane of live cells. *Protein J. 29*, 493−500.
(32) Lee, H., Venable, R. M., Mackerell, A. D., Jr., and Pastor, R. W. (2008) Molecular dynamics studies of polyethylene oxide and polyethylene glycol: hydrodynamic radius and shape anisotropy. *Biophys. J. 95*, 1590−9.
(33) Wexler-Cohen, Y., Ashkenazi, A., Viard, M., Blumenthal, R., and Shai, Y. (2010) Virus-cell and cell-cell fusion mediated by the HIV-1 envelope glycoprotein is inhibited by short gp41 N-terminal membrane-anchored peptides lacking the critical pocket domain. *FASEB J. 24*, 4196−202.
(34) Wexler-Cohen, Y., and Shai, Y. (2007) Demonstrating the C-terminal boundary of the HIV 1 fusion conformation in a dynamic ongoing fusion process and implication for fusion inhibition. *FASEB J. 21*, 3677−84.
(35) Wexler-Cohen, Y., and Shai, Y. (2009) Membrane-anchored HIV-1 N-heptad repeat peptides are highly potent cell fusion inhibitors via an altered mode of action. *PLoS Pathog. 5*, e1000509.
(36) Bader, B., Kuhn, K., Owen, D. J., Waldmann, H., Wittinghofer, A., and Kuhlmann, J. (2000) Bioorganic synthesis of lipid-modified proteins for the study of signal transduction. *Nature 403*, 223−6.
(37) Peisajovich, S. G., Gallo, S. A., Blumenthal, R., and Shai, Y. (2003) C-terminal octylation rescues an inactive T20 mutant: implications for the mechanism of HIV/SIMIAN immunodeficiency virus-induced membrane fusion. *J. Biol. Chem. 278*, 21012−7.
(38) Luo, C., Wang, K., Liu de, Q., Li, Y., and Zhao, Q. S. (2008) The functional roles of lipid rafts in T cell activation, immune diseases and HIV infection and prevention. *Cell Mol. Immunol. 5*, 1−7.
(39) Waheed, A. A., and Freed, E. O. (2010) The Role of Lipids in Retrovirus Replication. *Viruses 2*, 1146−1180.
(40) Vincent, N., Genin, C., and Malvoisin, E. (2002) Identification of a conserved domain of the HIV-1 transmembrane protein gp41 which interacts with cholesteryl groups. *Biochim. Biophys. Acta 1567*, 157−64.
(41) Van Laethem, F., Liang, X., Andris, F., Urbain, J., Vandenbranden, M., Ruysschaert, J. M., Resh, M. D., Stulnig, T. M., and Leo, O. (2003) Glucocorticoids alter the lipid and protein composition of membrane rafts of a murine T cell hybridoma. *J. Immunol. 170*, 2932−9.
(42) Schumann, J., Leichtle, A., Thiery, J., and Fuhrmann, H. (2011) Fatty acid and peptide profiles in plasma membrane and membrane rafts of PUFA supplemented RAW264.7 macrophages. *PLoS One 6*, e24066.
(43) Spector, A. A. (1975) Fatty acid binding to plasma albumin. *J. Lipid Res. 16*, 165−79.
(44) Benting, J., Rietveld, A., Ansorge, I., and Simons, K. (1999) Acyl and alkyl chain length of GPI-anchors is critical for raft association in vitro. *FEBS Lett. 462*, 47−50.
(45) Peng, L., Minbo, H., Fang, C., Xi, L., and Chaocan, Z. (2008) The interaction between cholesterol and human serum albumin. *Protein Pept. Lett. 15*, 360−4.
(46) Charbonneau, D. M., and Tajmir-Riahi, H. A. (2010) Study on the interaction of cationic lipids with bovine serum albumin. *J. Phys. Chem. B 114*, 1148−55.
(47) Fishburn, C. S. (2008) The pharmacology of PEGylation: balancing PD with PK to generate novel therapeutics. *J. Pharm. Sci. 97*, 4167−83.
(48) Dennis, M. S., Zhang, M., Meng, Y. G., Kadkhodayan, M., Kirchhofer, D., Combs, D., and Damico, L. A. (2002) Albumin binding as a general strategy for improving the pharmacokinetics of proteins. *J. Biol. Chem. 277*, 35035−43.

CHAPTER 5

IMPROVING THE PHARMACOKINETICS OF D-PEPTIDE HIV-1 ENTRY INHIBITORS

Joseph S. Redman, J. Nicholas Francis, Robert Marquardt, Brett D. Welch, Alan Mueller, Debra M. Eckert, and Michael S. Kay

Abstract

Unmodified peptides generally have *in vivo* half-lives on the order of minutes, making pharmacokinetic (PK) enhancement necessary. Herein we evaluate several strategies for enhancing PK in the context of our lead candidate PIE12-trimer, a protease-resistant D-peptide HIV entry inhibitor. Surprisingly, PIE12-trimer conjugates show a general reduction in half-life compared to equivalent monomeric conjugates. PEGylation with a 40 kDa Y-branched PEG greatly improves PIE12's half-life but reduces antiviral potency. Moreover, fatty acid conjugation (acylation) and alkane conjugation of comparable lengths were found to behave significantly differently. Fatty acids failed to improve potency, but reduced the volume of distribution and clearance 6-fold, while alkane conjugates significantly improved potency with only modest effects on half-life. Cholesterol conjugation dramatically improves potency while concurrently improving half-life. Because of its simultaneous improvements in potency and PK, cholesterol

conjugated PIE12-trimer is an especially promising therapeutic in the arsenal against HIV.

Introduction

Peptide therapeutics are an increasingly important class of medicines. Peptides have advantages over small molecules in terms of improved target affinity and specificity, as well as an ability to disrupt protein-protein interactions (generally considered "undruggable" by small molecules)[1]. Furthermore, peptides have advantages over proteins in that they can be chemically synthesized, can penetrate deeper into tissues, and are generally less immunogenic[1].

Despite these advantages, peptide therapeutics face considerable pharmacokinetic (PK) challenges. Peptides can be rapidly cleared by the kidneys and degraded by proteases, leading to short half-lives. They also do not readily penetrate through cell membranes[1], limiting access to potential intracellular targets and reducing transcellular migration. These same limitations prevent oral administration of peptides such that they must be delivered parenterally, usually by subcutaneous (SC) injection. Although generally not as preferable as oral delivery, self-administered subcutaneous drugs are readily accepted by patients for multiple indications, such as diabetes and HCV.

Recently we reported the development of a highly potent protease-resistant D-peptide inhibitor of HIV-1 entry, PIE12-trimer, that exhibits sub-pM binding affinity and high pM potency against every major circulating clade of HIV-1[2,3]. Using a polyethylene glycol (PEG) scaffold with three arms of discrete length for the attachment of PIE12 (a peptide composed solely of D-amino acids), synthesis of PIE12-trimer has

been simplified and yields increased. Moreover, an orthogonally reactive fourth linker arm makes conjugation to potency and PK enhancing moieties possible (Fig. 5-1).

PIE12-trimer's target, gp41, is only transiently exposed during HIV fusion. Because PIE12-trimer's off-rate greatly exceeds that time, PIE12-trimer potency is only limited by on-rate, which can be increased by membrane-tethering moieties on the fourth-arm. Prolonging the off-rate improves affinity for gp41, but not its potency. Thus, PIE12-trimer binds gp41 with an excess of binding energy. This excess affinity, dubbed the "resistance capacitor," significantly delays the onset of HIV resistance because mutations that reduce affinity are still inhibited with equal potency, preventing the stepwise accumulation of resistance mutations[3]. Overall, PIE12-trimer's broad potency combined with its "charged" resistance capacitor provides an ideal preclinical candidate for the prevention and treatment of HIV/AIDS.

Ultimately our goal is to develop a weekly or monthly subcutaneous injectable by conjugating potency and PK enhancing moieties to PIE12-trimer. For peptides in general, PK-enhancing moieties can improve half-life by reducing clearance (e.g., by avoiding renal filtration) or sheltering peptides from proteases. As a D-peptide, PIE12-trimer is unique because it is already protease stable. Thus, our conjugates will provide the first clear view of the pure clearance-reducing potential endowed by a given PK-enhancing moiety, without the need for considering a concurrent reduction in degradation.

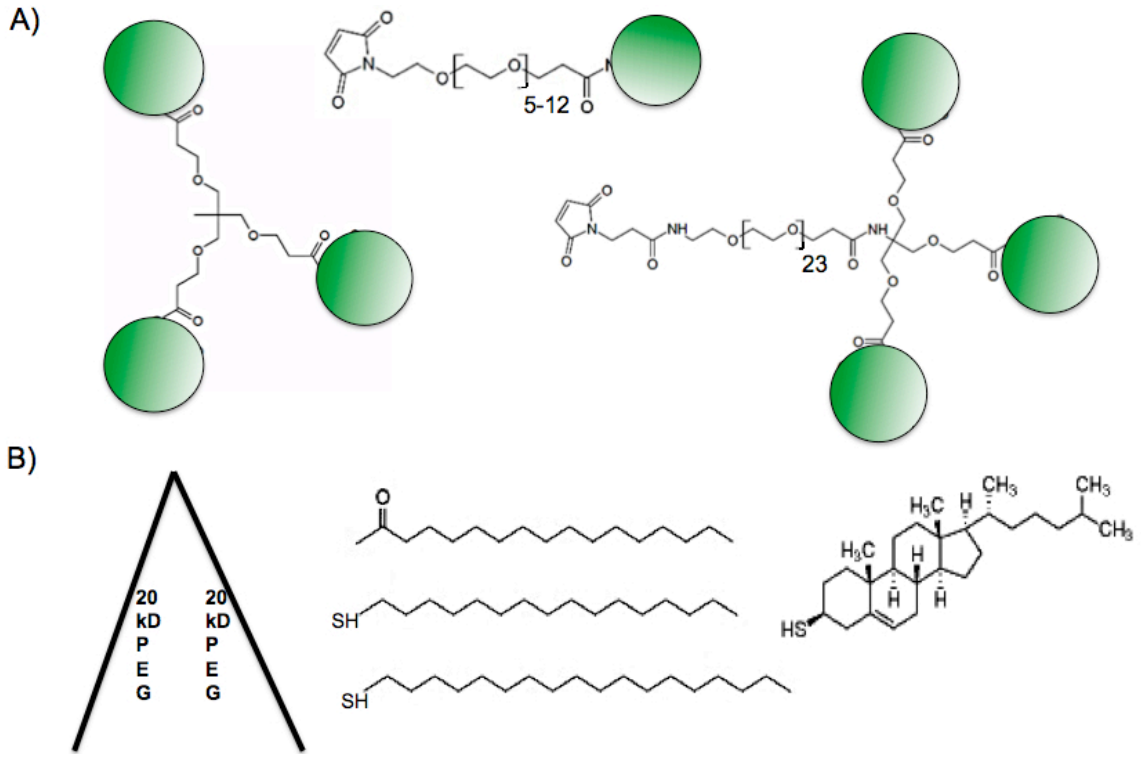

Figure 5-1. PIE12 and PIE12-trimer Scaffolds with PK-Enhancing Cargoes. PIE12 is represented by green circles. A) PIE12-trimer, activated PIE12, and activated PIE12-trimer are shown schematically (each PIE12 of PIE12-trimer is linked to the scaffold with a discrete PEG_4 linker, not shown). B) 40 kDa Y-branched PEG, palmitic acid, aliphatic C16 and C18 chains, and cholesterol are conjugated to PIE12 and PIE12-trimer by maleimide or NHS-ester chemistry. (modified from[3])

Selection of PK-Enhancing Moieties

When choosing PK-enhancing moieties, we considered both clinically validated strategies (such as PEGylation utilized for INFα2a in PEGASYS, and acylation utilized for a GLP-1 analogue in Victoza) as well as strategies in preclinical development (cholesterol and HSA conjugation)[4,5]. The benefits and challenges of each are described.

PEGylation

PEGylation is a validated strategy for enhancing PK with eleven approved products. PEG conjugation improves PK primarily by increasing drug size to reduce

renal filtration, while also decreasing proteolysis and reducing immunogenicity for susceptible proteins. The primary challenge of PEGylation is to add enough PEG to improve pharmacokinetics without sterically inhibiting the activity of the conjugate. Approved PEGylated compounds to date have utilized 20-40 kDa of PEG through single or multiple attachments. This amount of PEG is large enough to avoid renal filtration, but not too much as to completely inhibit activity or promote uptake into reticuloendothelial cells[6].

PEGASYS is a particularly well-studied PEGylated protein, and utilizes a single branched 40 kDa PEG. Branched PEGs are reported to increase half-life and better preserve conjugate activity compared to mass-equivalent straight-chains[7]. Branched PEGs also better protect against proteolysis[8]. Compared to unconjugated interferon, the 40 kDa branched PEG of PEGASYS increases IV half-life in humans from 3.8 to 65 h and reduces the volume of distribution 5-fold, thereby slowing clearance 100-fold[9] (Table 5-1). This enhanced PK profile enables once-weekly subcutaneous administration.

Unlike most PEGylated products, however, our peptide is an inhibitor, not a hormone or enzyme. Therefore doses must be higher and steadier, so questions regarding PEG toxicity become necessary to consider. Fortunately, PEG appears to be remarkably nontoxic. For example, the PEG 400 excipient in intravenous (IV) busulfan can be given at 300 mmoles (110 g) per week without noticeable toxicity[10]. With increasing dose, eventually PEG toxicity manifests as proximal renal tubule swelling. Recently a patient was given an average of 650 mmoles (240 g) per week of PEG 400 excipient in IV lorazepam for a duration of 43 days. Renal toxicity developed but completely resolved upon discontinuation of therapy[11]. In another report, 32 patients received IV

Table 5-1. Terminal Half-Lives and Volumes of Distribution for Relevant FDA-Approved and Investigational Products.

	Human (60-100 kg)			Rat (250-350 g)			Mouse (25-35 g)		
	IV	SC	Vd (L)	IV	SC	Vd (mL)	IV	SC	Vd (mL)
PEGylation									
Unconjugated INFα2a	3.8 h[9]	3-8 h[8]; 4-6 h[9]	31-73[8]	2.1 h[8]	0.7 h[12]				
PEGASYS [40 kD PEG-INFα2a]	60-80 h	160 h = 6.7 d	8-12[8]	15 h[8]	51 h[12]				
Cimzia (certolizumab pegol) [40 kDa anti-TNF-Fab]		14 d[13]	6-8[13]						
Omontys (peginesitide) [40 kDa PEG with 21aa dimerized peptides]	25 h[14]	53 h[14]	1.5-3.4 per 70 kg[14]						
Lipidation									
Acylation									
Unconjugated GLP-1 (7-37)	1-2 m[15]								
Liraglutide (Palmitated-GLP-1 analogue)	8 h[16]	13 h[17]; 11-15 h[18]	4.9 per 70 kg[17]		4 h[16]				
Unconjugated Insulin	4-6 m[19]	~2.5 h[20]	11.6-19.6[21]						
Insulin Detemir (myristoylated)	19-25 m[22]	5-7 h[23]	7 per 70 kg[23]						
Cholesterol									
T20 (Fuzeon)	1.83 h[24]	3.8 h[25]	6-7[24]	2.8 h[26]					
C34	ND	ND	N/A				0.6 h[4]	0.8 h[4]	210 per kg[4]
C34-Chol	ND	ND	N/A				3 h[4]	6.5 h[4]	30 per kg[4]
Albumin conjugation									
Unconjugated Albumin	19 d[27]		8.4 per 70 kg[28]	1.9 d[27]			1 d[27]		
C34-HSA	ND	ND	N/A				~1 d[29]	~1 d[29]	
Albuferon (INFα2b-HSA)		140 h[30]							
CJC-1131 (maleimide GLP-1 analogue)		9-15 d[30]			15-20 h[30]				

nitrofurantoin containing 120-225 g of PEG 300 (~650 mmoles) over 3-5 days. Of these, six developed renal toxicity and two died[11]. It is not clear whether the total mass of PEG or molar concentration contributes more to renal toxicity. However, the high molarity required to observe toxicity, often in the 10's of mM, exceeds the dose of current PEGylated products by approximately 600-fold[10], suggesting general safety of the material.

Acylation and Alkylation

PK-enhancement by acylation is based on the strong interaction of fatty acids with human serum albumin (HSA), which circulates for 19 days (Table 5-1). A secondary PK benefit of acylation is self-association that prolongs absorption from the subcutaneous space[17,31]. Physiologically, free fatty acids (FFAs) circulate bound to HSA, which has two high-affinity sites for FFAs and several secondary sites. [Note that "free" means it is not esterified to glycerol, and should not be taken to mean it is unbound]. Palmitate (C16 fatty acid) and stearate (C18 fatty acid) are the predominant forms of circulating FFAs[32]. FFA levels follow a diurnal pattern (rise during an overnight fast) that normally does not exceed a 2-fold molar excess over HSA[33], although >6-molar excess has been reported in diabetic and obese patients[34]. Circulating FFAs are anionic, although the charge is reputed to contribute little to albumin binding.[35]

The affinity of HSA for FFAs is in the mid-to-low nM range[35-37]. Notably, FFAs do not bind significantly to any other circulating particles, including low-density lipoproteins (LDL)[35]. Furthermore, FFAs bind sites on HSA that appear to be independent of those used by most small molecules. For example, although more than

98% of circulating myristoylated (C14 fatty acid) insulin detemir is bound to albumin, there have been no clinically relevant interactions noted with other protein-bound drugs[23,35].

Victoza (liraglutide), a GLP-1 analogue, utilizes palmitate conjugation to increase its half-life, enabling once-daily subcutaneous dosing. During the development of liraglutide, a myriad of other potential PK-enhancing lipids were evaluated[18]. Notably, stearate conjugates had a better half-life but reduced activity, so palmitate was chosen for development. Interestingly, liraglutide is not cleared by the kidneys or liver[17], consistent with its high association with albumin. Apparently the majority of liraglutide is catabolized and absorbed by cells.

Based on publications that identify a fatty acid's aliphatic chain as the critical moiety for albumin interaction[35], we also explored alkane-conjugation as a substitute for acylation. Alkanes only differ from fatty acyl groups by a single terminal carbonyl, and thiol-alkanes made synthesis straightforward using the maleimide chemistry of our scaffold's fourth-arm linker.

Cholesterol Conjugation

Cholesterol conjugation of an HIV C-peptide inhibitor improves PK in mice[4]. As a newer strategy for which there are no FDA-approved examples, it is as yet unclear exactly how cholesterol improves PK, although we suspect a combination of cell membrane and albumin association. Two studies report 435 μM[38] and 24.6 μM[39] cholesterol affinity for HSA. It is also reported, and consistent with our data, that

cholesterol provides superior membrane-binding over palmitate[4], although this interaction is readily reversible[3].

HSA Conjugation

Whereas acylation and, likely, cholesterol conjugation improve PK by noncovalently interacting with albumin, a direct linkage is reported to improve PK even further, consistent with albumin's long half-life (Table 5-1). Of HSA's 35 cysteines, only one is available for thiol-specific conjugation, Cys-34, found in the Ia subdomain[40]. Importantly, Cys-34 is buried and unavailable for conjugation unless the neighboring fatty acid binding site is occupied by fatty acid[40]. Physiologically, free thiols like Cys-34 are unusual, prompting the development of *in vivo* HSA conjugation prodrugs[40]. Among albumin conjugates studied to date, Albiglutide (GLP-1), Albugon (GLP-1), and Albuferon (INFα2b) are the most developed[5,30,41]. An albumin-C34 anti-HIV entry inhibitor has also been reported[29].

Materials and Methods

Synthesis of Monomeric PIE12 and Conjugates

PIE12 was synthesized by RS Synthesis (Louisville, KY) using standard solid-phase methods. PIE12-PEG_{12}-cholesterol was synthesized by reacting 3 mM PIE12 with 4 mM maleimide-PEG_{12}-NHS ester (Quanta Biodesign, 10284) in dimethylacetamide (DMAC) with 200 mM triethylamine (TEA) for 30 min at RT, and then purified by reverse-phase HPLC (water/acetonitrile gradient in 0.1% TFA) on a Waters BEH XBridge 10 μm, 300 Å C18 column (RP-HPLC). Two mM of the purified product,

PIE12-PEG_{12}-maleimide, was reacted with 4 mM thiocholesterol (Sigma-Aldrich, 136115) in DMAC with 200 mM TEA for 45 min at RT. PIE12-PEG_{12}-palmitate was synthesized by reacting 3 mM PIE12 with 3 mM Fmoc-N-amido-PEG_{12}-NHS ester (Quanta Biodesign, 10996) in DMAC with 200 mM TEA for 30 min at RT, and then purified by RP-HPLC. The lyophilized product, Fmoc-N-amido-PEG_{12}-PIE12, was dissolved in 20% piperidine in DMF to deprotect the terminal amine and repurified by RP-HPLC. Two mM of the purified product, PIE12-PEG_{12}-NH_2, was reacted with 4 mM palmitic acid NHS ester (Sigma-Aldrich, P1152) in DMAC with 500 mM TEA for 45 min at RT. PIE12-PEG_5-40 kDa Y-branched PEG was synthesized by reacting 2 mM PIE12 with 20 mM bis-NHS ester PEG_5 (Quanta Biodesign, 10224) in 100 mM HEPES pH 8.0 for 90 seconds. The reaction was quenched in 5% acetic acid and purified by RP-HPLC. Two mM of the purified product, PIE12-PEG_5-NHS ester, was reacted with 2.5 mM 40 kDa Y branched PEG-amine (JenKem, A0010), and then purified by RP-HPLC.

Synthesis of PIE12-trimer and PIE12-trimer Conjugates

PIE12-trimer and PIE12-trimer-PEG_{24}-maleimide were synthesized as previously described[3]. PIE12-trimer C8, C16, C18 and cholesterol conjugates were synthesized by reacting 3 mM PIE12-trimer-PEG_{24}-maleimide with 4.5 mM thiocholesterol (Sigma Aldrich, 136115), 1-octanethiol (Sigma-Aldrich, 471836), 1-hexadecanethiol (Sigma-Aldrich, 52270), or 1-octadecanethiol (Sigma Aldrich, 01858) in DMAC with 200 mM TEA for 60 min at RT, and then purified by RP-HPLC. Palmitate conjugated PIE12-trimer was synthesized by first reacting 3 mM PIE12-trimer-PEG_{24}-maleimide with 4.5 mM D-Cysteine in DMAC with 200 mM TEA for 60 min at RT, and then purified by RP-

HPLC. Two mM of the purified product was reacted with 5 mM palmitic acid NHS ester (Sigma-Aldrich, P1152) in DMAC with 500 mM TEA for 45 min at RT and then purified by RP-HPLC.

Pseudoviral Assay

Pseudovirion infectivity assays were conducted as previously described[2,42]. Briefly, a six-point dilution series of inhibitor was generated in quadruplicate in HOS-CD4-CXCR4 (for HXB2) or HOS-CD4-CCR5 (for JRFL) target cell seeded plates, after which HXB2 (X4) and JRFL (R5) luciferase reporter psuedovirions were added. After 2 days, cells were lysed using GloLysis buffer (Promega) and BrightGlo (Promega) luciferase reagent was added. Luminescence was read on a PolarStar Optima (BMG) plate reader. Counts were normalized to uninhibited controls. Curves were plotted and fit to a standard IC_{50} equation for normalized data $[1 - c/(IC_{50} + c)]$, weighting each point by its standard error using KaleidaGraph (Synergy software). Reported IC_{50} values are the average of at least two independent assays.

HSA Affinity Studies

A 4 x 100 mm, 5 μm Chiral-HSA column was generously donated from Chiral Technologies Inc. to enable HSA affinity studies. Samples were injected on an Agilent HPLC system and eluted isocratically at 0.9 mL/min with 15 mM potassium phosphate buffer, pH 7.4 with 7.5% ACN and 7.5% isopropanol at 37 °C. All absorbance traces were measured at 214 nm except for warfarin, which was measured at 308 nm.

Pharmacokinetic Studies

Animals, Dosing, and Collection

For monomers PIE12, Chol-PIE12 and PEG40-PIE12, PK studies were conducted by Invitek. All other studies were conducted by Navigen. Studies were conducted by dosing three Sprague Dawley rats (0.22-0.44 kg) for each compound and route (doses listed in Table 5-5). ~300 μL blood samples were taken over 10 timepoints and anticoagulated with lithium heparin. Samples were spun and ~150 μL plasma was collected for quantitation.

LC/MS/MS Quantitation

Drug concentrations in plasma were determined using an AB Sciex API 3000 triple-quad LC/MS/MS by MRM methods. Standard curves were produced in pooled Sprague Dawley rat plasma anticoagulated with lithium heparin (Bioreclamation). Plasma samples were prepared for LC/MS/MS by spiking with internal standard followed by precipitation 2:1 with 98% acetonitrile (ACN) / 2% formic acid. Supernatants were run over a C18 reverse-phase column (Waters, 4.6 x 50 mm, 5 μm, XBridge BEH300) on an Agilent HPLC system. Lipid conjugates required lower source temperatures (300 °C vs. 500 °C) for best reproducibility. For all studies except PEG40-PIE12 the column was regenerated after every group of 3 rats by running an isocratic gradient of 25% ddH_2O, 25% MeOH, 25% IPA, and 25% ACN for 30 min. This procedure was found to be sufficient for removing retained phospholipids. For PEG40-PIE12, a blank run and isocratic wash of 25% ddH_2O, 25% MeOH, 25% IPA, and 25% ACN for 5 min were required after every sample to prevent carryover.

Determining an appropriate starting ACN concentration was also necessary for effective elution. For PIE12 (mass transition 1022.3/180.1), Palm-PIE12 (mass transition 721.4/282.3), and Chol-PIE12 (mass transition 1066.6/229.1), the starting concentrations were 15%, 40%, and 82% ACN, respectively. PEG40-PIE12 was fragmented in the source (5000 Volts) and the mass transition monitored was 133.1/89 with a starting concentration of 37% ACN. For PIE12-trimer (mass transition 1431.7/180.1), Palm-PIE12-trimer (mass transition 1466.5/554.5), C16-PIE12-trimer (mass transition 1450.1/453.4), C18-PIE12-trimer (mass transition 1454.5/481.3), and Chol-PIE12-trimer (mass transition 1474.2/1694.9), the starting concentrations were 35%, 40%, 65%, 65%, and 75% ACN, respectively.

Fitting the Data

IV-dosed time-points were plotted and fit to a noncompartmental model to determine C_0 and the terminal half-life ($T_{1/2}$) using the equation $C(t) = C_0*((1/2)^{(t/T_{1/2})})$, where C_0 represents the theoretical starting concentration if drug were instantly distributed (no alpha phase). The terminal half-life is then converted into the decay rate k_e ($k_e = \ln 2/T_{1/2}$). SC-dosed time-points were plotted and fit to the model $C(t) = K*(ka/(ka-ke))*[\exp(-ke*t) - \exp(-ka*t)]$, where K is a constant, k_a is the rate of absorption, and k_e is the decay rate determined from the IV fit (weighting to the standard deviation of duplicate measurements, KaleidaGraph). Volume of distribution (Vd) is determined by dividing dose (in moles) by C_0. Because elimination is first order, clearance (CL) can be determined by the relationship $CL = ((\ln 2)*(Vd))/(T_{1/2})$. Areas

under the curve (AUCs) were calculated by integrating fits from zero to infinity. Bioavailability (F) is determined by $F = 100*(AUC_{SC} / AUC_{IV})*(Dose_{IV} / Dose_{SC})$

Metabolism Studies

PK plasma samples were prepared for pseudoviral assay by 2:1 precipitation with 98%ACN/2%FA, followed by centrifugation for 10 min in a microcentrifuge at 13,000 rpm. Supernatants were spun to dryness on speed-vac, followed by resuspension in 50 mM HEPES pH 7.4 to their original volumes. Pooled plasma was prepared as a control. Samples were then diluted 1:10 or 1:100 in DMEM/10% FBS and assessed in a pesudoviral assay as described (diluting samples 2-fold further) with normalization for uninhibited controls in the presence of prepared control plasma (1:20 prepared plasma slightly reduced viral infectivity). A standard IC_{50} curve was prepared alongside plasma samples and was used to convert percent inhibition to a concentration of drug present in each sample.

Results

Our Designs

Using clinically successful and promising preclinical PK-enhancing moieties, we designed and synthesized several PIE12 and PIE12-trimer conjugates (Table 5-2). The effects of each conjugation on antiviral potency are shown in Table 5-3. As expected, the large 40 kDa Y-branched PEG reduces the potency of our inhibitors, likely due to steric interference with target binding. Specifically, the potency of monomeric PIE12 is reduced by 2.5 (HxB2) and 10-fold (JRFL), and the potency of PIE12-trimer is reduced

Table 5-2. Conjugate Designs and Naming Scheme

Abbreviated name	**Full name**
Monomers	
PIE12	PIE12GK
PEG40-PIE12	PIE12GK-PEG5-40 kDa Y-branched PEG
Palm-PIE12	PIE12GK-PEG12-Palmitate
Chol-PIE12	PIE12GK-PEG12-Maleimide-Thiocholesterol
Trimers	
PIE12-trimer	$(PIE12GK\text{-}PEG4)_3$
PEG40-PIE12-trimer	$(PIE12GK\text{-}PEG4)_3$-PEG_{24}-Maleimide-D-Cys-40 kDa Y-branched PEG
C8-PIE12-trimer	$(PIE12GK\text{-}PEG4)_3$-PEG_{24}-Maleimide-Octanethiol
Palm-PIE12-trimer	$(PIE12GK\text{-}PEG4)_3$-PEG_{24}-Maleimide-D-Cys-Palmitate
C16-PIE12-trimer	$(PIE12GK\text{-}PEG4)_3$-PEG_{24}-Maleimide-Hexadecanethiol
C18-PIE12-trimer	$(PIE12GK\text{-}PEG4)_3$-PEG_{24}-Maleimide-Octadecanethiol
Chol-PIE12-trimer	$(PIE12GK\text{-}PEG4)_3$-PEG_{24}-Maleimide-Thiocholesterol

Table 5-3. Potency Effects of PK Conjugation

Inhibitor	**%ACN elution on reverse-phase C18**	**HxB2** IC_{50} (nM)	**JRFL** IC_{50} (nM)
Monomers			
PIE12	41	$37 \pm 2.3^{\dagger}$	$580 \pm 21.4^{\dagger}$
PEG40-PIE12	47	93 ± 32	5640 ± 950
Palm-PIE12	67	243 ± 23	1660 ± 14
Chol-PIE12	88	$12 \pm 3.6^{*}$	28 ± 2.4
Trimers			
PIE12-trimer	51	$0.72 \pm 0.04^{*}$	$2.1 \pm 0.28^{*}$
PEG40-PIE12-trimer	47	9.5 ± 1.4	71 ± 12
C8-PIE12-trimer	55	$0.42 \pm 0.01^{*}$	2 ± 0.58
Palm-PIE12-trimer	62	0.225 ± 0.008	0.540 ± 0.041
C16-PIE12-trimer	71	$0.09 \pm 0.014^{*}$	$0.11 \pm 0.012^{*}$
C18-PIE12-trimer	76	$0.054 \pm 0.018^{*}$	$0.087 \pm 0.012^{*}$
Chol-PIE12-trimer	80	$0.013 \pm 0.0013^{*}$	$0.019 \pm 0.003^{*}$

(†from[2], *from[3])

by 13 (HxB2) and 34-fold (JRFL). In comparison, the same PEG on PEGASYS reduces activity 14-fold[9].

In contrast, the smaller hydrophobic conjugations mostly increased the potency of our inhibitor, but to varying extents, from little or no increase with C8 conjugation to a 2 log improvement with cholesterol conjugation. The C8 alkane only modestly improves potency, while C16 and C18 alkanes improve potency significantly. A C16 fatty acid (palmitate) also improves potency, but to a much lesser extent than C16 alkane, suggesting that acyl groups interact with membranes differently than alkanes. Cholesterol interacts with membranes even more strongly[4], improving potency over other lipid conjugates. Notably, cholesterol conjugates remain very soluble[3].

PIE12-trimer conjugations to albumin are still preliminary, but have been informative. Using incompletely purified material (approximately 4:1 HSA to HSA-PIE12-trimer), there appears to be only a modest five-fold loss in potency compared to PIE12-trimer in pseudoviral infectivity assays. However, challenges remain regarding complete purification of HSA-PIE12-trimer, and reliable quantitation of HSA-PIE12-trimer in plasma samples. Gel filtration is successful at removing unreacted PIE12-trimer, but does not remove unreacted HSA. Unreacted HSA and HSA-PIE12-trimer conjugates can be separated by reverse-phase HPLC, but this process completely denatures albumin. It has been reported, however, that not only can HSA be completely recovered off a reverse-phase column[43], it can also be efficiently refolded following HPLC denaturation and lyophilization[44,45]. Soluble microaggregates, if present, can be detected by light scattering[44].

HSA Affinity Studies

Acyl and alkane conjugates were synthesized with the intention to improve PK through HSA binding. To assess the relative HSA affinities of PIE12 and PIE12-trimer conjugates we utilized an immobilized HSA affinity column. Longer retention times on this column correlate with higher HSA affinity[46] (Table 5-4, Fig. 5-2). Small molecules with known affinities for HSA have been included for reference; L-Tryptophan (90.9 μM K_D) and (R)- and (S)-warfarin (4.8 and 3.8 μM K_D respectively)[46].

Notably, Chol-PIE12-trimer shows reduced affinity for HSA compared to Palm-PIE12-trimer, but comparable affinity to C18-PIE12-trimer. PEG40-PIE12 shows the least affinity for HSA. Interestingly, C8-PIE12-trimer, with its long fourth-arm PEG linker, shows slightly reduced affinity for HSA compared to the three-armed PIE12-trimer, while C16-PIE12-trimer is not so limited.

Table 5-4. HSA Affinity Column Retention Times

Inhibitor	Retention Time (min)
PEG40-PIE12	0.65
C8-PIE12-trimer	1.35
PIE12-trimer	1.5
PIE12	1.6
L-Tryptophan	1.68
C16-PIE12-trimer	4.0
C18-PIE12-trimer	5.7
Chol-PIE12-trimer	5.7
Palm-PIE12-trimer	10.0
R-Warfarin	11.5
S-Warfarin	17.9
Palm-PIE12	21.5

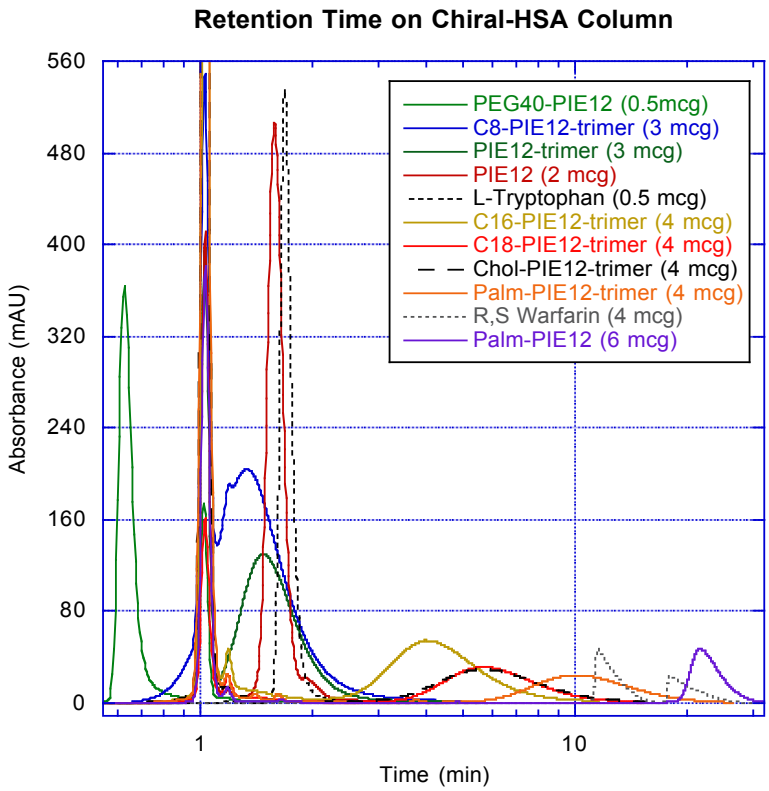

Figure 5-2. HSA Affinity Column Retention Times. Compounds are listed in order of elution. HEPES buffer from the samples elutes at 1.01 min.

PK Studies

In order to understand the PK effects of the different PK-enhancing moieties, we studied conjugates of both PIE12 monomer as well as PIE12-trimer (our lead anti-HIV drug candidate). PK studies of C8 conjugates were not pursued due to poor potency improvements and low affinity for HSA. Similarly, significant losses in potency for PEG40-PIE12-trimer reduced our interest in it as a lead preclinical candidate. Although we did not pursue PK studies for PEG40-PIE12-trimer, we did study PEG40-PIE12 to assess the general PK-enhancing properties of PEGylation. Representative PK data are shown in Figures 5-3 and 5-4, and a summary of PK parameters is given in Tables 5-5 (IV data) and 5-6 (SC data).

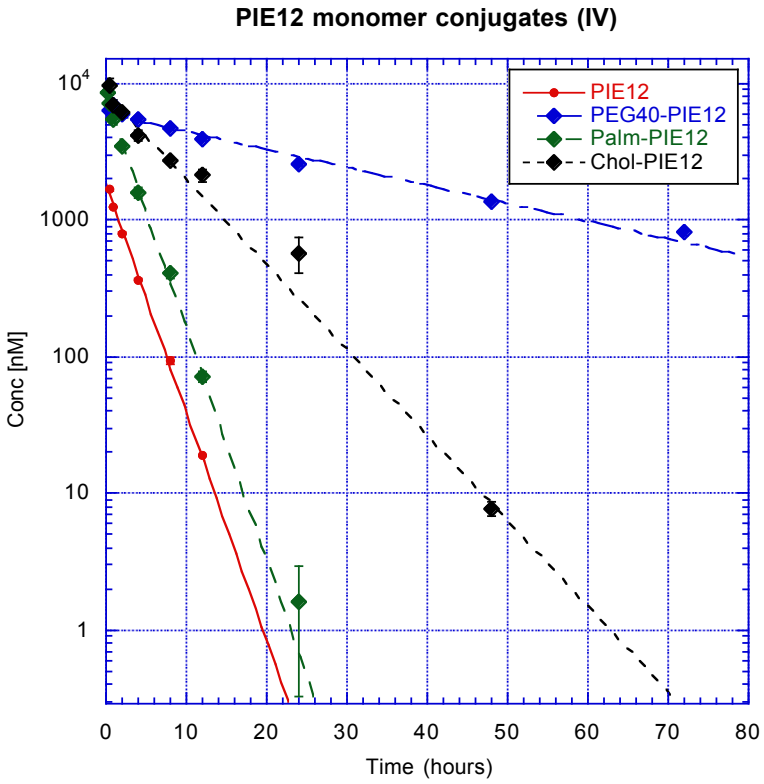

Figure 5-3. Pharmacokinetics of four intravenously administered monomers in rats. Data are from single representative animals. Terminal half-life fits are shown, with linearity establishing first-order clearance. Error bars are the standard deviation of duplicate measurements.

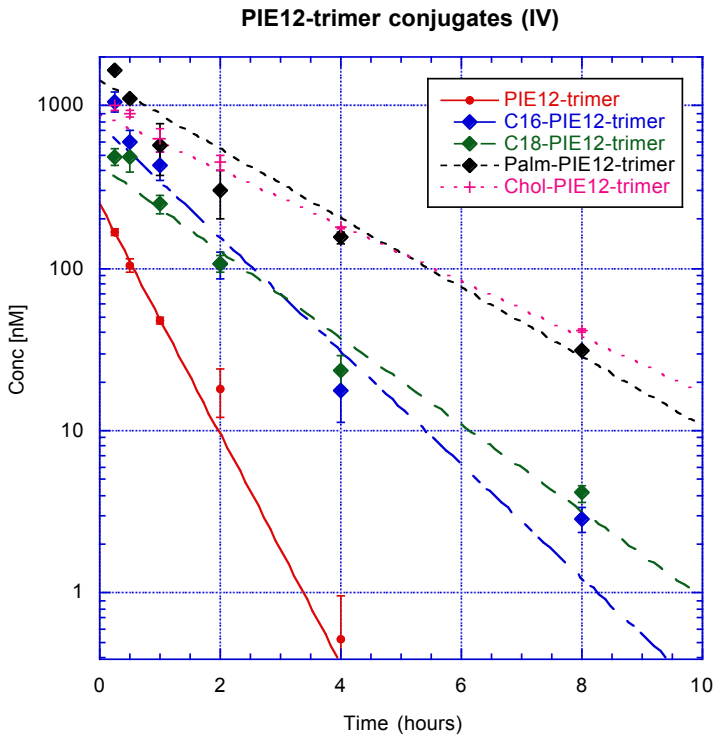

A)

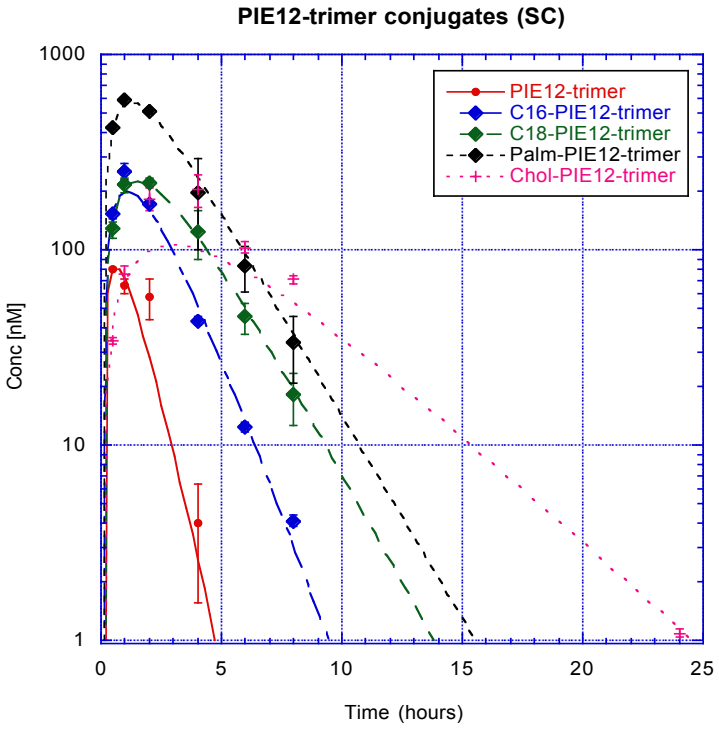

B)

Figure 5-4. Pharmacokinetic data of five trimers in rats. A) Intravenously-administered trimer data from single representative animals. Terminal half-life fits are shown, with linearity establishing first-order clearance. B) Subcutaneously-administered trimer data from single representative animals. Standard two-phase absorption-elimination fits are shown. Error bars are the standard deviation of duplicate measurements.

Table 5-5. IV Pharmacokinetic Parameters of PIE12 and PIE12-trimer Conjugates in Rats.

Inhibitor	m.w.	Dose	Term. $T_{1/2}$ (IV)	IV $AUC_{0\rightarrow\infty}$ (nM*hr)†	Vd (mL)	CL (mL/hour)
Monomers						
PIE12	2043.3	1.4 mg/kg	1.9 h	2,891	116	42
PEG40-PIE12	42345.8	0.9 mg/kg*	26.8 h	223,658	20	0.5
Palm-PIE12	2881.6	1.2 mg/kg	1.8 h	15,534	17.5	6.7
Chol-PIE12	3196.9	2.2 mg/kg	5.1 h	26,451	22	3
Trimers						
PIE12-trimer	7153.2	1 mg/kg	0.54 h	153	211	271
C16-PIE12-trimer	8692.2	1 mg/kg	0.65 h	876	37	39
C18-PIE12-trimer	8720.2	1 mg/kg	0.84 h	814	50	41
Palm-PIE12-trimer	8793.3	1.2 mg/kg	1.5 h	1675	42	20
Chol-PIE12-trimer	8835.4	1 mg/kg	1.6 h	2049	38	16

*PIE12 portion of the weight; † normalized to dose (AUC per mg/kg)

Table 5-6. SC Pharmacokinetic Parameters of PIE12-trimer Conjugates in Rats.

Inhibitor	Dose	Term. $T_{1/2}$ (SC)	Abs $T_{1/2}$	SC $AUC_{0\rightarrow\infty}$ (nM*hr)†	F (%)	Tmax (hr)	Cmax (nM)
Trimers							
PIE12-trimer	1 mg/kg	1 h	0.7 h	451	295	0.84 h	84
C16-PIE12-trimer	1 mg/kg	1.3 h	0.9 h	936	107	1.1 h	183
C18-PIE12-trimer	1 mg/kg	1.5 h	1.2 h	745	92	1.4 h	187
Palm-PIE12-trimer	1.2 mg/kg	2.1 h	0.5 h	609	36	1.2 h	603
Chol-PIE12-trimer	1 mg/kg	3.4 h	2.7 h	340	17	3 h	146

† normalized to dose (AUC per mg/kg)

The terminal half-life is the most commonly reported PK parameter, often referred to simply as “half-life”; it is the steady half-life that occurs after a compound is distributed throughout an animal. PIE12 has a 1.9 hour IV terminal half-life vs. only 0.54 hours for PIE12-trimer. Similarly, Chol-PIE12 and Chol-PIE12-trimer IV terminal half-lives differ by 3- to 4-fold, 5.1 hours and 1.6 hours, respectively. Whereas PEG40-PIE12 greatly enhances half-life to 26.8 hours, Palm-PIE12 did not affect the terminal half-life compared to PIE12 (1.8 vs. 1.9 hours, respectively). However, the palmitate moiety did reduce the volume of distribution and clearance 6-fold. Palmitate on Palm-PIE12-trimer

did improve half-life compared to PIE12-trimer (1.5 vs. 0.54 hours, respectively), reduced clearance ~10-fold, and reduced volume of distribution ~6-fold.

Notably, identical compounds have different terminal half-lives depending on the route of administration, because terminal half-lives are apparent half-lives (a mix of absorption from tissue compartments and elimination[47]). All PIE12-trimer conjugates acquired an approximate 2-fold improvement in terminal half-life after subcutaneous administration, with the exception of Palm-PIE12-trimer (~1.3-fold improved).

Discussion

Potency Effects

It is interesting to note that for PIE12-trimer conjugates, elution time off a C18 reverse-phase column correlates with potency, indicating that potency enhancement is directly related to hydrophobicity of the lipid moiety. PIE12-trimer potency is limited by on-rate, so improvements in potency reflect improvements in membrane binding[3]. This indicates a relationship where the more hydrophobic lipids interact more effectively with membranes.

Given the potency increase with palmitate conjugation to PIE12-trimer, it is surprising that monomeric PIE12 is not similarly enhanced. Although the PEG_{12} linker between PIE12 and palmitate is shorter than optimal[3], the same linker between PIE12 and cholesterol still improves potency over PIE12. Considering palmitate's higher affinity for HSA over cholesterol, it is possible that fatty acid conjugates are being sequestered by albumin in the assay, and that PIE12-trimer's branched PEG scaffold prevents sequestration to the same degree.

PK Effects

Because of PIE12-trimer's large volume of distribution and rapid equilibration (no alpha phase noted), the resultant low concentrations were near the sensitivity limit of our method of quantitation. Reduced accuracy regarding AUC calculations are likely responsible for the apparent higher bioavailability of SC vs. IV administered PIE12-trimer.

The difference in half-life between alkylated and acylated conjugates, which differ only by a carbonyl group, is surprising (comparing data for C16 acylation and C16 alkylation). The uncharged acyl group significantly reduces hydrophobicity compared to an equivalent alkane, lowering membrane affinity and antiviral potency while simultaneously improving albumin affinity and half-life. Differences can also be observed in the absorption rate, with the more hydrophobic alkanes prolonging absorption from the subcutaneous space. Like PEG, acylation reduces the volume of distribution, consistent with albumin binding. Compared to Palm-PIE12, Palm-PIE12-trimer has reduced albumin affinity and a larger volume of distribution, suggesting the PEG scaffold may be interfering with beneficial HSA interactions.

Half-life comparisons between related PIE12 and PIE12-trimer conjugates are also surprising. While originally we assumed that increasing molecular weight from a monomer to a trimer could only improve half-life by reducing renal filtration, there is actually an across-the-board 3- to 5-fold higher clearance for each PIE12-trimer conjugate. Conjugations to PIE12 monomer improve PK consistent with the literature; PEGylation increases half-life to 26 hours (compared to 15 hours for PEGASYS[8]), acylation reduces the volume of distribution and clearance 6-fold (despite no apparent

change in half-life), and cholesterol conjugation increases half-life to 5.1 hours in rat (comparable to 3 hours for C34-Chol in mice[4]). Notably, for PIE12-trimer the rank order of PK-enhancement is still retained for each moiety, as is the magnitude of improvements endowed by each conjugate. Therefore something specific to PIE12-trimer itself must be reducing its half-life.

One explanation is reduced efficacy of PK-enhancing moieties in the context of PIE12-trimer. There are indications that PIE12-trimer's PEG scaffold may be restricting beneficial interactions between PK-enhancing moieties and HSA and cell membranes. PIE12-trimer conjugates show reduced affinity for HSA and C18 on reverse-phase columns compared to monomer equivalents (Tables 5-3 and 5-4, Fig. 5-2). Furthermore, a C8 alkane conjugated to the long PEG fourth-arm scaffold demonstrates even less affinity for HSA than regular PIE12-trimer. Volumes of distribution are also greater for PIE12-trimer conjugates compared to monomers, consistent with reduced albumin binding. Finally, palmitate conjugation improves PIE12-trimer potency while reducing PIE12 potency, a finding that might be explained by significant HSA sequestration for Palm-PIE12, but less HSA interaction for Palm-PIE12-trimer.

Of the affinity-boosting conjugates, cholesterol produces the best terminal half-life. Cholesterol interacts more weakly with HSA than palmitate, so the enhanced retention is likely due to superior cell membrane binding. This explanation is also consistent with the prolonged absorption rate of Chol-PIE12-trimer from the subcutaneous space (2.7 hours half-life). Cholesterol also reduces the volume of distribution like acylation. However, the cholesterol moiety may be causing sequestration of Chol-PIE12-trimer. The bioavailability of SC-administered Chol-PIE12-

timer is only ~20%, suggesting that long durations of exposure to cell surfaces may lead to cell surface sequestration, endocytosis, or local metabolism. The cholesterol moiety might also direct clearance to the liver through LDL binding. It is known that siRNA-cholesterol conjugates, even pre-bound to HDL or albumin, are redistributed and taken up into LDL particles in mice[48], and humans circulate significantly more LDL than rodents[49]. This disparity may change the pharmacokinetics of cholesterol conjugates in humans. Animal models with more human-like lipid profiles (e.g., Guinea pig, Golden Syrian hamsters, and the LDLR-/- mouse)[49-51] could provide some insight on *in vivo* kinetics in the context of increased circulating LDL concentrations, and may more accurately predict PK in humans.

In the end, the best clinical candidate must balance potency with pharmacokinetics. Although PEGylation improves half-life the most, potency suffers. Palmitate conjugation improves half-life and potency modestly, but to a lesser extent than cholesterol. Alkane conjugation improves potency but does little to improve half-life. Of unknown significance is the decreased volume of distribution created by each conjugation because it is not clear which tissue compartments must be accessed for successful inhibition of HIV transmission. However, it is clear that Fuzeon is highly HSA-bound[25], has a reduced volume of distribution in humans (Table 5-1), and successfully inhibits HIV. Taken as a whole, Chol-PIE12-trimer has become our lead candidate for future studies.

Metabolism Studies

We envision four possibilities to explain the enhanced clearance of PIE12-trimer conjugates. Reduced affinity for membranes and albumin is the simplest explanation. However, enzyme modifications, breakdown, and sequestration are also possible.

To rule out enzyme modification we developed a method to determine the concentration of active compound in plasma samples using our pseudovirus infectivity assay. We reasoned that although molecular weight-shifted metabolites may be missed by LC/MS/MS analysis, it is unlikely that such metabolites would lose antiviral potency, especially given PIE12-trimer's charged resistance capacitor. We analyzed C18-PIE12-trimer because it was the first to reveal a surprisingly low terminal half-life by LC/MS/MS. C18-PIE12-trimer concentrations calculated from the antiviral activity of plasma samples agree with the LC/MS/MS values, indicating that there were no detectable active metabolites in the plasma being missed by LC/MS/MS. Therefore if drug clearance is due to a metabolic process, the metabolites must have greatly reduced antiviral activity. Notably, PIE12-trimer is stable in rat plasma, even after weeks of incubation at 37 °C. Chol-PIE12-trimer is also quite stable in rat plasma, although ~20% becomes oxidized (+16 Daltons) after 24 hours.

We are also pursuing additional methods to discover metabolites. For instance, all PIE12-containing analytes produce an acetylated histidine ion fragment (180.1 Da, +1 charge) with 5% efficiency. By utilizing the "Precursor Ion" mode on the LC/MS, any parent molecule that produces the 180.1 Da daughter ion can be identified with a ~1 μM sensitivity limit (following acetonitrile precipitation of plasma samples), enabling the detection of mass-shifted PIE12-containing metabolites. The sensitivity of this method

might be improved with better cleanup of the sample, so we also plan to utilize affinity purification with IZN17. IZN17 binds PIE12 and PIE12-trimer with 20 nM and sub-pM affinity, respectively. By adding it to plasma samples, all PIE12-containing molecules could be selectively purified. These cleaner samples should enable sensitive identification of metabolites.

Future Directions

Future studies will include a pilot efficacy study in SHIV-infected macaques in order to demonstrate the pharmacokinetics and viral response to unmodified and cholesterol-conjugated PIE12-trimer. Suppression of viral load would indicate successful exposure and efficacy of our D-peptide antivirals *in vivo*. To rule out nonspecific mechanisms of viral clearance, treatment will be halted after one month to demonstrate viral rebound.

Dose-escalation studies in rats are also planned. We would like to assess how PK is affected by changes in stock concentrations (e.g., by creating local depots of self-associated peptide) and total mass delivered. Moreover, these high-dose studies should enable investigation into the clearance mechanism(s) of PIE12-trimer and conjugates. Urine, feces, and bile will be collected to determine the roles of renal filtration and biliary excretion.

Next, we plan to track fluorescently labeled PIE12-trimer conjugates *in vivo* (in rodents) to better understand clearance, volumes of distribution, and possible sites of sequestration. A companion PK study will be done to control for possible PK changes created by the fluorescent moiety. This *in vivo* study will help reveal routes of

elimination and assess access to different tissue compartments (e.g., lymphatic tissue, brain, etc.).

Further, the protease-resistant design of PIE12-trimer enables novel applications. For instance, PIE12-trimer is a promising microbicide candidate (antiviral prophylactic) because it can withstand the protease-rich environment of the vaginal mucosa. Moreover, our several lipid conjugations may enhance PIE12-trimer exposure by augmenting cell surface binding. Oral bioavailability may also be possible. By surviving gut proteases, PIE12-trimer might be formulated with a gut permeabilizing agent to achieve significant circulating concentrations. Promising gut permeabilizers have been extensively reviewed[52,53].

Finally, sustained delivery technologies may also be readily compatible with PIE12-trimer and its conjugates. Microsphere delivery like that utilized by the recently approved Bydureon (once-weekly extended release exenatide) may enable a similarly favorable dosing schedule for PIE12-trimer.

Acknowledgments

We thank Chiral Technologies Inc. for donating the Chiral-HSA affinity column. We thank Rebecca Macchione and the animal team at Navigen for conducting the rat PK studies. We also thank Chad Bradford for an independent WinNonlin analysis of our PK data.

References

1 McGregor, D. P. Discovering and improving novel peptide therapeutics. *Current Opinion in Pharmacology* **8**, 616-619 (2008).

2 Welch, B. D., J. Nicholas Francis, Joseph S. Redman, Suparna Paul, Matthew T. Weinstock, Jacqueline D. Reeves, Yolanda S. Lie, Frank G. Whitby, Debra M. Eckert, Christopher P. Hill, Michael J. Root, and Michael S. Kay. Design of a potent D-peptide HIV-1 entry inhibitor with a strong barrier to resistance. *Journal of Virology* **84**, 11235-11244 (Nov. 2010).

3 Francis, J. N., Joseph S. Redman, Debra M. Eckert, and Michael S. Kay. Design of a modular tetrameric scaffold for the synthesis of membrane-localized D-peptide inhibitors of HIV-1 entry. *Bioconjugate Chemistry* (2012).

4 Ingallinella, P., Elisabetta Bianchi, Neal A. Ladwa, Ying-Jie Wang, Renee Hrin, Maria Veneziano, Fabio Bonelli, Thomas J. Ketas, John P. Morre, Michael D. Miller, and Antonello Pessi. Addition of a cholesterol group to an HIV-1 peptide fusion inhibitor dramatically increases its antiviral potency. *Proceedings of the National Academy of Sciences* **106**, 5801-5806 (April 2009).

5 Thibaudeau, K., Roger Leger, Xicai Huang, Martin Robitaille, Omar Quraishi, Chantal Soucy, Nathalie Bousquet-Gagnon, Pieter van Wyk, Veronique Paradis, Jean-Paul Castaigne, and Dominique Bridon. Synthesis and evaluation of insulin-human serum albumin conjugates. *Bioconjugate Chemistry* **16**, 1000-1008 (2005).

6 Yamaoka, T., Yasuhiko Tabata, and Yoshito Ikada. Distribution and tissue uptake of poly(ethylene glycol) with different molecular weights after intravenous administration to mice. *Journal of Pharmaceutical Sciences* **83**, 601-606 (1994).

7 Fee, C. Size comparison between proteins PEGylated with branched and linear poly(ethylene glycol) molecules. *Biotechnology and Bioengineering* **98**, 725-731 (Nov. 2007).

8 Reddy, K. R., Marlene W. Modi, Simon Pedder. Use of peginterferon alfa-2a (40 kD) (Pegasys (R)) for the treatment of hepatitis C. *Advanced Drug Delivery Reviews* **54**, 571-586 (2002).

9 Fishburn, C. S. The pharmacology of PEGylation: balancing PD with PK to generate novel therapeutics. *Journal of Pharmaceutical Sciences* **97**, 4167-4183 (2008).

10 Webster, R., Victoria Elliott, B. Kevin Park, Donald Walker, Mark Hankin and Philip Taupin. PEG and PEG conjugates toxicity: towards an understanding of the toxicity of PEG and its relevance to PEGylated biologicals. *PEGylated Protein Drugs: Basic Science and Clinical Applications*, 127-146, doi:10.1007/978-3-7643-8679-5_8 (2009).

11 Laine, G., SM Hossain, RT Solis, SC Adams. Polyethylene glycol nephrotoxicity secondary to prolonged high-dose intravenous lorazepam. *The Annals of Pharmacotherapy* **29**, 1110-1114 (1995).

12 Bailon, P., Alicia Palleroni, Carol A. Schaffer, Cheryl L. Spence, Wen-Jian Fung, Jill E. Porter, George K. Ehrlich, Wen Pan, Zhi-Xin Xu, Marlene W. Modi, Adrienne Farid, and Wolfgang Berthold. Rational design of a potent, long-lasting form of interferon: a 40 kDa branched polyethylene glycol-conjugated interferon alpha-2a for the treatment of hepatitis C. *Bioconjugate Chemistry* **12**, 195-202 (2001).

13 (UCB), U. 1-31 (UCBeyond (UCB), http://www.cimzia.com, April 2012 revised version).

14 Affymax. 1-39 (Affymax, http://omontys.com, March 2012 revised version).

15 Kim, B.-J., Jie Zhou, Bronwen Martin, Olga D. Carlson, Stuart Maudsley, Nigel H. Grieg, Mark P. Mattson, Ellen E. Ladenheim, Jay Wustner, Andrew Turner, Homayoun Sadeghi, and Josephine M. Egan. Transferrin fusion technology: a novel approach to prolonging biological half-life of insulinotropic peptides. *The Journal of Pharmacology and Experimental Therapeutics* **334**, 682-692 (2010).

16 Rolin, B., Marianne O. Larsen, Carsten F. Gotfredsen, Carolyn F. Deacon, Richard D. Carr, Michael Wilken and Lotte Bjerre Knudsen. The long-acting GLP-1 derivative NN2211 ameliorates glycemia and increases beta-cell mass in diabetic mice. *American Journal of Physiology - Endocrinology and Metabolism* **283**, E745-E752 (2002).

17 Nordisk, N. 1-12 (Novo Nordisk, http://www.victozaPro.com, 2012).

18 Madsen, K., Lotte Bjerre Knudsen, Henrik Agersoe, Per Franklin Nielsen, Henning Thogersen, Michael Wilken, and Nils Langeland Johansen. Structure-activity and protraction relationship of long-acting glucagon-like peptide-1 derivatives: importance of fatty acid length, polarity, and bulkiness. *Journal of Medicinal Chemistry* **50**, 6126-6132 (2007).

19 Duckworth, W. C., Robert G. Bennett, and Frederick G. Hamel. Insulin degradation: progress and potential. *Endocrine Reviews* **19**, 608-624 (1998).

20 Gosain, V. V. Insulin analogs and intensive insulin therapy in type-1 diabetes. *Int. J. Diab. Dev. Countries* **23**, 26-36 (2003).

21 Hipszer, B., Jeffrey Josph, Moshe Kam. Pharmacokinetics of intravenous insulin delivery in humans with type 1 diabetes. *Diabetes Technology & Therapeutics* **7**, 83-93 (2005).

22 EMEA. 1-29 (http://www.ema.europa.eu/docs/en_GB/document_library/EPAR_-_Scientific_Discussion/human/000528/WC500036658.pdf, 2004).

23 Nordisk, N. 1-9 (Novo Nordisk, http://www.levemir.com, 2012).

24 Zhang, X., Keith Nieforth, Jean-Marie Lang, Regine Rouzier-Panis, Jacques Reynes, Albert Dorr, Stanley Kolis, Mark R. Stiles, Tosca Kinchelow, Indravadan H. Patel. Pharmacokinetics of plasma enfuvirtide after subcutaneous administration to patients with human immunodeficiency virus: inverse Gaussian density absorption and 2-compartment disposition. *Clin Pharmacol Ther.* **72**, 10-19 (2002).

25 Trimeris. 1-18 (Trimeris, http://www.fuzeon.com, Aug 2011 revised version).

26 Huet, T., Oliver Kerbarh, Dominique Schols, Pascal Clayette, Cecile Gauchet, Guy Dubreucq, Loic Vincent, Heidi Bompais, Romain Mazinghien, Olivier Querolle, Arnaud Salvador, Jerome Lemoine, Bruno Lucidi, Jan Balzarini, and Maurice Petitou. Long-lasting enfuvirtide carrier pentasaccharide conjugates with potent anti-human immunodeficiency virus type 1 activity. *Antimicrobial Agents and Chemotherapy* **54**, 134-142 (Jan 2010).

27 Nguyen, A., Arthur E. Reyes II, Min Zhang, Paul McDonald, Wai Lee T. Wong, Lisa A. Damico and Mark S. Dennis. The pharmacokinetics of an albumin-binding Fab (AB.Fab) can be modulated as a function of affinity for albumin. *Protein Engineering, Design & Selection* **19**, 291-297 (2006).

28 Greissman, A., P. Silver, L. Nimkoff, M. Sagy. Albumin bolus administration versus continuous infusion in critically ill hypoalbuminemic pediatric patients. *Intensive Care Med.* **22**, 495-499 (1996).

29 Stoddart, C. A., Genevieve Nault, Sofiya A. Galkina, Karen Thibaudeau, Peter Bakis, Nathalie Bousquet-Gagnon, Martin Robitaille, Maryanne Bellomo, Veronique Paradis, Patricia Liscourt, Alexandra Lobach, Marie-Eve Rivard, Roger G. Ptak, Marie K. Mankowski, Dominique Bridon, and Omar Quraishi. Albumin-conjugated C34 peptide HIV-1 fusion inhibitor; equipotent to C34 and T-20 in vitro with sustained activity in Scid-Hu Thy/Liv mice. *The Journal of Biological Chemistry* **283**, 34045-34052 (2008).

30 Kratz, F. Albumin as a drug carrier: design of prodrugs, drug conjugates and nanoparticles. *J Control Release.* **132**, 171-183 (2008).

31 Havelund, S., Anne Plum, Ulla Ribel, Ib Jonassen, Aage Volund, Jan Markussen, and Peter Kurtzhals. The mechanism of protraction of insulin detemir, a long-acting, acylated analog of human insulin. *Pharmaceutical Research* **21**, 1498-1504 (2004).

32 Tuei, V. C., Ji-Sook Ha, Chung-Eun Ha. Effects of human serum albumin complexed with free fatty acids on cell viability and insulin secretion in the hamster pancreatic beta-cell line HIT-T15. *Life Sciences* **88**, 810-818 (2011).

33 Suh, B., William A. Craig, Albert C. England, and Richard L. Elliott. Effect of free fatty acids on protein binding of antimicrobial agents. *The Journal of Infectious Diseases* **143**, 609-616 (April 1981).

34 Mishra, R., and Michael S Simonson. Saturated free fatty acids and apoptosis in microvascular mesangial cells: palmitate activates pro-apoptotic signaling involving caspase 9 and mitochondrial release of endonuclease G. *Cardiovascular Diabetology* **4**, 1-12 (Jan 2005).

35 Spector, A. A. Fatty acid binding to plasma albumin. *Journal of Lipid Research* **16**, 165-179 (1975).

36 Richieri, G. V., Alberto Anel, and Alan M. Kleinfeld. Interactions of long-chain fatty acids and albumin: determination of free fatty acid levels using the fluorescent probe ADIFAB. *Biochemistry* **32**, 7574-7580 (1993).

37 Richieri, G. V., and Alan M. Kleinfeld. Unbound free fatty acid levels in human serum. *Journal of Lipid Research* **36**, 229-240 (1995).

38 Charbonneau, D. M., and Heider-Ali Tajmir-Riahi. Study on the interaction of cationic lipids with bovine serum albumin. *The Journal of Physical Chemistry B* **114**, 1148-1155 (2010).

39 Peng, L., He Minbo, Chen Fang, Li Xi and Zhang Chaocan. The interaction between cholesterol and human serum albumin. *Protein & Peptide Letters* **15**, 360-364 (2008).

40 Kratz, F., A. Warnecke, K. Scheuermann, C. Stockmar, J. Schwab, P. Lazar, P. Druckes, N. Esser, J. Drevs, D. Rognan, C. Bissantz, C. Hindergling, G. Folkers, I. Fichtner, C. Unger. Probing the cysteine-34 position of endogenous serum albumin with thiol-binding doxorubicin derivatives. Improved efficacy of an acid-sensitive doxorubicin derivative with specific albumin-binding properties compared to that of the parent compound. *J. Med. Chem.* **45**, 5523-5533 (2002).

41 Madsbad, S., U. Kielgast, M. Asmar, C. F. Deacon, S. S. Torekov, J. J. Holst. An overview of once-weekly glucagon-like peptide-1 receptor agonists -- available efficacy and safety data and perspectives for the future. *Diabetes Obes Metab.* **13**, 394-407 (2011).

42 Welch, B. D., Andrew P. VanDemark, Annie Heroux, Christopher P. Hill, and Michael S. Kay. Potent D-peptide inhibitors of HIV-1 entry. *Proceedings of the National Academy of Sciences* **104**, 16828-16833 (2007).

43 Eertmans, F., Veerle Bogaert and Barbara Puype. Development and validation of a high-performance liquid chromatography (HPLC) method for the determination

of human serum albumin (HSA) in medical devices. *Analytical Methods* **3**, 1296-1302 (April 2011).

44 Lin, J.-J., Jeffrey D. Meyer, John F. Carpenter, and Mark C. Manning. Stability of human serum albumin during bioprocessing: denaturation and aggregation during processing of albumin paste. *Pharmaceutical Research* **17**, 391-396 (2000).

45 Muzammil, S., Yogesh Kumar, Saad Tayyab. Anion-induced refolding of human serum albumin under low pH conditions. *Biochimica et Biophysica Acta* **1476**, 139-148 (2000).

46 Kim, H. S., Irving W. Wainer. Rapid analysis of the interactions between drugs and human serum albumin (HSA) using high-performance affinity chromatography (HPAC). *J Chromatogr B Analyt Technol Biomed Life Sci.* **870**, 22-26 (2008).

47 Toutain, P. L., A. Bousquet-Melou. Plasma terminal half-life. *Journal of Veterinary Pharmacology and Therapeutics* **27**, 427-439 (2004).

48 Wolfrum, C., S. Shi, K. N. Jayaprakash, M. Jayaraman, G. Wang, R. K. Pandey, K. G. Rajeev, T. Nakayama, K. Charrise, E. M. Ndungo, T. Zimmermann, V. Koteliansky, M. Manoharan, M. Stoffel. Mechanisms and optimization of in vivo delivery of lipophilic siRNAs. *Nat Biotechnol.* **25**, 1149-1157 (2007).

49 Fernandez, M. L., Richard J. Wood. *Chapter 23; Guinea Pigs as Models for Human Cholesterol and Lipoprotein Metabolism*. 201-212 (Humana Press Inc., 2008).

50 Singh, V., Rajiv L. Tiwari, Madhu Dikshit, Manoj K. Bathwal. Models to study atherosclerosis: a mechanistic insight. *Curr Vasc Pharmacol.* **7**, 75-109 (2009).

51 Fernandez, M. L., Jeff S. Volek. Guinea pigs: A suitable animal model to study lipoprotein metabolism, atherosclerosis and inflammation. *Nutr Metab (Lond)*. **3**, 17-23 (2006).

52 Park, K., Ick Chan Kwon, Kinam Park. Oral protein delivery: current status and future prospect. *Reactive & Functional Polymers* **71**, 280-287 (2011).

53 Peppas, N. A., Nikhil J. Kavimandan. Nanoscale analysis of protein and peptide absorption: Insulin absorption using complexation and pH-sensitive hydrogels as delivery vehicles. *Eur J Pharm Sci.* **29**, 183-197 (2006).

CHAPTER 6

DISCUSSION AND FUTURE DIRECTIONS

Utilizing Other PK-Enhancing Strategies

Numerous PK-enhancing strategies are discussed in the Introduction, but only 40 kDa Y-branched PEGylation and lipidation (i.e., acylation, alkane conjugation, and cholesterol conjugation) have been carefully assessed in our lab to date. Other techniques, especially direct HSA conjugation and Fuzeon's hydrophobic tail, should also be evaluated for their PK-enhancing potential.

Synthesis of the HSA-PIE12-trimer has been straightforward, but purification has been more challenging. Gel filtration can remove unreacted peptide, but does not effectively remove unreacted HSA. Fortunately, it has been reported that HSA might be readily purified and appropriately refolded after reverse-phase HPLC and lyophilization[1,2]. These results are encouraging, because HSA and HSA-PIE12-trimer do separate on a C18 reverse phase column. Using gel-filtered material (about 1:4 HSA-PIE12-trimer to unreacted HSA), I have shown that the IC_{50} of HSA-PIE12-trimer is about 5-fold worse than PIE12-trimer itself. With improved purification (e.g., RP-HPLC), more accurate IC_{50}'s could be determined.

Significant analytical method development will also be required for HSA-PIE12-trimer before PK experiments can be conducted. Although HSA-PIE12-trimer may

acquire enough charges to become detectable by LC/MS, this has not yet been established. It is also unlikely that HSA-peptide conjugates would survive an acetonitrile precipitation of plasma samples, and it is not yet clear how much crosstalk exists between HSA-PIE12-trimer and endogenous albumin on LC/MS. Affinity purification of plasma samples or a non-LC/MS quantitative assay are likely the best strategies for quantifying peptide-HSA conjugates.

The 8 amino acid tail, or hydrophobic foot, of Fuzeon is also worth future investigation. Fuzeon-tail conjugates would be trivial to produce and easy to evaluate in both pseudoviral assay and PK studies. It would also be interesting to discover whether this sequence functions equally well in L and D. If so, this moiety could also become a nondegradable component of PIE12-trimer.

Conjugations to albumin-binding peptides might also be of interest, but would require a substantial amount of development. The peptides discussed in the introduction are quite large (making scale-up difficult and costly) and contain disulfide bonds that complicate conjugation to our existing PIE12-trimer scaffold's thiol-reactive maleimide. It is also unclear whether these constructs would offer any benefit over simple lipidation.

Fc domains are unlikely to be of practical use to us, primarily because they require mammalian cell expression for appropriate folding and glycosylation, making them too complicated to produce synthetically (though simpler production methods are being investigated[3]). Further, D-peptides cannot be genetically fused to an Fc domain. However, it might be possible to express Fc domains in mammalian cells and then post-translationally link them to D-peptides, but this strategy is unlikely to produce conjugates amenable to scale-up for large therapeutic production.

Two future directions are envisioned for PEGylation. First is assessing the effects of smaller PEG conjugations. While PEGylation with a single 40 kDa Y-branched PEG has proven beneficial for improving PIE12's half-life, it reduced the potency of PIE12 (2.5- to 10-fold) and PIE12-trimer (13- to 34-fold). It is possible that smaller PEGs (e.g., 5 kDa or 20 kDa) may provide significant PK enhancement while retaining potency.

The second future direction involves improving the way PEGylated compounds are quantified. Because of the polydispersity of large PEGs and their propensity to acquire multiple charges in LC/MS, determining a reliable Q1 parent mass for LC/MS quantitation is difficult. Although much of the PEG can be fragmented off PIE12 in the source, the resulting peptide-containing fragments still contain a polydisperse amount of PEG, making detection of a discrete peptide fragment unreliable. Instead, for quantifying PEGylated PIE12 I was forced to follow ionizable PEG fragments as a surrogate for intact parent mass.

Quantifying PEGylated PIE12-trimer by this method is risky. If PIE12-trimer is susceptible to metabolism, we would be unaware if we only followed PEG fragments as a surrogate for the parent. A possible solution for robust quantitation of polydisperse PEGylated PIE12-trimer is to develop a non-LC/MS quantitative assay. We have had trouble with this task before, and my recommendations are given in the Appendix.

Combining PK-Enhancing Moieties

Of the PK-enhancing strategies we assessed so far, PEGylation provided the longest half-life. However, the large 40 kDa Y-branched PEG reduces potency. Cholesterol conjugation, on the other hand, greatly improves potency while modestly

improving half-life. As the two most promising strategies, it is tempting to consider whether PEGylation and cholesterol conjugation can be combined.

Cholesterol's ability to increase potency is based on its ability to tether PIE12-trimer close to cell surfaces so that it is prepositioned to bind HIV's gp41 pocket approximately 60 Å away. Although the fourth arm linker is not taut and can accommodate excess linker length, it is not clear exactly how much it can tolerate. In Chapter 4 we showed that for cholesterol conjugates, 60 PEG units appeared ideal for increasing potency, while lengths of up to 140 PEG units were well tolerated and demonstrated comparable potencies. Further studies are required to determine how long the linker can become before potency drops off significantly.

PK enhancement from PEGylation exhibits a sigmoidal relationship between size and reduction in clearance. PEGs less than 5 kDa provide little PK benefit because they are rapidly cleared by renal filtration. Forty kDa PEGs provide near-maximal PK benefit, while exceeding 40 kDa provides little additional benefit. Replacing the fourth arm of our scaffold with a linear 40 kDa PEG would almost certainly reduce clearance and improve half-life, but would likely reduce potency because of long linker length and steric blocking. However, adding less than 5 kDa of PEG is unlikely to provide much PK benefit. Five kDa appears to have about one tenth the clearance-reducing benefit of a 40 kDa PEG, while 20 kDa appears to have about half the clearance-reducing benefit of a 40 kDa PEG[4].

To see if the PK and potency-enhancing benefits of PEGylation and cholesterol can be combined, cholesterol conjugates that utilize 5 kDa PEG and 20 kDa PEG fourth-arm linkers should be developed and assessed by pseudoviral assay. If tolerated, PEG

length should be increased until a potency reduction is observed. The longest PEG that maintains potency should then be analyzed in a PK study to assess its clearance-reducing benefit.

There is one caveat; if cholesterol dominates how the conjugate is cleared (e.g., it directs clearance through the liver), increasing the fourth arm PEG length may provide little PK benefit. PEG size improves half-life by reducing renal filtration. Thus, if the conjugate is not cleared renally, PEG size may be irrelevant.

Multimerization

A multimer of PIE12 might be made large enough to avoid renal filtration. The renal filtration cutoff for globular proteins is ~70 kDa and ~40-60 kDa for PEGylated peptides/proteins. Because each PIE12 is ~2 kDa and each PIE12-trimer is ~7-8 kDa, about 20-30 monomers or 5-10 trimers might be linked together to become large enough to avoid rapid filtration. Polydisperse 4-arm and 8-arm activated PEG scaffolds are readily available in radial symmetry or comb designs. For more precise control over the number, position and length of each bond, a poly-Lys or poly(Lys-Gly-Gly) peptide scaffold could be utilized through primary-amine reactive linkages (e.g., NHS-ester).

Analytical Challenges

To date, all the PEG linkers utilized for PIE12-trimer and conjugates have been discrete in length. However, for ease of large-scale synthesis, or for improvements in potency and PK (by using long fourth-arm linkers), polydisperse PEGs may become our preferred material for synthesizing PIE12-trimer. There are analytical challenges

associated with large polydisperse PEGs that need to be overcome. As discussed, polydisperse PEGs make LC/MS/MS analysis challenging. I was able to quantitate large 40 kDa PEGylated PIE12 conjugates only by fragmenting PEG in the source and following charged PEG ions in Q1 and Q3. It is possible that if our scaffold's fourth-arm linker becomes long enough, this same strategy might be applied to all PIE12-trimer conjugates. It is not yet clear how long the linker must become before this technique becomes sufficiently sensitive. Studies that explore this question might be coupled to studies that seek to combine the PK benefits of PEG and cholesterol. Ultimately, mass-independent assays might be required for effective quantitation of polydisperse compounds.

Developing an antibody to PIE12 would provide a powerful tool for a variety of applications, including immunohistochemistry and quantitation. For example, an ELISA assay might utilize an anti-PIE12 antibody coupled to a fluorescent or enzymatic readout (e.g., horseradish peroxidase). Efforts to develop a PIE12 antibody are currently underway, but because small peptides are generally nonimmunogenic, PIE12 must first be coupled to a carrier protein (e.g., KLH). Adjuvants must also be included to improve the immune response. Additional challenges surround PIE12's nondegradable nature such that antigen presenting cells are unlikely to become involved in the process. This may limit the kinds of antibodies produced to lower affinity IgM, which may nonetheless be sufficient for assay development. Alternatively, an ELISA kit that utilizes antibodies to PEG itself is commercially available (Enzo Life Sciences)[5,6]. Although expensive, this option would also be compatible with polydisperse PEG.

Webster et al. suggest two other methods for quantifying polydisperse PEGylated proteins and peptides; Western blot and NMR. In my own experience, Coomassie-blue stain of an SDS-PAGE is insufficient to detect PEGylated peptides because PEG excludes the dye. However, PEGylated protein bands can be transferred to nitrocellulose and probed with anti-PEG antibodies.

NMR is an intriguing possibility because of the cumulative signal of PEG protons (all protons on PEG are identical). Some practical considerations are worth mentioning. Jack Skalicky, local NMR expert at the University of Utah, suggests that for a single species in buffer, 10 μM is the lower limit of detection for a single unique proton. If there are 200 identical protons in a molecule, such as in a linker of 50 PEG units (2.2 kDa), the limit of detection would drop to 50 nM. However, methylene protons, like those found in PEG, might be quite abundant in plasma. It is not clear yet what kind of background noise would be present in acetonitrile-precipitated plasma samples. NMR has the added benefit of directly detecting changes in the parent molecule (i.e., metabolites), although it is unclear how sensitive detection of these changes might be nor how the FDA might perceive such a strategy for primary quantitation.

Evaluating the Species-Dependence of PK

So far, cholesterol conjugation has proven to be the most promising overall strategy for improving the potency and pharmacokinetics of PIE12-trimer conjugates. However, there is no precedent for approved cholesterol conjugates (or D-peptides for that matter!). While the body of literature is just beginning to flourish[7-13], it suggests that

circulating lipids may directly affect the clearance of lipid conjugates, indicating that PK for cholesterolated peptides might differ significantly between species.

Rodents have significantly different lipid profiles than humans, both in quantity of LDL and HDL particles as well is in the profile of lipid receptors that direct lipid circulation[14]. Fortunately, several animal models have been developed that better simulate human lipid content, including Guinea pig, Golden Syrian hamster, the LDLR (-/-) knockout mouse, and several rabbit models[14-16]. Assessing Chol-PIE12-trimer in one of these animal models seems prudent and may provide the best indication for PK behavior in humans.

Evaluating Dose-Dependence

Dose escalation studies are necessary to demonstrate a correlated increase in drug exposure (AUC) and to establish an accurate therapeutic index. For example, if higher doses initiate alternate clearance mechanisms in rodents, one might be led to believe that high doses are well tolerated, and incorrectly establish a therapeutic index that can lead to toxic doses in humans. Exposure (AUC) evaluations reduce this risk by establishing a correlation with the administered dose.

We have recently conducted dose escalation studies for PIE12-trimer and Chol-PIE12-trimer (3 mg/kg, 10 mg/kg, and 30 mg/kg in rat). Early evaluation suggests that terminal half-lives may increase with an increase in dose. While these doses are much higher than would reasonably be given to actual human patients, it provides us with an opportunity to understand the mechanism behind clearance.

Two possible scenarios explain the data. Either increased overall dosage (in mg/kg) leads to a saturation of the clearance-process, or simply increasing the concentration of the subcutaneous dose (in mg/mL) leads to a local self-association or precipitation of the compound with a delayed resolubilization and circulation. Unfortunately, our existing studies have changed both dose and stock concentrations. Therefore, an independent future study that deliberately evaluates the effects of just dose or stock concentration will be required in order to completely answer this question. Still, if high stock concentrations lead to a PK-enhancing local precipitation, then there are important implications regarding how to formulate our compound in order to achieve the same benefits at lower doses appropriate for patients.

Determining Toxicity

Paracelsus, Renaissance alchemist, physician, and father of toxicology, once said "All things are poison and nothing [is] without poison. Only the dose makes a thing not to be poison."[17] Toxicity is of particular interest to the Kay lab because, as of yet, no D-peptides or cholesterol conjugates have been approved by the FDA. It is not known how toxicity might manifest for a nondegradable D-peptide. Will they permanently accumulate somewhere? Will accumulation have physiological consequences?

Speculation is of little benefit on this subject; toxicity must be empirically determined. We can, however, surmise what organs might become affected. Given that Fuzeon produced dose-limiting injection-site reactions after subcutaneous administration, it is prudent to evaluate whether PIE12-timer injection sites develop similar reactions.

Moreover, because of the cholesterol moiety on Chol-PIE12-trimer, liver accumulation and toxicity might also be anticipated.

A set of defined toxicity studies are required by the FDA as part of filing an IND (investigational new drug) and again for the NDA (new drug application) following clinical trials. IND toxicity studies must be conducted in two animal species, one rodent and one nonrodent. Early requirements include an acute, 7-day and 28-day toxicity studies. In general, chronic toxicity studies in animals should always be longer (often twice as long) as intended studies in humans. These studies are currently underway with our company collaborator Navigen.

Exploring Metabolism

Metabolism of therapeutics presents a daunting challenge because almost anything can happen to modify a parent compound. In industry, generally a precise set of experiments is done to evaluate a defined number of most-likely metabolic changes. These include plasma stability studies, microsomal incubations, and tissue homogenate incubations.

Microsomal incubations help to identify phase-I metabolic products from the intracellular Cyp-450 oxidative system, a common site of small molecule metabolism. If susceptible, these enzymes will add +16 and +32 to the molecular weight of a parent compound (single or double oxidation). For peptides, however, we are skeptical that the intracellular Cyp-450 system will play much of a metabolic role because peptides do not readily cross cell membranes. However, cryopreserved hepatocytes are also commercially available, and may provide a superior alternative to liver microsome

studies. Intact hepatocyte incubation will determine whether peptides are actively transported intracellularly where they might become metabolized by Cyp-450 enzymes.

A number of other defined metabolic molecular weight changes that are common for small molecules can be assayed, one at a time, using defined MRM methods on plasma samples containing metabolized analyte[18]. Unfortunately, this process is tedious, sample-consuming, and unable to detect catabolism, uncommon metabolic changes, or sequestration. Furthermore I have recently demonstrated by pseudoviral assay that our LC/MS determined concentrations match the amount of functional PIE12-trimer-cholesterol in plasma samples, indicating that no detectable active metabolites are present in our Chol-PIE12-trimer plasma samples. If metabolism is occurring, metabolites would have to be inactive. Because such inactivation seems unlikely, breakdown of PIE12-trimer or sequestration seems more plausible.

Open Q1 scans might directly reveal metabolites if they are especially abundant. Unfortunately, plasma is rife with confounding signals, even after acetonitrile precipitation, limiting detection of analytes and metabolites to those with >5 μM concentrations. Open scans of urine are more promising because it contains less of a background signal, although urine requires careful handling to prevent analyte loss to tubes (no proteins in urine to prevent tube sticking), and urine too contains a surprisingly high number of confounding signals, complicating metabolite identification.

Fortunately, the MS "Precursor Ion" mode is capable of scanning a range of masses on Q1, fragmenting them in Q2, detecting a selected daughter ion on Q3 (i.e., a unique daughter ion common to PIE12-trimer and its conjugates) and then reporting what parent mass produced that ion. This mode has the capability of directly reporting any

metabolite that can produce a known daughter ion. Furthermore, I have observed that the N-terminal residue of PIE12, an acetylated histidine (mw 180.1), is common to all PIE12-containing molecules. This ion is relatively unique compared to plasma, and is produced at about 5% efficiency from parents in Q2. Some troubleshooting of the precursor ion mode may improve sensitivity, but current assessments allow for detection of any parent that produces the unique 180.1 m/z daughter ion if that parent concentration is 1 μM or higher in plasma or urine. This is still a fairly high concentration for a metabolite, but several of our highly dosed animals contain analyte concentrations that easily exceed this limit.

Future studies to find metabolites might also utilize affinity purification to help isolate metabolites from confounding signals in urine and plasma. IZN17 is a synthetically produced HIV pocket mimic for which PIE12 has a ~20 nM affinity. Attaching IZN17 to retrievable magnetic beads and incubating them in biological samples is a feasible strategy to pull out any PIE12-containing analyte, metabolite or fragment. Eluting some analytes, like the high-affinity PIE12-trimer, from IZN17-coated beads might require very strong conditions, but should be possible. The eluted samples should have vastly improved signal to noise on LC/MS, allowing for higher sensitivity detection modes such as the open Q1 scan (low nM sensitivity) to search for metabolites.

In Vivo Imaging

Because of the higher-than-expected clearance of PIE12-trimer and its conjugates, and the benefits of actually visualizing distribution, excretion, and possible accumulation of these compounds, we envision actively utilizing *in vivo* imaging to monitor the fate of

labeled drug (e.g., via MRI, CT, PET and fluorescence tomography). Unfortunately, synthesizing labeled peptides with identical physical properties (i.e., radiolabeling) is a significant technical challenge. Instead, we intend to utilize fluorescently labeled PIE12-trimer and/or its conjugates as a substitute. A fluorescent molecule might redistribute PIE12-trimer in a manner unrepresentative of its unlabeled correlate, but parallel PK studies using labeled compounds will serve as controls.

References

1 Lin, J.-J., Jeffrey D. Meyer, John F. Carpenter, and Mark C. Manning. Stability of human serum albumin during bioprocessing: denaturation and aggregation during processing of albumin paste. *Pharmaceutical Research* **17**, 391-396 (2000).

2 Muzammil, S., Yogesh Kumar, Saad Tayyab. Anion-induced refolding of human serum albumin under low pH conditions. *Biochimica et Biophysica Acta* **1476**, 139-148 (2000).

3 Beck, A., Thierry Wurch, Christian Bailly, Nathalie Corvaia. Strategies and challenges for the next generation of therapeutic antibodies. *Nat Rev Immunol.* **10**, 345-352 (2010).

4 Yamaoka, T., Yasuhiko Tabata, and Yoshito Ikada. Distribution and tissue uptake of poly(ethylene glycol) with different molecular weights after intravenous administration to mice. *Journal of Pharmaceutical Sciences* **83**, 601-606 (1994).

5 Enzon Life Sciences, E. (Enzo Life Sciences, http://www.enzolifesciences.com, 2012).

6 Cheng, T.-L., Chiu-Min Cheng, Bing-Mae Chen, Der-An Tsao, Kuo-Hsiang Chuang, Sheng-Wen Hsaio, Yi-Hung Lin, Steve R. Roffler. Monoclonal antibody-based quantitation of poly(ethylene glycol)-derivatized proteins, liposomes, and nanoparticles. *Bioconjugate Chem.* **16**, 1225-1231 (2005).

7 Francis, J. N., Joseph S. Redman, Debra M. Eckert, and Michael S. Kay. Design of a modular tetrameric scaffold for the synthesis of membrane-localized D-peptide inhibitors of HIV-1 entry. *Bioconjugate Chemistry* (2012).

8 Ingallinella, P., Elisabetta Bianchi, Neal A. Ladwa, Ying-Jie Wang, Renee Hrin, Maria Veneziano, Fabio Bonelli, Thomas J. Ketas, John P. Morre, Michael D. Miller, and Antonello Pessi. Addition of a cholesterol group to an HIV-1 peptide fusion inhibitor dramatically increases its antiviral potency. *Proceedings of the National Academy of Sciences* **106**, 5801-5806 (April 2009).

9 Harman, S., Carolina Herrera, Naomi Armanasco, Jeremy Nuttall, Robin J. Shattock. Preclinical evaluation of the HIV-1 fusion inhibitor L'644 as a potential candidate microbicide. *Antimicrob Agents Chemother.* **56**, 2347-2356 (2012).

10 Lee, K. K., Antonello Pessi, Long Gui, Alessia Santoprete, Aparna Talekar, Anne Moscona, Matteo Porotto. Capturing a fusion intermediate of influenza hemagglutinin with a cholesterol-conjugated peptide, a new antiviral strategy for influenza virus. *J Biol Chem.* **286**, 42141-42149 (2011).

11 Porotto, M., Christine C. Yokoyama, Laura M. Palermo, Bruce Mungall, Mohammad Aljofan, Riccardo Cortese, Antonello Pessi, Anne Moscona. Viral entry inhibitors targeted to the membrane site of action. *Journal of Virology* **84**, 6760-6768 (July 2010).

12 Porotto, M., Barry Rockx, Christine C. Yokoyama, Aparna Talekar, Ilaria DeVito, Laura M. Palermo, Jie Liu, Riccardo Cortese, Min Lu, Heinz Feldmann, Antonello Pessi, Anne Moscona. Inhibition of nipah virus infection in vivo: targeting an early stage of paramyxovirus fusion activation during viral entry. *PLoS Pathog.* **6**, 1-17 (Oct 2010).

13 Wolfrum, C., S. Shi, K. N. Jayaprakash, M. Jayaraman, G. Wang, R. K. Pandey, K. G. Rajeev, T. Nakayama, K. Charrise, E. M. Ndungo, T. Zimmermann, V. Koteliansky, M. Manoharan, M. Stoffel. Mechanisms and optimization of in vivo delivery of lipophilic siRNAs. *Nat Biotechnol.* **25**, 1149-1157 (2007).

14 Fernandez, M. L., Jeff S. Volek. Guinea pigs: A suitable animal model to study lipoprotein metabolism, atherosclerosis and inflammation. *Nutr Metab (Lond).* **3**, 17-23 (2006).

15 Singh, V., Rajiv L. Tiwari, Madhu Dikshit, Manoj K. Bathwal. Models to study atherosclerosis: a mechanistic insight. *Curr Vasc Pharmacol.* **7**, 75-109 (2009).

16 Fernandez, M. L., Richard J. Wood. *Chapter 23; Guinea Pigs as Models for Human Cholesterol and Lipoprotein Metabolism*. 201-212 (Humana Press Inc., 2008).

17 Stumpf, W. E. The dose makes the medicine. *Drug Discovery Today* **11**, 550-555 (2006).

18 Holcapek, M., L. Kolarova, M. Nobilis. High-performance liquid chromatography–tandem mass spectrometry in the identification and determination of phase I and phase II drug metabolites. *Anal Bioanal Chem.* **391**, 59-78 (2008).

APPENDIX

PROGRESS TOWARDS A FLUORESCENT BIOANALYTICAL ASSAY FOR PIE12-TRIMER IN PLASMA SAMPLES; CHALLENGES AND LESSONS

Background

While preparing for our initial PK studies with Invitek, we prepared stocks of PIE12 and its conjugates to reach starting concentrations of 5 μM in plasma (>1000-fold over PIE12-Trimer IC_{50}'s for HxB2 and JRFL). We reasoned that an assay that could detect analytes down to 10 nM should provide adequate sensitivity and allow us to capture 9 half-lives of elimination data. But with limited access to LC/MS/MS instrumentation (at the time), and with numerous different moieties attached to PIE12 with several more being planned for PIE12-Trimer, we wanted an assay that could easily accommodate all PIE12 variants. We therefore decided to develop a fluorescence resonance energy transfer (FRET) assay.

The Dream

A FRET assay promised numerous benefits. Fluorescent dyes have extraordinary extinction coefficients and can be detected with high sensitivity and throughput on

commonly available 96-well fluorescent plate readers. Furthermore, a FRET assay would be based entirely upon binding events, which made it amenable to our plethora of PIE12 conjugates independent of their molecular weights. Lastly, we envisioned that our FRET assay could be amenable to a "homogenous" design, requiring only the addition of a few components into one mixture with little or no sample preparation.

Other commercial tools made FRET sound even more appealing. Licor's IRDye800 fluoresces in the near-IR spectrum, a region where biological samples absorb and emit little. Further, Licor developed a FRET pair that utilizes an unusual "dark quencher" (QC1) along with its standard IRDye800. Unlike normal FRET where a new signal is detected when two fluors approach each other, dark quenchers absorb the energy of a nearby fluor, quenching its fluorescence. Fluorescence is only restored (dequenched) when the two moieties are separated.

Such a quenching pair can be utilized for a competition-based assay where addition of unlabeled analyte displaces labeled ligand, resulting in increased fluorescence with increasing unlabeled analyte. Specifically, excess QC1 dark quencher conjugated PIE12 (300-500 nM) is added to a limited amount of IRDye800-labeled pocket-containing target (10-20 nM of 5-Helix or IZN17) resulting in the binding a large fraction of pockets according to the equation $F = C/ (C+ K_D)$ where F is fraction occupied, C is concentration and K_D is the affinity of PIE12-QC1 for HIV pockets (~20 nM; 300 nM PIE12-Q1 occupies ~94% of sites). FRET occurs according to the equation $E = 1 / (1 + (R/R_0)^6)$, where E is the FRET efficiency, R is the distance between the fluors, and R_0 is the Forster distance defined for a given FRET pair (65 Å for QC1 with IRDye800). Using IZN17 labeled with IRDye800 on its N terminus, the highest

observed quenching (FRET efficiency) approached 80%, corresponding to a distance of 52 Å between the two fluors.

When a plasma sample containing unlabeled analyte is added (PIE12, PIE12-trimer, or any PK-modified conjugate thereof), it competes with QC1-PIE12 for binding to the pockets. When QC1-PIE12 is displaced, an incremental increase in fluorescence is observed. Notably, the dark quencher and IRDye800 fluors cannot be switched between the pocket-containing target and PIE12 because the PIE12-dye is always in excess, which means only a fraction of it will be bound to the pocket at all times such that free PIE12-IRDye800 would constantly produce an extraordinarily high background signal.

The maximum achievable FRET signal is determined by the concentration of IRDye800-labeled pocket-containing target. More target means higher maximum signal, however, with more target, a higher concentration of PIE12-QC1 has to be added to effectively quench that target. Eventually a balance must be struck because too much QC1-PIE12 begins contributing significantly to the background fluorescent signal, and too much QC1-PIE12 also prevents effective competition from analyte in plasma.

The "IC_{50}" of this assay is also somewhat arbitrary. It reflects the amount of analyte required to displace 50% of previously bound pockets, which is a function of how much QC1-PIE12 is originally added. Complications arise when considering PIE12 monomer analytes vs. PIE12-Trimer analytes, which have extraordinarily different affinities; thus, the IC_{50} of the assay must be tailored to each.

The Reality

Throughout my experiments I encountered multiple unanticipated challenges. By careful planning, many of them were overcome. Eventually I succeeded in developing a functional FRET assay in buffer. However, plasma samples affected the assay with animal-to-animal variation, preventing its utility for reliable quantitation. At the risk of waxing too comprehensive, I will chronicle only the most meaningful lessons learned.

The two most insurmountable challenges that ultimately halted the pursuit of a FRET-based assay involved inexplicable increases in fluorescence. First, fluorescence was affected by the addition of every component to the assay, even those that should not have had any impact whatsoever. For example, IRDye800 conjugated to PIE12 would increase in fluorescence following the addition of unlabeled PIE12; there is no logical reason why this should happen, and it certainly shook our confidence in accurately understanding the FRET response. Furthermore, I found that these inexplicable responses also depended on the order of addition of components, implying that the assay never truly came to equilibrium (even after days).

The second insurmountable problem was that the fluor was drastically affected by something in plasma that varied from animal to animal, making reproducible quantitation impossible. The same amount of fluor in plasma samples from different animals produced wildly different signals, preventing the development of a meaningful standard curve. Moreover, the offending component could not be removed from plasma following acetonitrile crash, speed-vac, and resuspension of plasma samples (Table A-1).

A third challenge was producing enough identical dye-labeled materials that could reproduce the results of a previous batch of material. Dye-labeled conjugates were

Table A-1. Animal-to-Animal Variable Effect on IRDye800

10 nM IRDye800-PIE12 placed in:	Fluorescent Units
50 mM HEPES, pH 7.4 + 10% Superblock	12.3
50% plasma from Rat A	111.4
50% plasma from Rat B	121.8
50% plasma from Rat C	141.3
50% plasma from Rat D	102.2
50% pooled rat plasma	92.4
10% pooled rat plasma	95.0
ACN-crashed rat plasma, spun, speed-vacuumed, and resuspended in 50 mM HEPES, pH 7.4 + 10% Superblock	149.1

always limited because of the expensive and short supply of dye and never seemed to behave the same from batch to batch, further complicated by the challenges of cutting pure fractions from the HPLC (especially after labeling on resin, when several truncated products would co-elute). Subtle differences in pH, organic content, denaturant, temperature and timing in the stock or assay would produce significant changes in fluorescent signal. This finicky behavior was not unique to Licor's IRDye800; Cy7.5 and DyLight-800 both shared similar unpredictable sensitivities.

Several plates were assessed for compatibility with the FRET assay. Many plates had autoflorescence in the IR range, but usually less than 1% of the signal produced by the assay. What mattered most was well-to-well reproducibility. I found that Greiner Bio-One μ-Clear high-bind Fluotrac-200 384-well black plates with clear bottom were best (Greiner 781097), with coefficients of variance (standard deviation divided by average signal) of less than 2%. Plasma was also found to produce an autofluorescent background signal that was significant at 700 nm but negligible at 800 nm. We eventually found that the volume in each well also mattered. Twenty-five μL of dye-

containing plasma actually produced a larger signal than fifty μL (at the same concentration); this was an illogical but reproducible finding. The discovery also complicated the assay, because evaporation readily changed the volume in wells within 1 hour. To address this, all plasma incubations were done in independent tubes before transferring contents to the plate. An automatic pipetter also helped to reduce variability.

A Licor Odyssey instrument was used to read the plates. The limit of detection was 150 pg of IRDye800 labeled antibody in 50 μL of plasma (~3 fmoles of fluor, or 60 pM fluor). The instrument itself produced a slight left-to-right signal bias (high to low), so assays were generally constructed in vertical columns. Thirty-two nM unconjugated IRDye800 saturated the instrument detector (at 600 units). The fluorescence was generally reduced after protein conjugation, so 50 nM of labeled conjugate was the maximum before saturating the detector.

Because of difficulties producing and properly folding 5-Helix (a target with one free pocket), we directed our efforts to labeling IZN17 with IRDye800. IZN17 trimerizes in solution to produce a three-pocket target. To avoid three fluors on every trimer of IZN17, we decided to add unlabeled IZN17 in order to cause shuffling of the monomers, aided by incubation for 1 hour at 50 °C. Surprisingly, we found the ratio of unlabeled IZN17 to IRDye800-IZN17 was increasingly beneficial (up to 10:1) for quenching by QC1-PIE12 and dequenching with PIE12; rationally, at some point adding unlabeled IZN17 would produce a sink of unlabeled IZN17 trimers that would bind PIE12 analyte without any corresponding signal, but we never reached a point where adding unlabeled IZN17 hurt sensitivity to D-peptide. This was illogical, but was nevertheless a reality.

To explain it we had to invoke some sort of solubilizing activity of D-peptide on IRDye800-labeled IZN17.

While troubleshooting the assay, we did confirm that dark-quencher labeled PIE12 had good affinity for the pocket. In pseudoviral infectivity assays, QC1-KGPIE12 and PIE12GK-QC1 had IC_{50}'s (HxB2 strain) of 40 nM and 66 nM respectively (vs. 37 nM for PIE12). Attempts were also made to develop better targets (in terms of solubility and responsiveness to quenching and dequenching). I developed "five and a half" helix and truncated IZN17 targets to bring the fluors closer together for improved FRET. However, neither of these constructs behaved much better than regular IZN17. I also developed a pocket-mutant of IZN17 and added this in a 10:1 ratio to IRDye800 labeled IZN17 to create one-pocket targets. This strategy also did not readily improve the assay.

Eventually we succeeded in developing a functioning FRET assay in 50 mM HEPES, pH 7.4 buffer. Unlabeled IZN17 and IRDye800 labeled IZN17 were combined in a 10:1 ratio with QC1-PIE12 in 6 M Guanidine at 10x concentrations. Upon dilution into buffer, the signal was appropriately quenched. Diluting into analyte-containing buffer recovered the signal, but oddly, the signal could be recovered to higher values than the uninhibited control (Fig. A-1). This assay also quenched and dequenched successfully in plasma, but did not match the responses observed in buffer, and varied in response from animal to animal, crippling the utility of the assay.

After discovering the animal-to-animal variability we gave up on the homogenous FRET assay design and developed an ELISA assay that could accommodate a washing step. We reasoned that a wash step might remove whatever fluorescence-altering

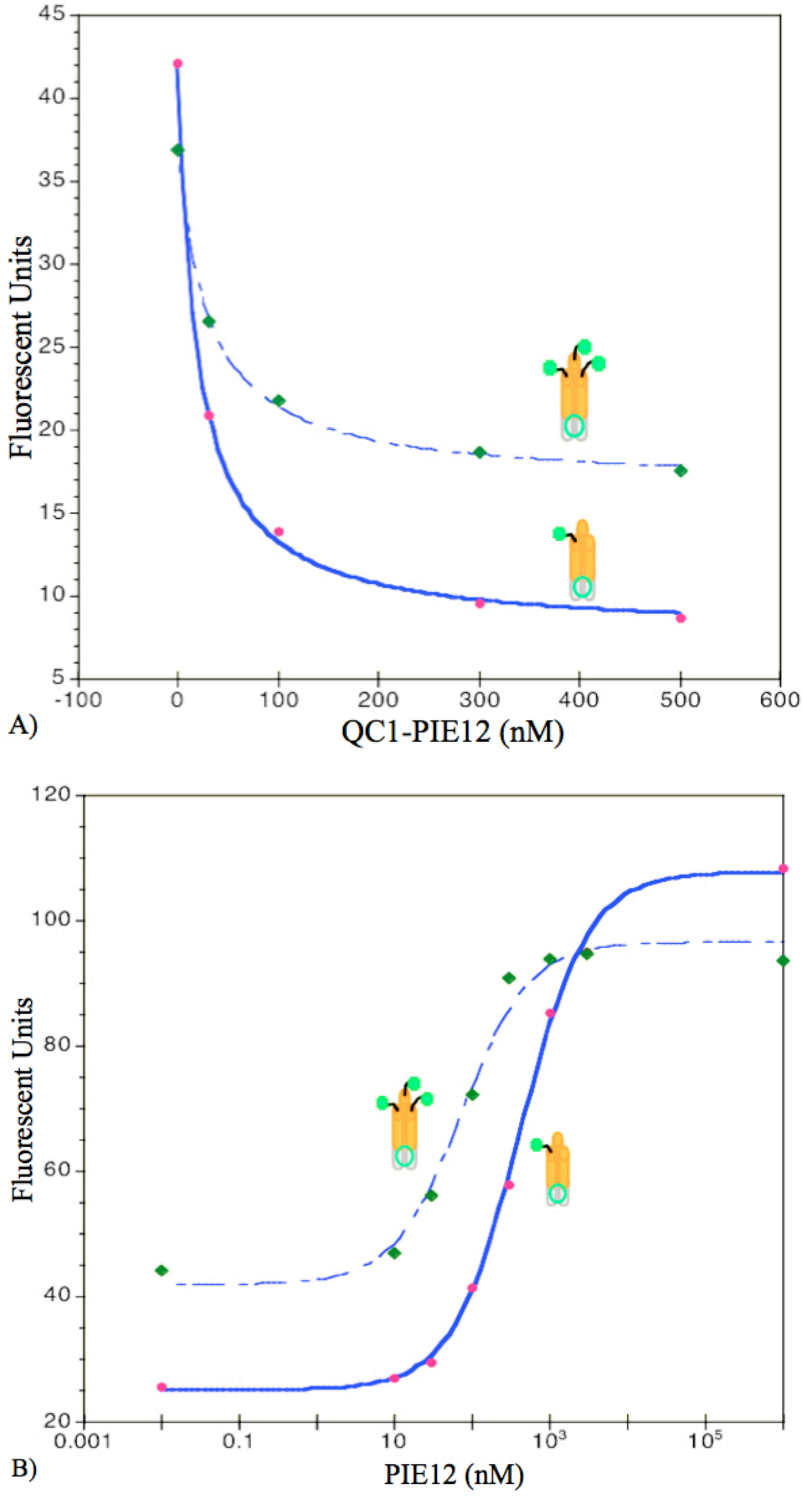

Figure A-1. Functioning FRET Assay. Dashed lines are associated with 10 nM IZN17 (3.3 nM trimers), where each monomer component is labeled with IRDye800. Solid lines are associated with 10 nM IRDye800 labeled IZN17 spiked with 100 nM unlabeled IZN17 in order to preferentially create trimers with only one IRDye800. A) IZN17 targets are quenched with increasing concentrations of QC1-PIE12. B) Quenched IZN17 can be dequenched by adding increasing concentrations of unlabeled PIE12.

component was present in plasma. We analyzed plates with streptavidin and Neutravidin pre-blocked with Superblock or bovine serum albumin (BSA) (Pierce). We found the Superblock/Neutravidin combination was able to bind the most IZN17. We developed the assay with PIE12-trimer in mind so that binding to IZN17 would be irreversible, and synthesized PIE12-trimer labeled with IRDye800. Although IRDye800-PIE12-trimer did not bind to the Neutravidin plates, we did observe nonspecific binding once IZN17 was immobilized on the plate (compared to IRDye800-PIE12-trimer prebound with IZN17 and then pulled onto Neutravidin).

Unfortunately, no variant of the assay removed the effects of plasma. Once the IRDye800 fluor became exposed to plasma its fluorescence was altered and could not be recovered by washing. Further, too many (or too long) washes began removing Neutravidin from the bottom of the plate. I redesigned the ELISA so that the fluor would be added last after plasma was removed. Biotinylated IZN17 was added to plasma to bind PIE12-trimer analyte, which was then added to the Neutravidin wells and incubated for $\leq$ 2 hours to pull down biotylated-IZN17. The plasma was washed away, and IRDye800-PIE12-trimer was added to bind any remaining available IZN17 target. This design worked in buffer, but still it failed to avoid plasma effects (Fig. A-2).

One surprising complication was that the binding of biotinylated IZN17 to Neutravidin or streptavidin was not rapid, and was further reduced in the presence of plasma (Fig. A-3). Once again, the assay never appeared to come to equilibrium. To overcome the challenge of delayed equilibrium I employed IZN17-labeled magnetic beads. Unfortunately, IRDye800-PIE12-trimer was found to bind nonspecifically to

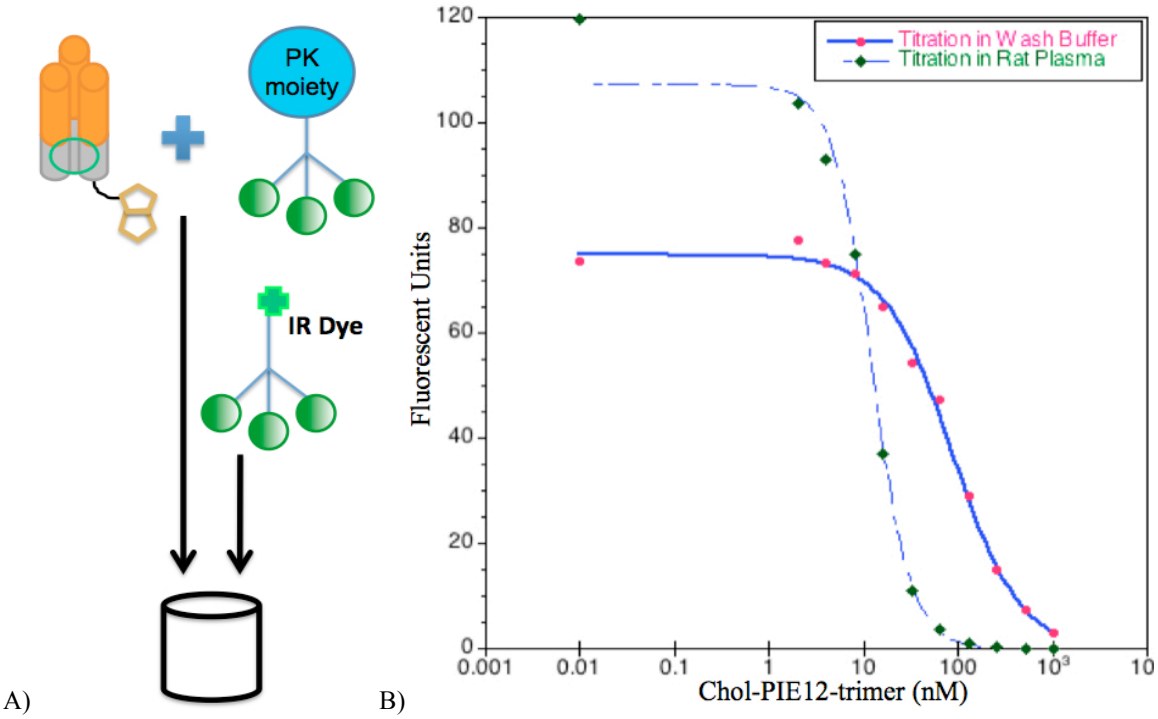

Figure A-2. ELISA Design and Function. A) Biotinylated IZN17 was added to samples (buffer or plasma) to bind analyte. These samples were then transferred to Neutravidin plates to pull down IZN17. The wells were then washed to remove unbound sample components. IRDye800-PIE12-trimer was then added to bind any IZN17 lacking analyte. B) The assay worked well in buffer, but was still affected by plasma.

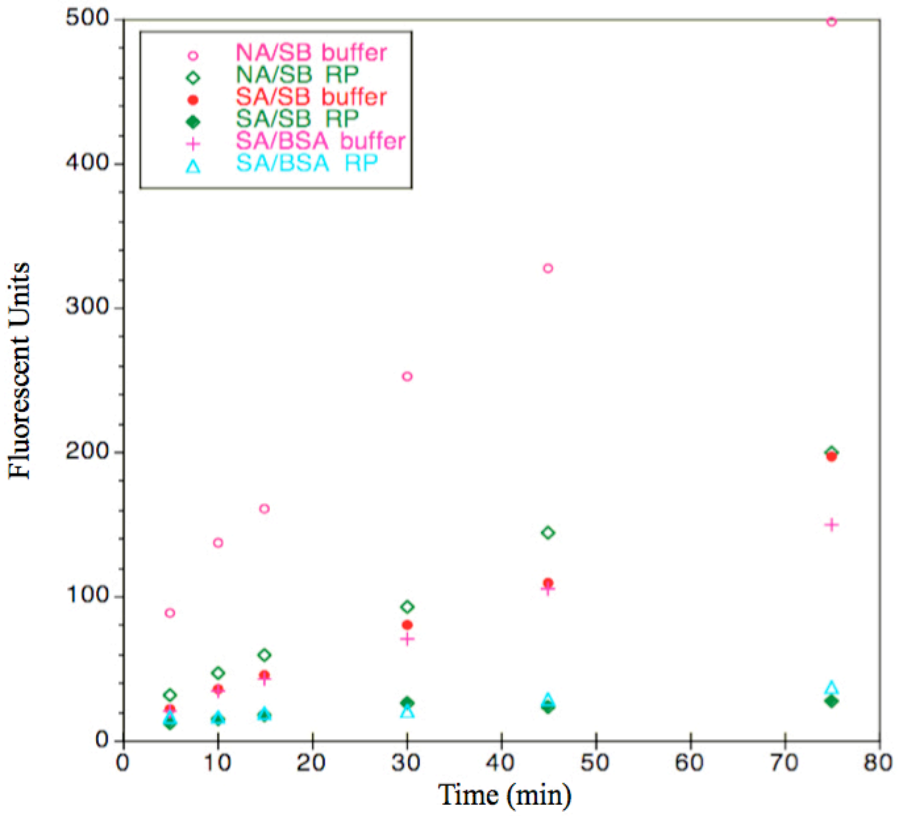

Figure A-3. Kinetics of Binding Biotinylated IZN17 to Neutravidin and Streptavidin in Plasma and Buffer Samples. IRDye800-PIE12-trimer was incubated with biotinylated IZN17 in buffer and rat plasma (RP). The samples were then transferred at different times to Neutravidin plates blocked with Superblock (NA/SB), and streptavidin plates blocked with Superblock or BSA (SA/SB and SA/BSA, respectively) to control the timing of pull-down. Wells were washed to remove unbound IZN17. The data indicate pull-down is surprisingly slow, and is exacerbated by plasma.

them, independent of blocking agent used. This was the last fluorescence-based assay attempt I made before turning to the more robust LC/MS/MS technique.

Suggestions for Future Troubleshooting

With anticipated changes to our PIE12-trimer designs (e.g., polydisperse PEG scaffolds), a functional ELISA may provide more reliable quantitation than LC/MS/MS, although an ELISA would be unable to distinguish between active metabolites. If efforts to develop an ELISA are to be undertaken, I most fervently recommend using a non-fluor-based readout, like an enzyme; every fluor I used in FRET and ELISA was too unpredictable for reliable quantitation of plasma samples.

I also recommend a cleanup of plasma samples before analysis by ELISA. Untreated plasma interferes with protein-protein interactions like the biotin pull-down by Neutravidin. Several washes, like those required to remove untreated plasma, also negatively affect the assay. Instead, I recommend using an acetonitrile crash of plasma samples, followed by speed-vac to dryness and resuspension in aqueous buffer (e.g., 50 mM HEPES, pH 7.4). My efforts to cleanup plasma samples for functional quantitation in pseudoviral assays have shown that PIE12-trimer conjugates can be successfully recovered by this method. Note that this method does not remove plasma components that affect fluorescence. I would minimize washes of Neutravidin plates, unless covalently-linked Neutravidin plates can be developed or acquired.

As interest in a mass-independent assay is rekindling in the Kay lab, I give my very best wishes to the future students whose opportunity it is to progress beyond my own efforts. May these lessons be a boon to you. Amen.